

Exclusive proton final-states and kinematic imbalance in differential neutrino cross sections with the MicroBooNE detector

[arXiv:2301.03706](https://arxiv.org/abs/2301.03706) & [arXiv:2301.03700](https://arxiv.org/abs/2301.03700)

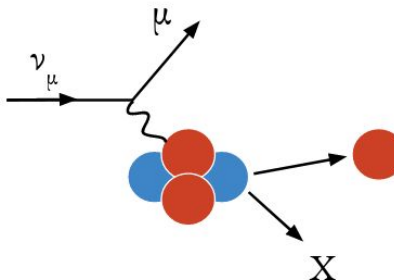
Afroditi Papadopoulou apapadopoulou@anl.gov
on behalf of the MicroBooNE Collaboration
MITP Workshop
6/27/2023



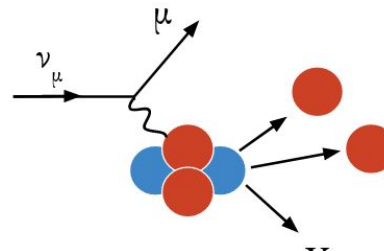
Neutrino Interaction Challenge

- Broad neutrino spectra
- Various complex interaction mechanisms

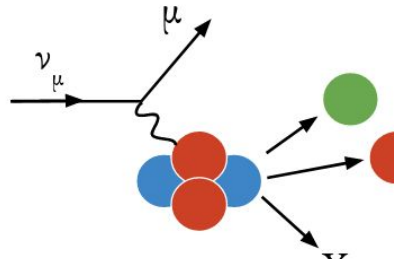
Any mismodeling in neutrino event generator simulation predictions can limit experimental sensitivity



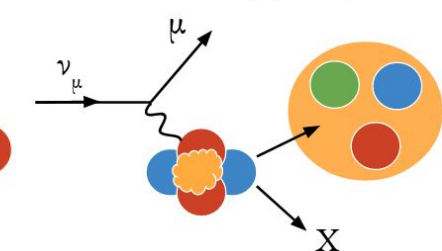
Quasi-elastic (QE)



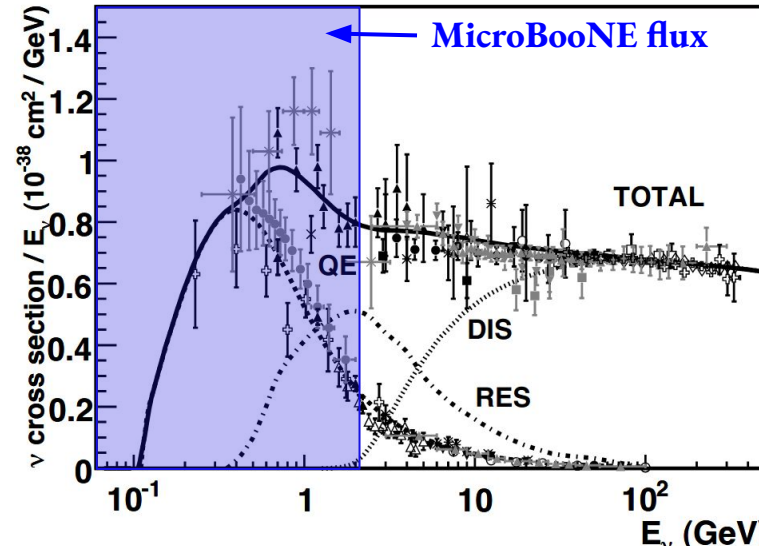
Meson Exchange Current (MEC)



Resonance (RES)

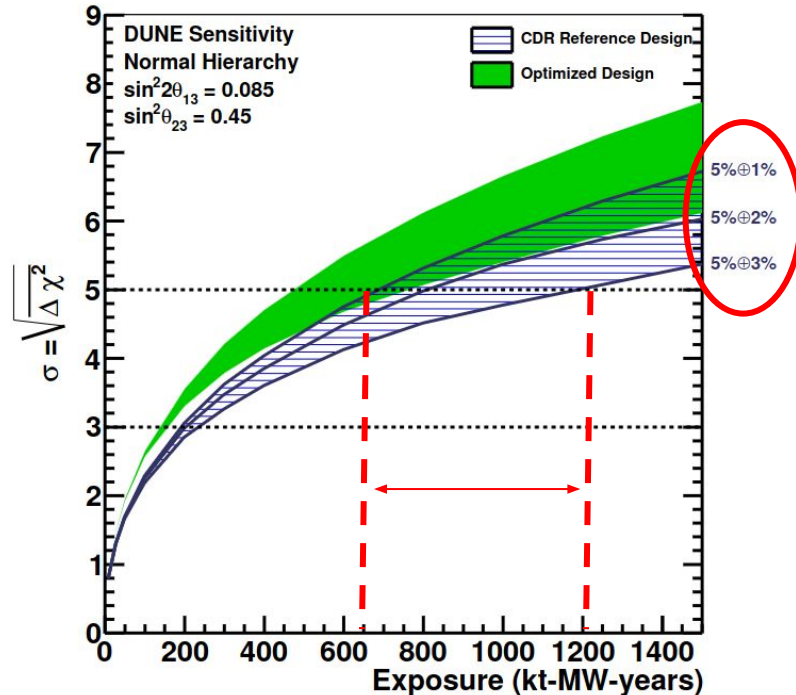


Deep Inelastic Scattering (DIS)



Future Experiments

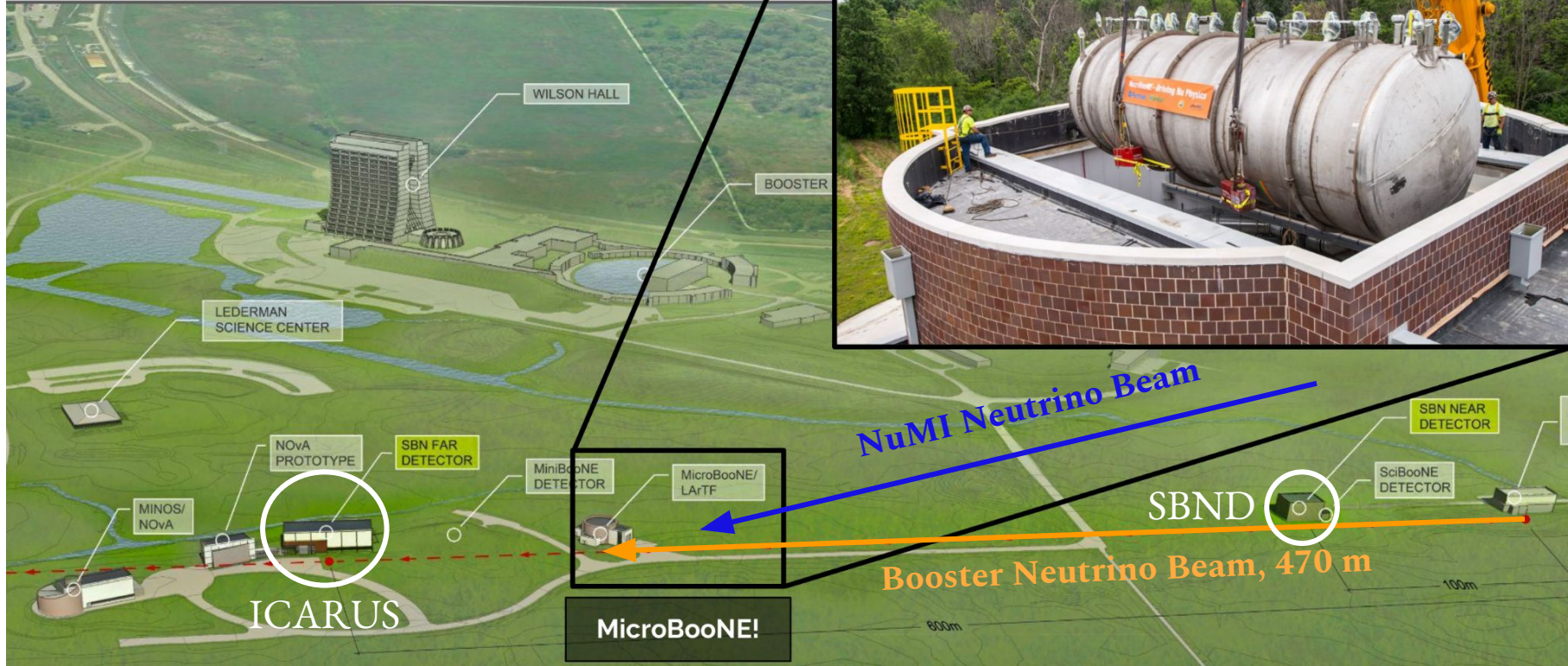
50% CP Violation Sensitivity



- Mismodeling can impact required run time of forthcoming flagship experiments
- But ... head start with Short-Baseline Neutrino (SBN) Program (MicroBooNE, SBND, ICARUS)

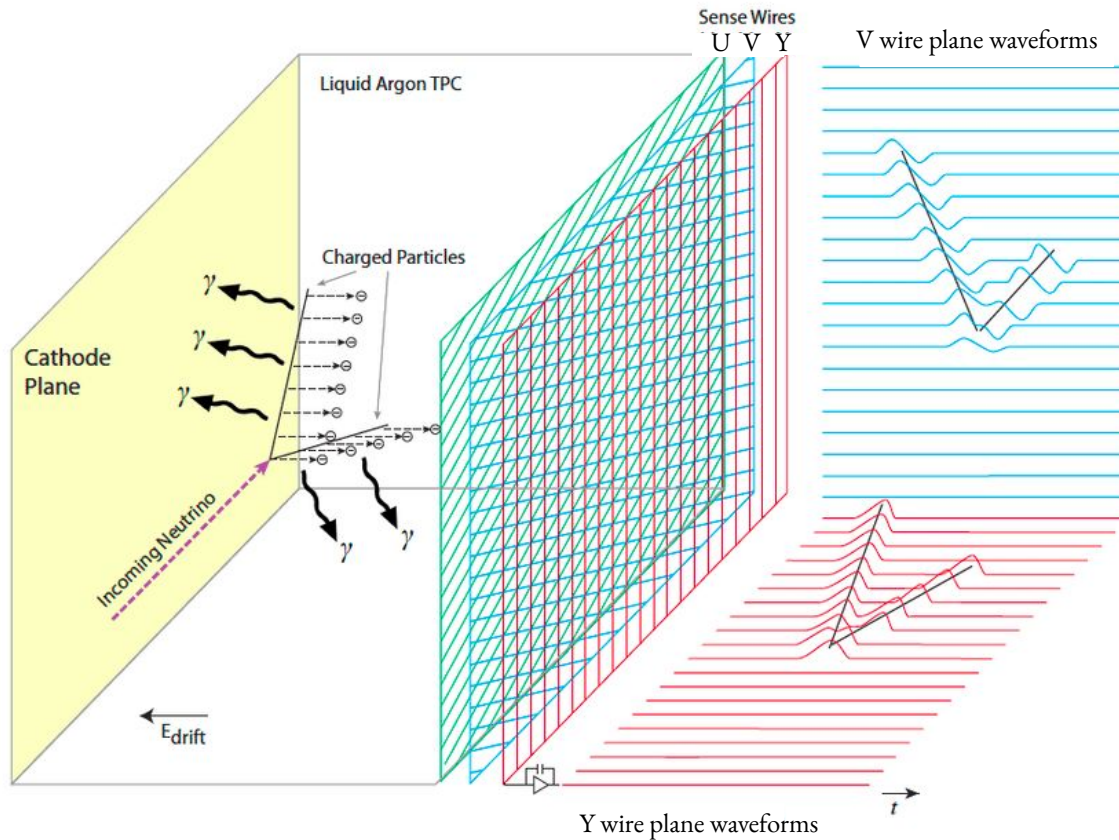
DUNE CDR, [arXiv:1512.06148](https://arxiv.org/abs/1512.06148)

MicroBooNE@FNAL



85 tonne Liquid Argon Time Projection Chamber (LArTPC)
[JINST 12, P02017 \(2017\)](#)

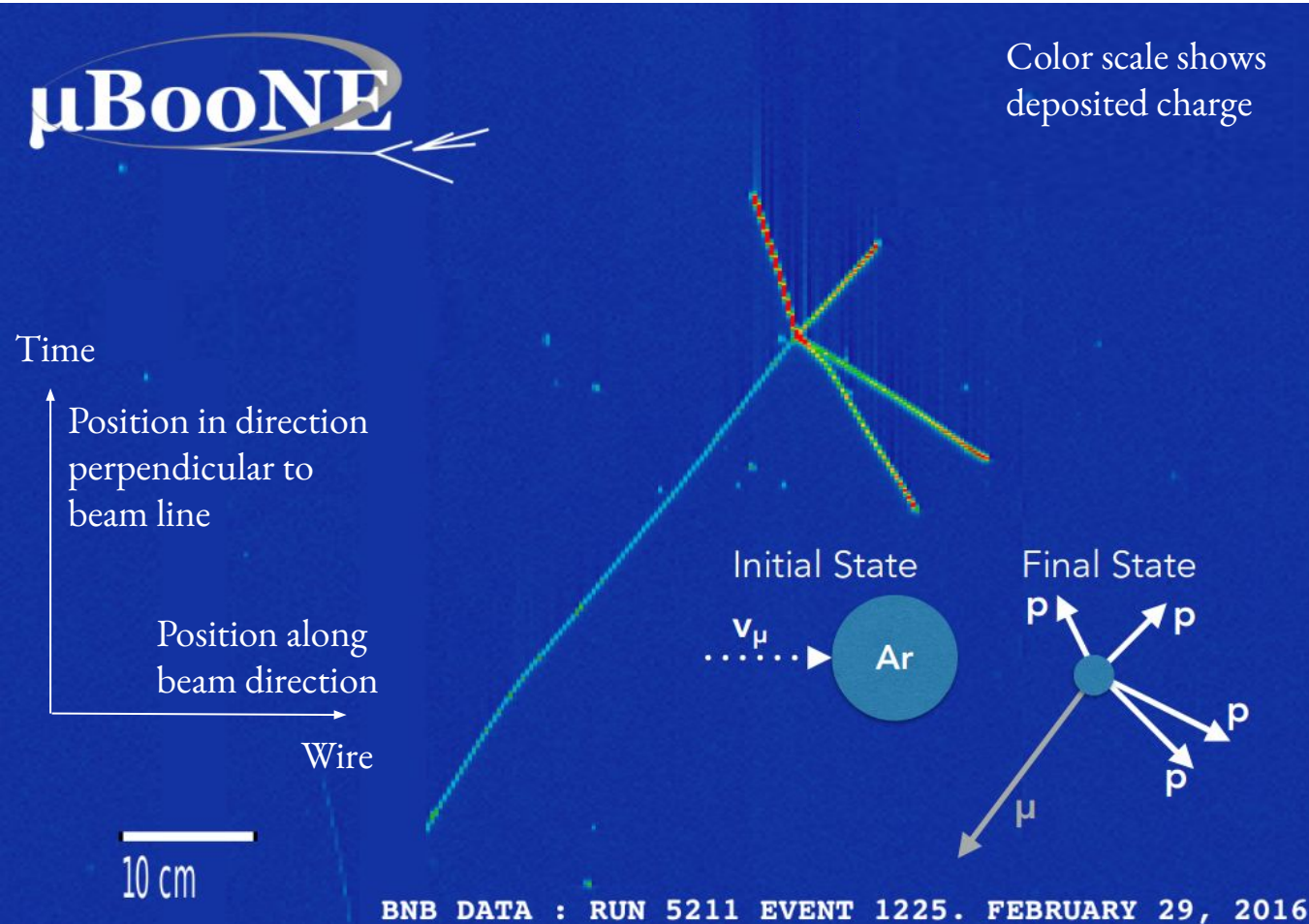
LArTPC Operation Principle



MicroBooNE

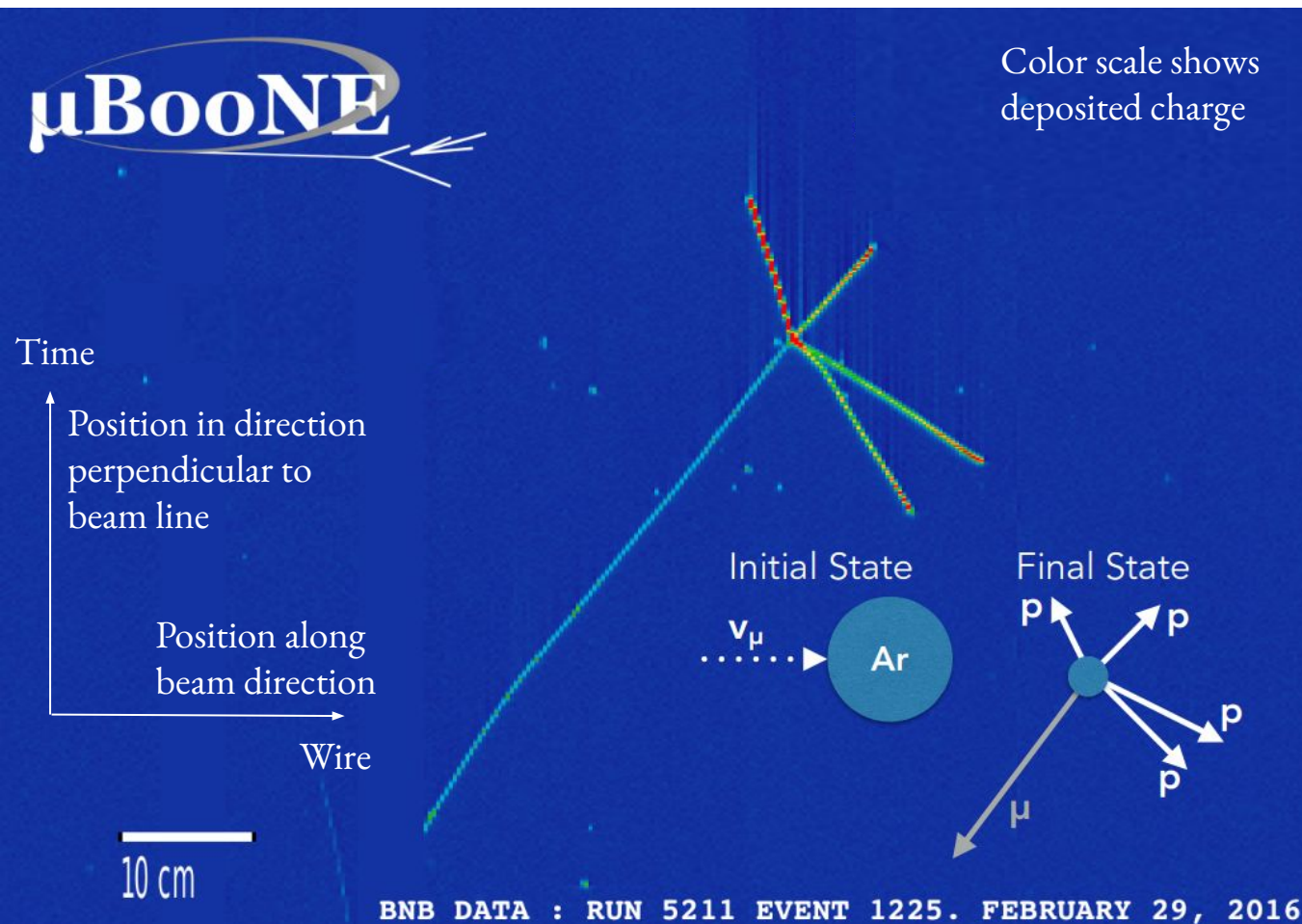
- 3 wire planes
- 8192 gold coated wires
- 3 mm wire spacing
- 32 PMTs

MicroBooNE Data Events



- Excellent spatial resolution
- Low detection thresholds
- Precise calorimetric information
- Powerful particle identification

MicroBooNE Data Events



- Largest available neutrino-argon data set with ~500k recorded neutrino interactions
- Over 10 released and more than 30 active MicroBooNE cross section analyses
- Multiple topologies investigated

Already Public Results

CC inclusive

- 1D ν_μ CC inclusive @ BNB
[Phys. Rev. Lett. 123, 131801 \(2019\)](#)
- 1D ν_μ CC E_ν @ BNB
[Phys. Rev. Lett. 128, 151801 \(2022\)](#)
- 1D ν_e CC inclusive @ NuMI
[Phys. Rev. D105, L051102 \(2022\)](#)
[Phys. Rev. D104, 052002 \(2021\)](#)

Pion production

- ν_μ NC π^0 @ BNB
[Phys. Rev. D 107, 012004 \(2023\)](#)

CC0 π

- 1D ν_e CCNp0 π @ BNB
[Phys. Rev. D 106, L051102 \(2022\)](#)
- 1D & 2D ν_μ CC1p0 π Kinematic Imbalance @ BNB
[arXiv:2301.03700](#), [arXiv:2301.03706](#)
submitted to PRL & PRD
- 1D ν_μ CC1p0 π @ BNB
[Phys. Rev. Lett. 125, 201803 \(2020\)](#)
- 1D ν_μ CC2p @ BNB
[arXiv:2211.03734](#), submitted to PRL
- 1D ν_μ CCNp0 π @ BNB
[Phys. Rev. D102, 112013 \(2020\)](#)

Rare channels

- η production @ BNB, submitted to PRL
[arXiv:2305.16249](#)
- Λ production @ NuMI
[arXiv:2212.07888](#), accepted by PRL

Already Public Results

CC inclusive

- 1D ν_μ CC inclusive @ BNB
[Phys. Rev. Lett. 123, 131801 \(2019\)](#)
- 1D ν_μ CC E_ν @ BNB
[Phys. Rev. Lett. 128, 151801 \(2022\)](#)
- 1D ν_e CC inclusive @ NuMI
[Phys. Rev. D105, L051002 \(2022\)](#)
[Phys. Rev. D104, 052003 \(2021\)](#)

CC0 π

- 1D ν_e CCNp0 π @ BNB
[Phys. Rev. D 106, L051102 \(2022\)](#)
- 1D & 2D ν_μ CC1p0 π Kinematic Imbalance @ BNB
[arXiv:2301.03700](#), [arXiv:2301.03706](#)
submitted to PRL & PRD

Opportunity to extensively benchmark neutrino event generator predictions

Pion production

- ν_μ NC π^0 @ BNB
[Phys. Rev. D 107, 012004 \(2023\)](#)

submitted to PRL

- 1D ν_μ CCNp0 π @ BNB
[Phys. Rev. D102, 112013 \(2020\)](#)

Rare channels

- η production @ BNB
[arXiv:2305.16249](#)
- Hyperon (Λ, Σ) production @ NuMI
[arXiv:2212.07888](#), accepted to PRL

Nuclear Effects in Event Generators

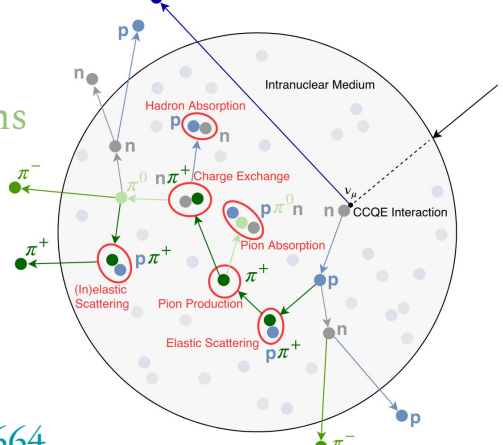
[Rev. Mod. Phys. 89, 045002 \(2017\)](#)

- Fermi motion
- Final state interactions
- Meson exchange currents
- ...

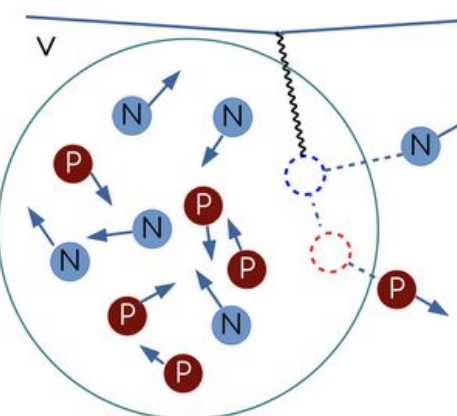
}

Known unknowns that need to be accurately simulated

Hadron
reinteractions

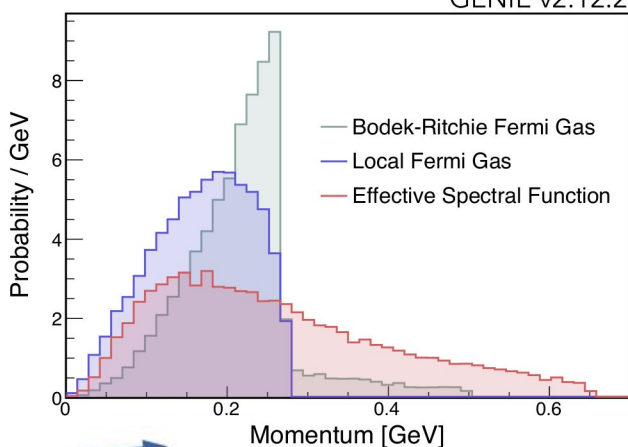


[arXiv:2201.04664](#)

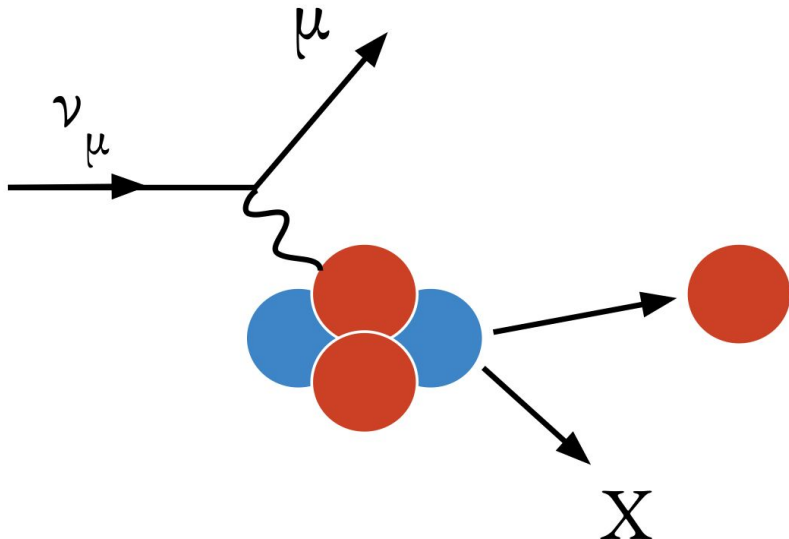


Nucleon-nucleon relative angle
and momenta

[J. Wolcott](#)
[Wine & Cheese Seminar](#)



Double-Differential Single-Proton Knockout

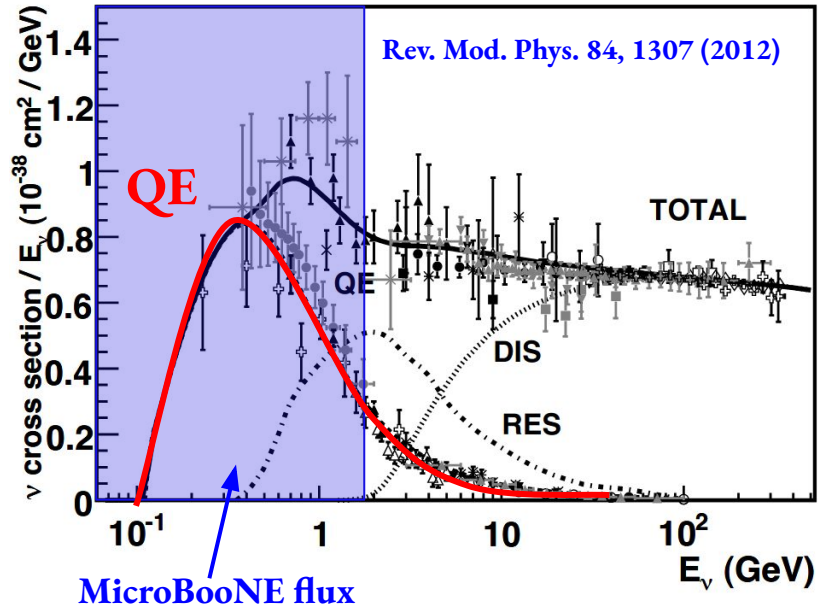
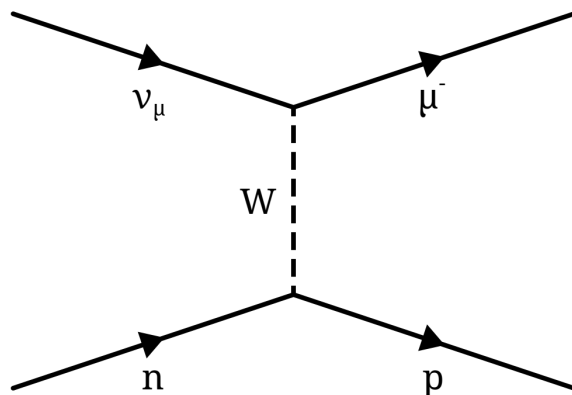


- First double-differential single-proton cross section measurement on argon
- Identified kinematic variables and phase-space regions with sensitivity to Fermi motion & final state interactions
- Uses ~50% of available MicroBooNE data sets & Booster Neutrino Beam (BNB)

[arXiv:2301.03700](https://arxiv.org/abs/2301.03700)

[arXiv:2301.03706](https://arxiv.org/abs/2301.03706)

Single-Proton Knockout



- Dominated by Charged Current Quasi-elastic (CCQE) interactions
- Simple single muon-proton events
- Dominant at MicroBooNE energies

CC1p0 π Quasielastic-like Signal Definition

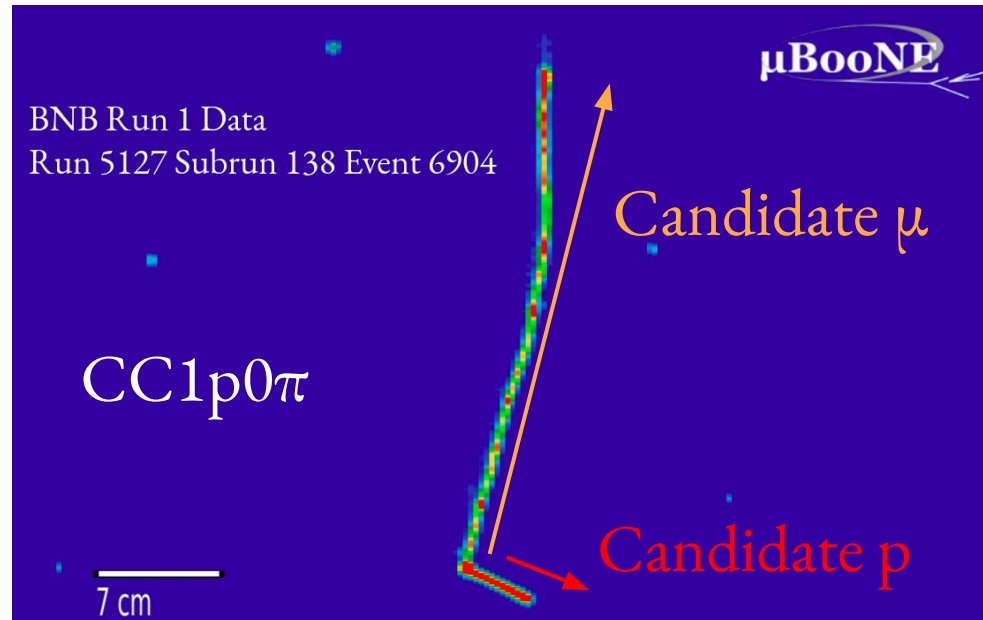
Ranges driven by minimum track length, track containment, hadronic reinteractions, and systematics

- 1 muon
 $100 < P_\mu < 1200$ MeV/c
- 1 proton
 $300 < P_p < 1000$ MeV/c
- No π^\pm with $P_\pi > 70$ MeV/c
- No π^0 or heavier mesons
- Any number of neutrons

9051 CC1p0 π candidate data events

CC1p0 π ~10% efficiency

~70% purity

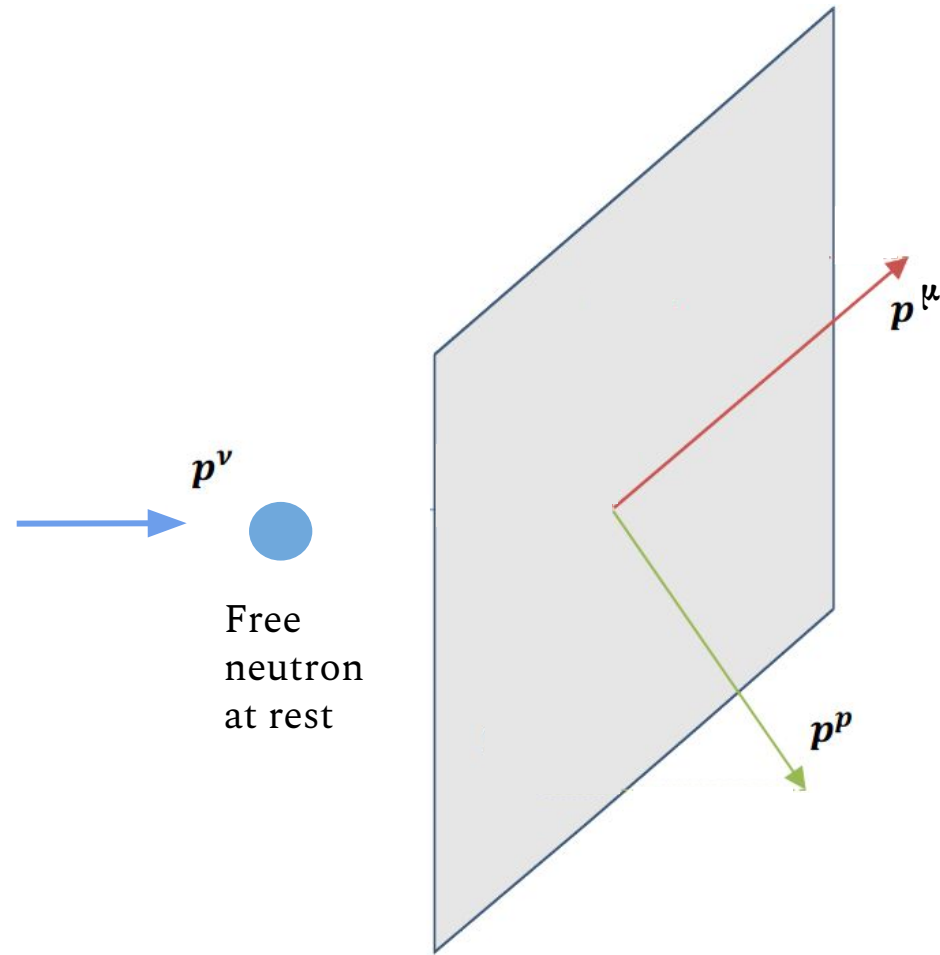


[arXiv:2301.03706](https://arxiv.org/abs/2301.03706)

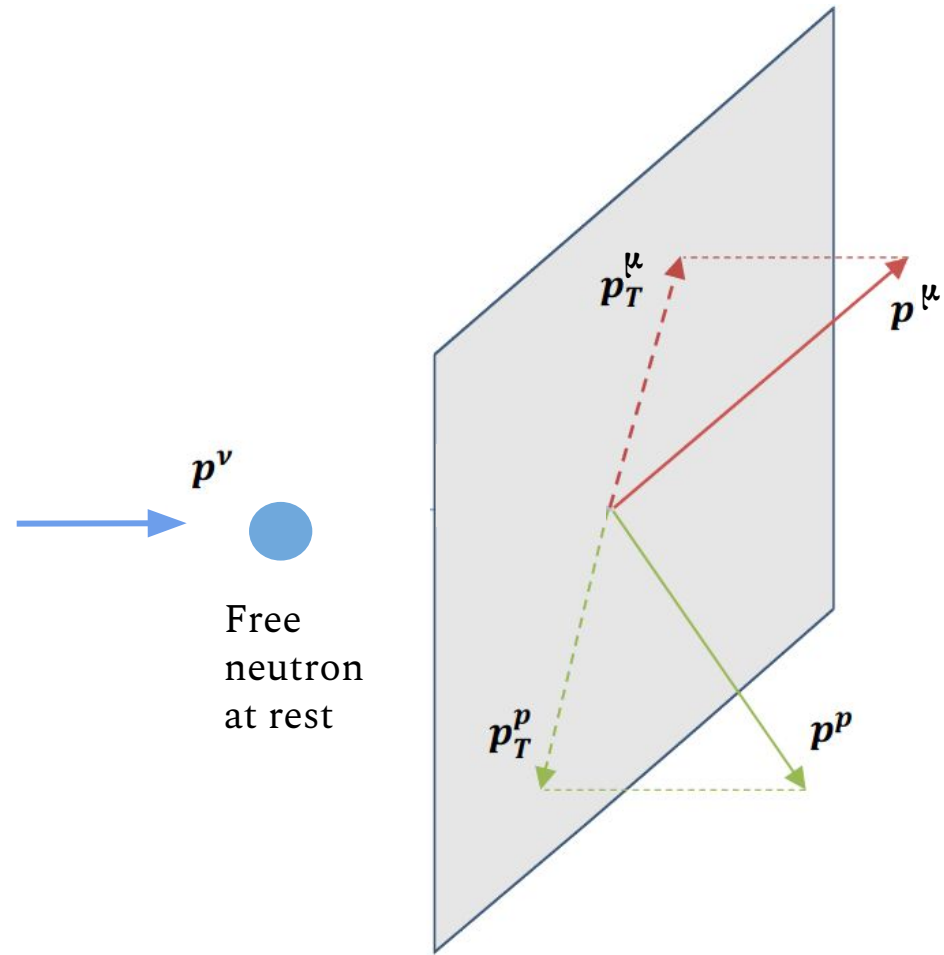
* [Phys. Rev. D 105, 072001 \(2022\)](https://doi.org/10.1103/PhysRevD.105.072001)

MC: GENIE v3.0.6 G18_10a_02_11b + tune*
Nieves QE & MEC, Berger Sehgal RES

Transverse Kinematic Imbalance (TKI)



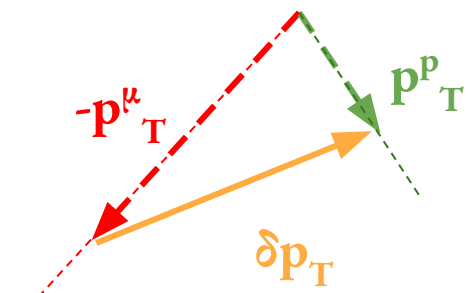
Transverse Kinematic Imbalance (TKI)



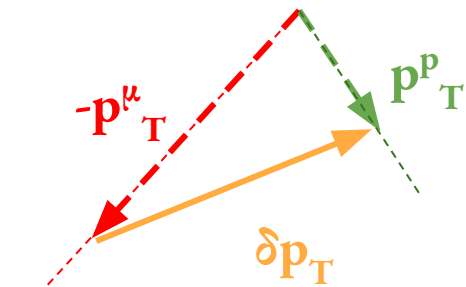
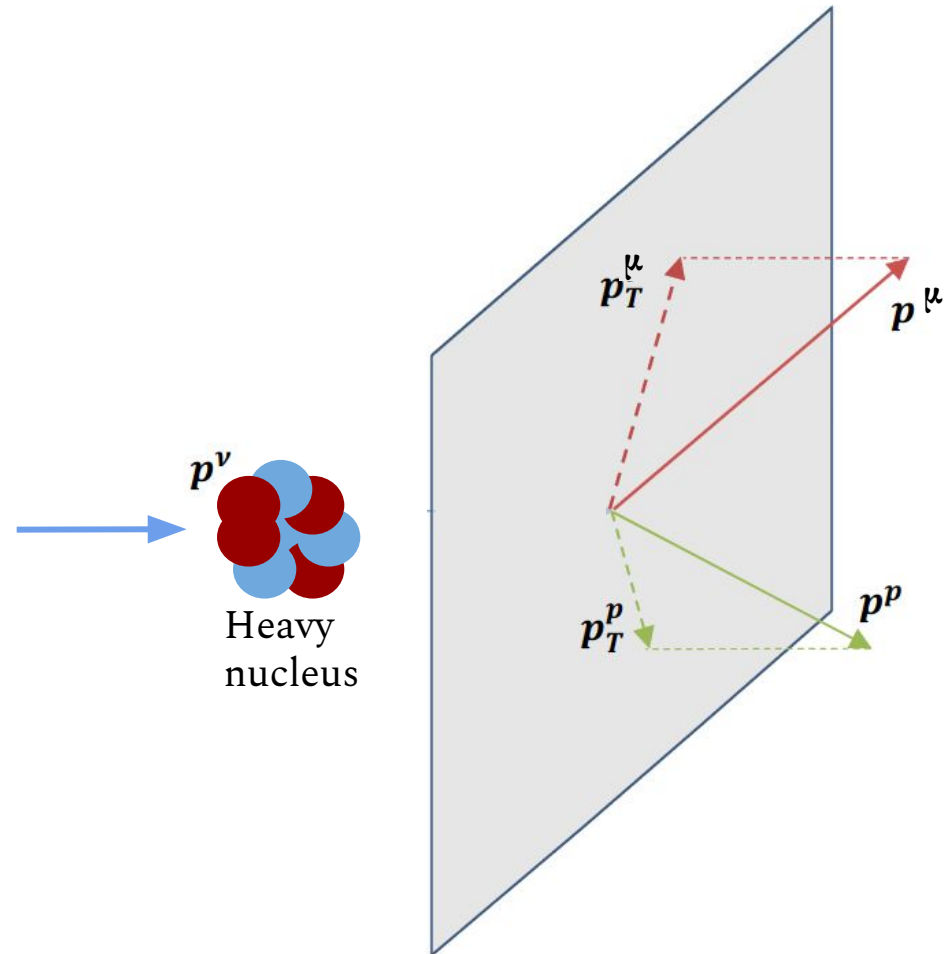
Free
neutron
at rest

Transverse missing momentum
 $\delta p_T = | p_T^\mu + p_T^p | = 0$

Transverse projections
equal and opposite due to
momentum conservation



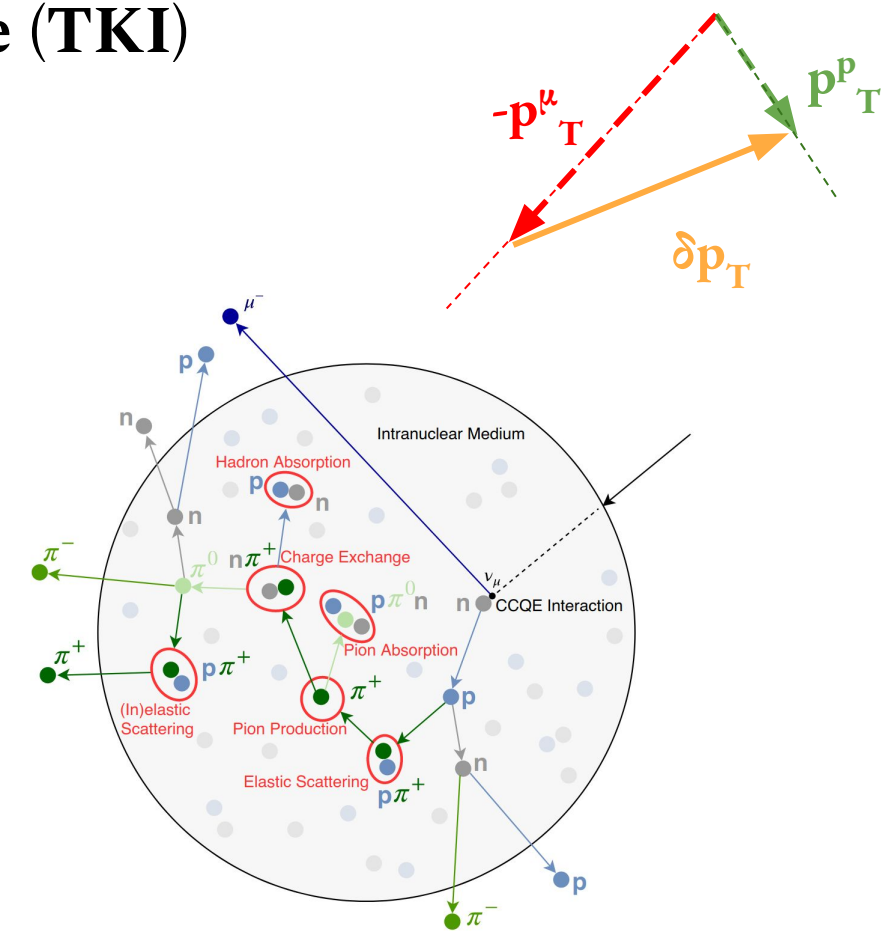
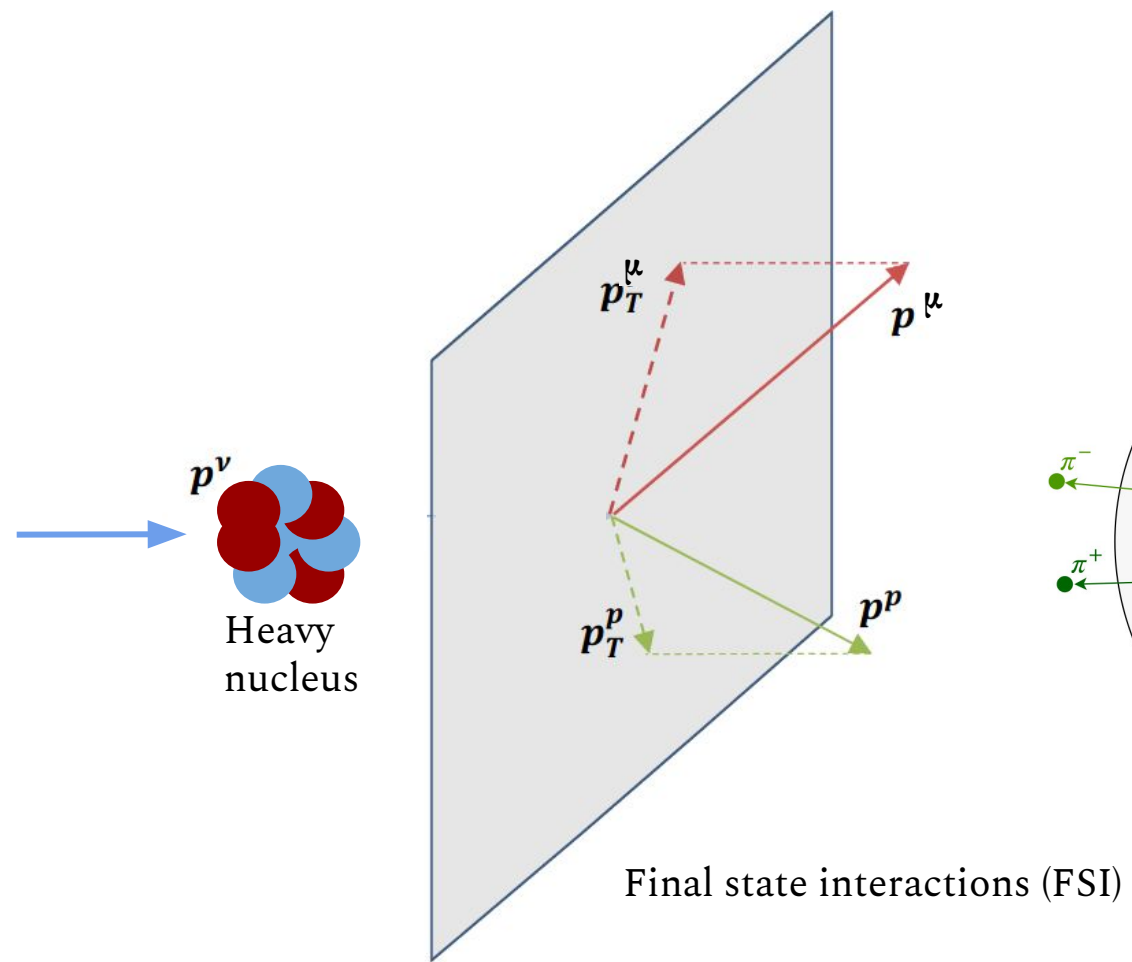
Transverse Kinematic Imbalance (TKI)



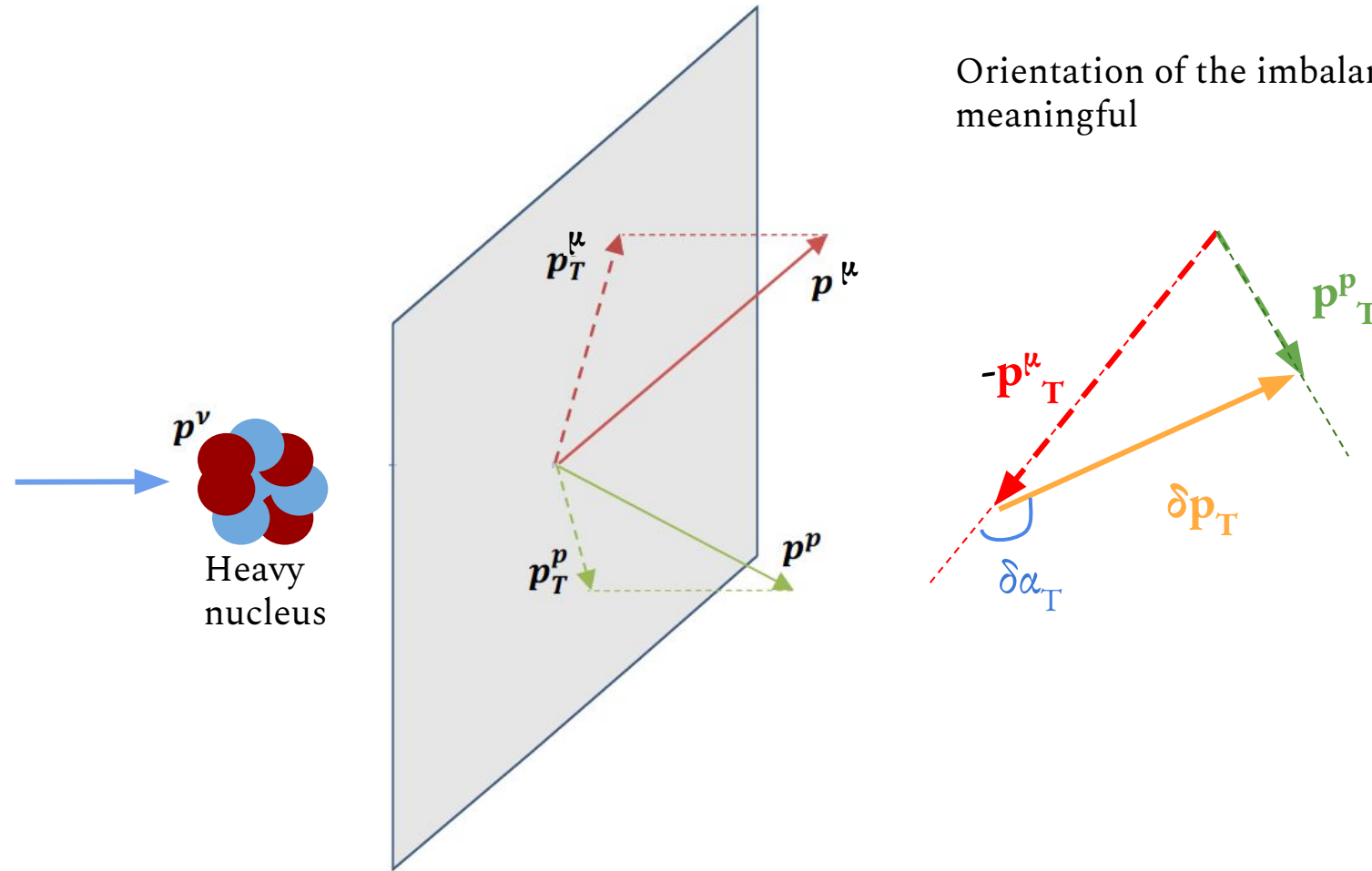
Transverse missing momentum
 $\delta p_T = | \mathbf{p}_T^\mu + \mathbf{p}_T^p | > 0$

Broad distribution due to initial nucleon motion and other nuclear effects

Transverse Kinematic Imbalance (TKI)

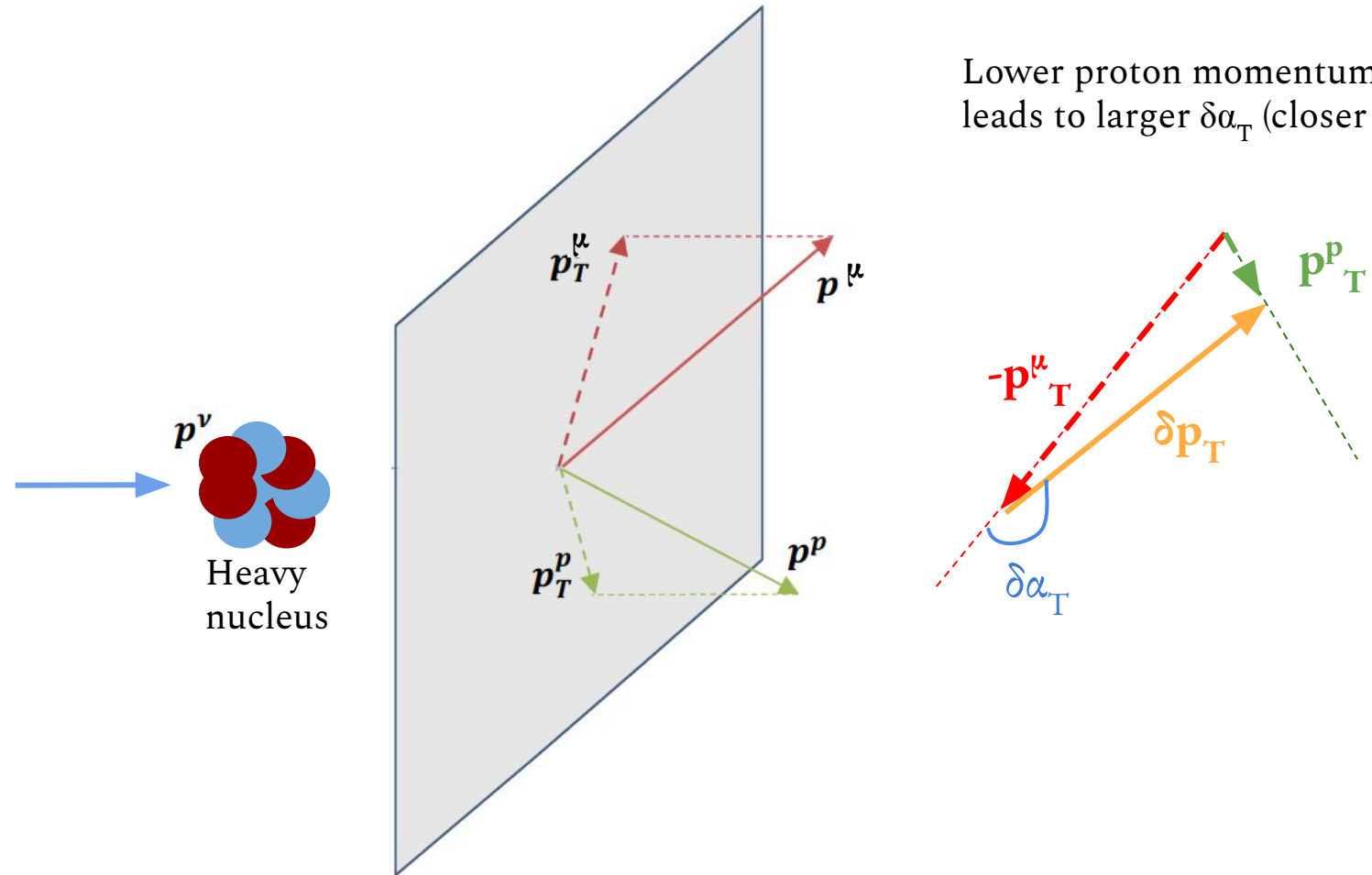


Transverse Kinematic Imbalance (TKI)



Orientation of the imbalance ($\delta\alpha_T$) also meaningful

Transverse Kinematic Imbalance (TKI)



Lower proton momentum due to FSI
leads to larger $\delta\alpha_T$ (closer to 180°)

TKI Neutrino Measurements

Experiment	Target	References
T2K	CH	Phys. Rev. D 103 11, 112009 (2021) Phys. Rev. D 98, 032003 (2018)
MINERvA	CH	Phys. Rev. Lett. 121, 022504 (2018) Phys. Rev. D 101, 092001 (2020) Phys. Rev. D 102, 072007 (2020)

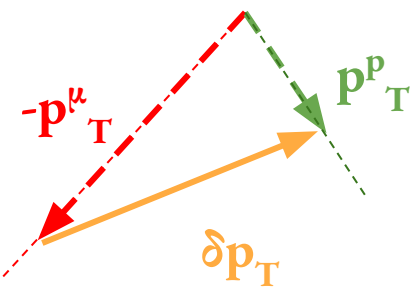
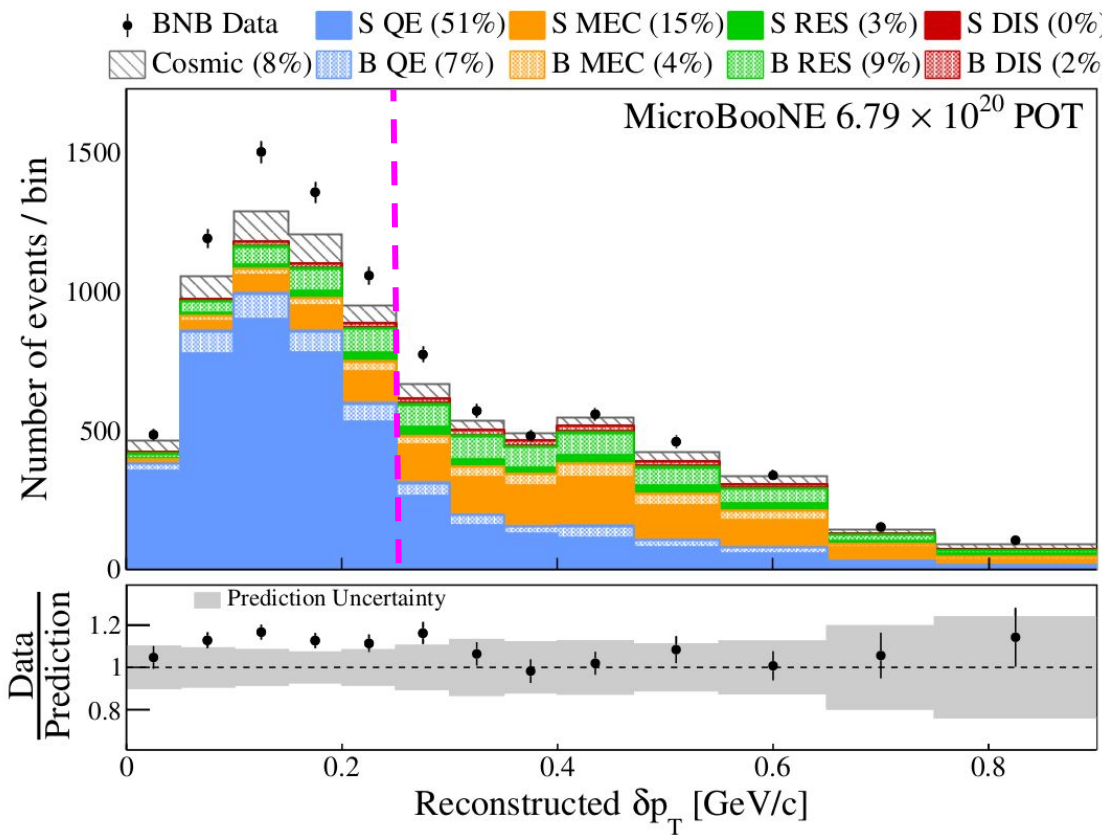
But none on argon up to now!

TKI Neutrino Measurements

Experiment	Target	References
T2K	CH	Phys. Rev. D 103 11, 112009 (2021) Phys. Rev. D 98, 032003 (2018)
MINERvA	CH	Phys. Rev. Lett. 121, 022504 (2018) Phys. Rev. D 101, 092001 (2020) Phys. Rev. D 102, 072007 (2020)
This talk: MicroBooNE	Ar	arXiv:2301.03706 (submitted to PRL) arXiv:2301.03700 (submitted to PRD)

First single- and double-differential single-proton cross section measurements on argon in transverse kinematic imbalance

Transverse Missing Momentum δp_T



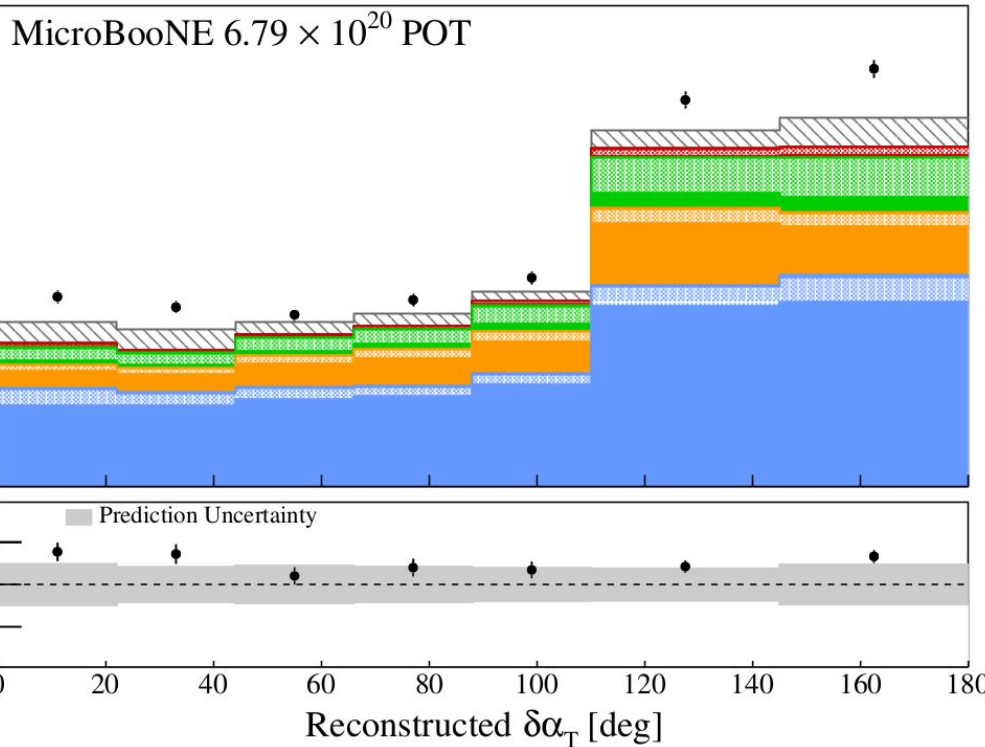
- S = Signal, B = Background
- QE dominance in peak below Fermi momentum (~ 250 MeV/c)
- MEC/RES mainly in high momentum tail

arXiv:2301.03700
* Phys. Rev. D 105, 072001 (2022)

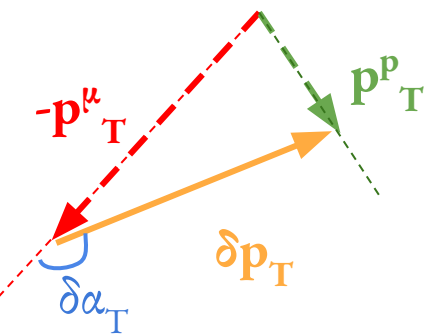
GENIE v3.0.6 G18_10a_02_11b + tune*
Nieves QE & MEC, Berger Sehgal RES

Transverse Orientation $\delta\alpha_T$

♦ BNB Data S QE (51%) S MEC (15%) S RES (3%) S DIS (0%)
 ◻ Cosmic (8%) B QE (7%) B MEC (4%) B RES (9%) B DIS (2%)



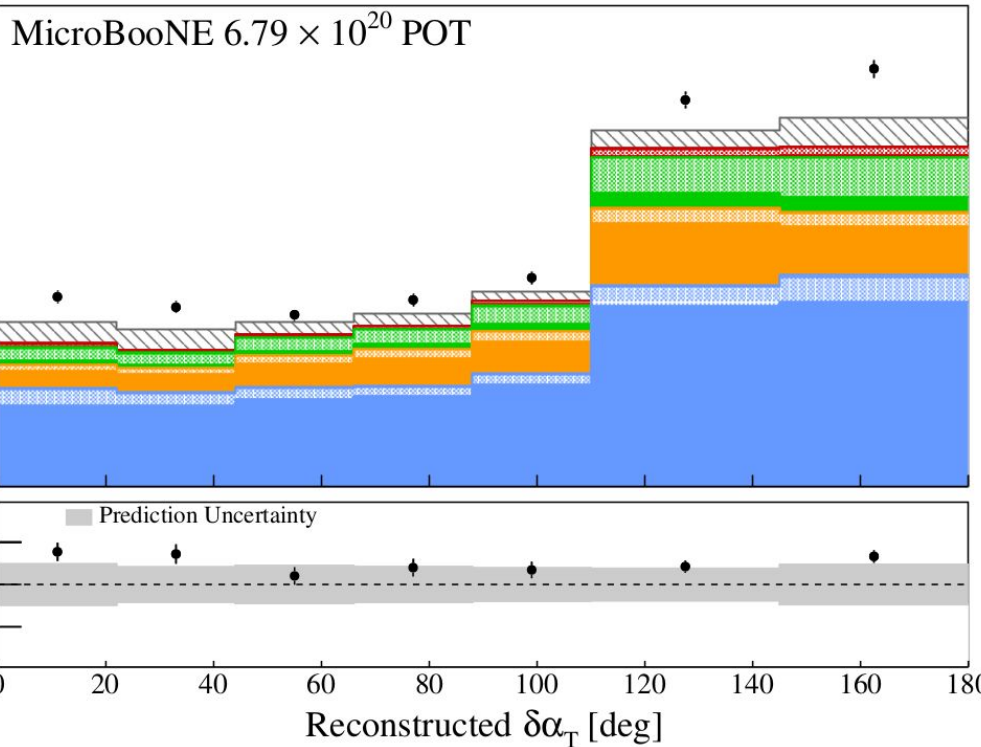
- $\delta\alpha_T$ asymmetry due to proton FSI
- **MEC/RES** fractional contribution enhanced in $\sim 180^\circ$ region



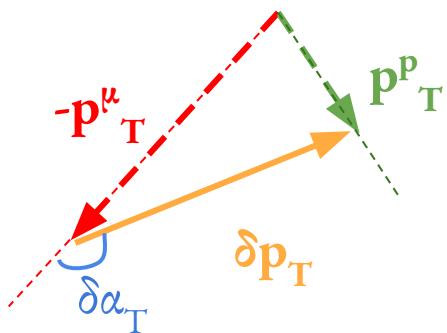
GENIE v3.0.6 G18_10a_02_11b + tune*
 Nieves QE & MEC, Berger Sehgal RES

Transverse Orientation $\delta\alpha_T$

♦ BNB Data S QE (51%) S MEC (15%) S RES (3%) S DIS (0%)
 ◻ Cosmic (8%) B QE (7%) B MEC (4%) B RES (9%) B DIS (2%)



Need to move from event distributions to cross sections → *unfolding*

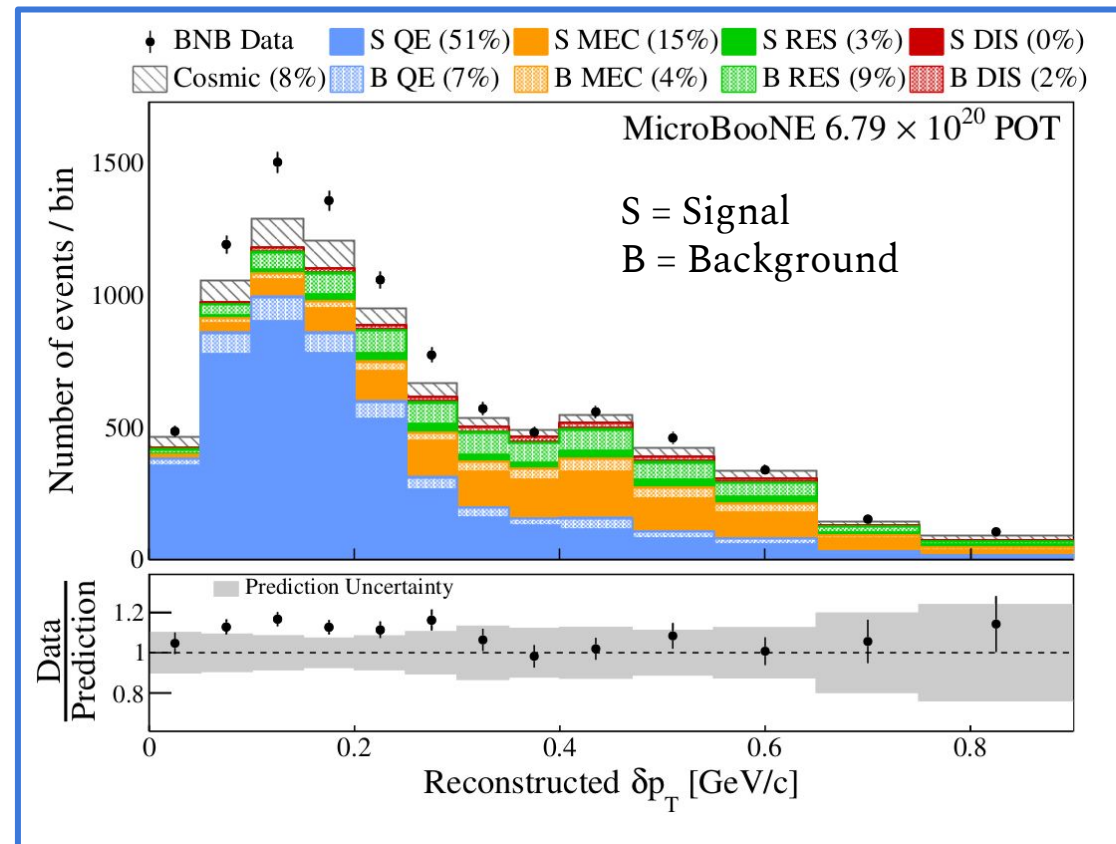


Cross Section Extraction with Wiener SVD Unfolding

JINST 12 P10002 (2017)

Input Quantities

- Measurement (Data)
- Background (Cosmics + MC)
- Response Matrix (MC)
- Total Covariance Matrix (MC)



Cross Section Extraction with Wiener SVD Unfolding

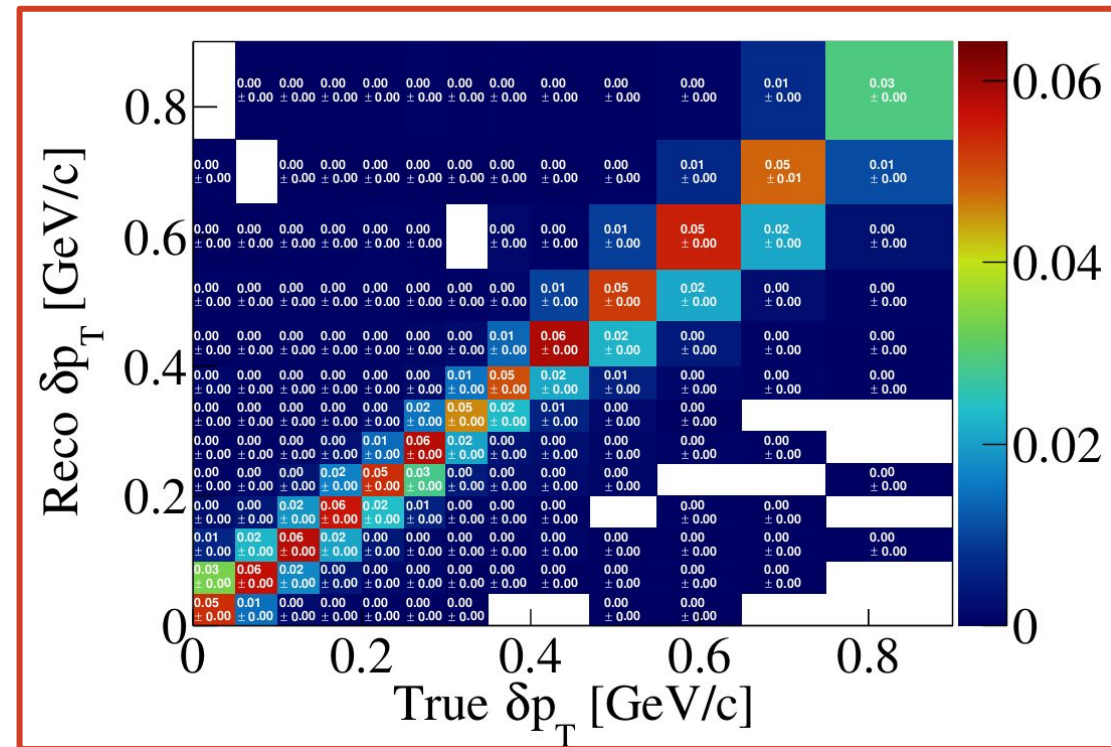
JINST 12 P10002 (2017)

Input Quantities

- Measurement (Data)
- Background (MC)
- Response Matrix (MC)
- Total Covariance Matrix (MC)

Probability that a generated event is reconstructed and selected

Diagonal matrix with flat ~6% efficiency



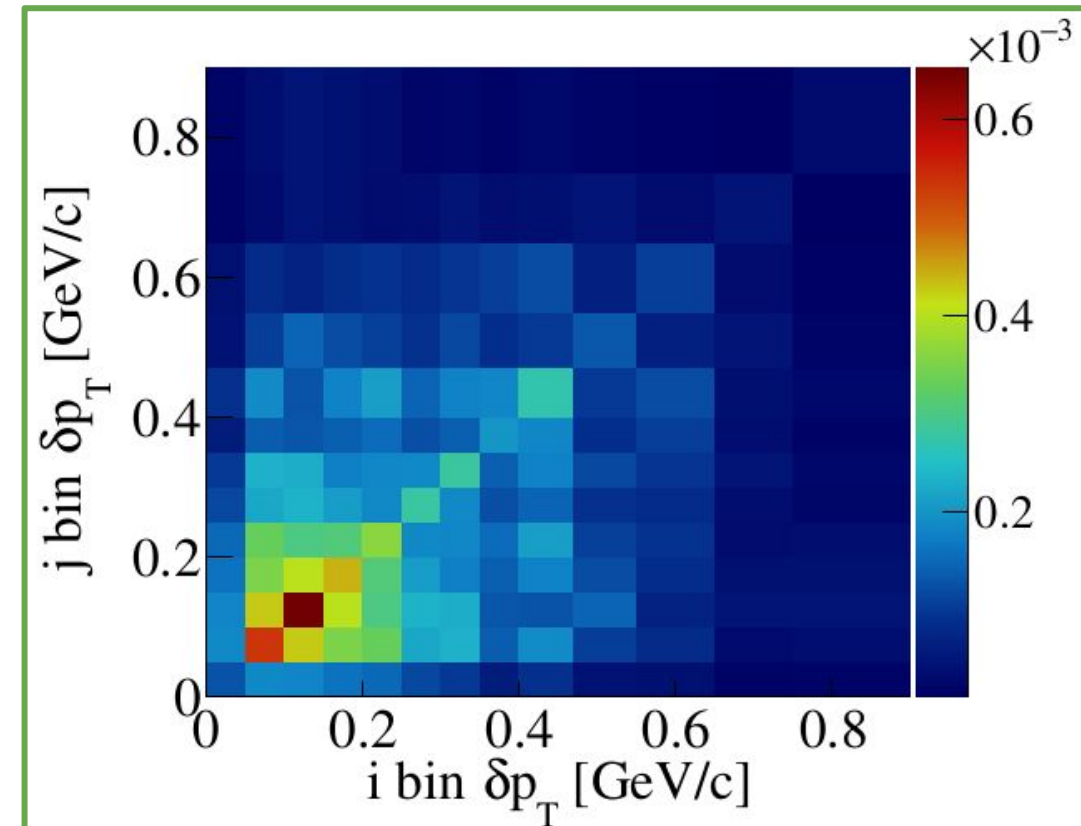
Cross Section Extraction with Wiener SVD Unfolding

[JINST 12 P10002 \(2017\)](#)

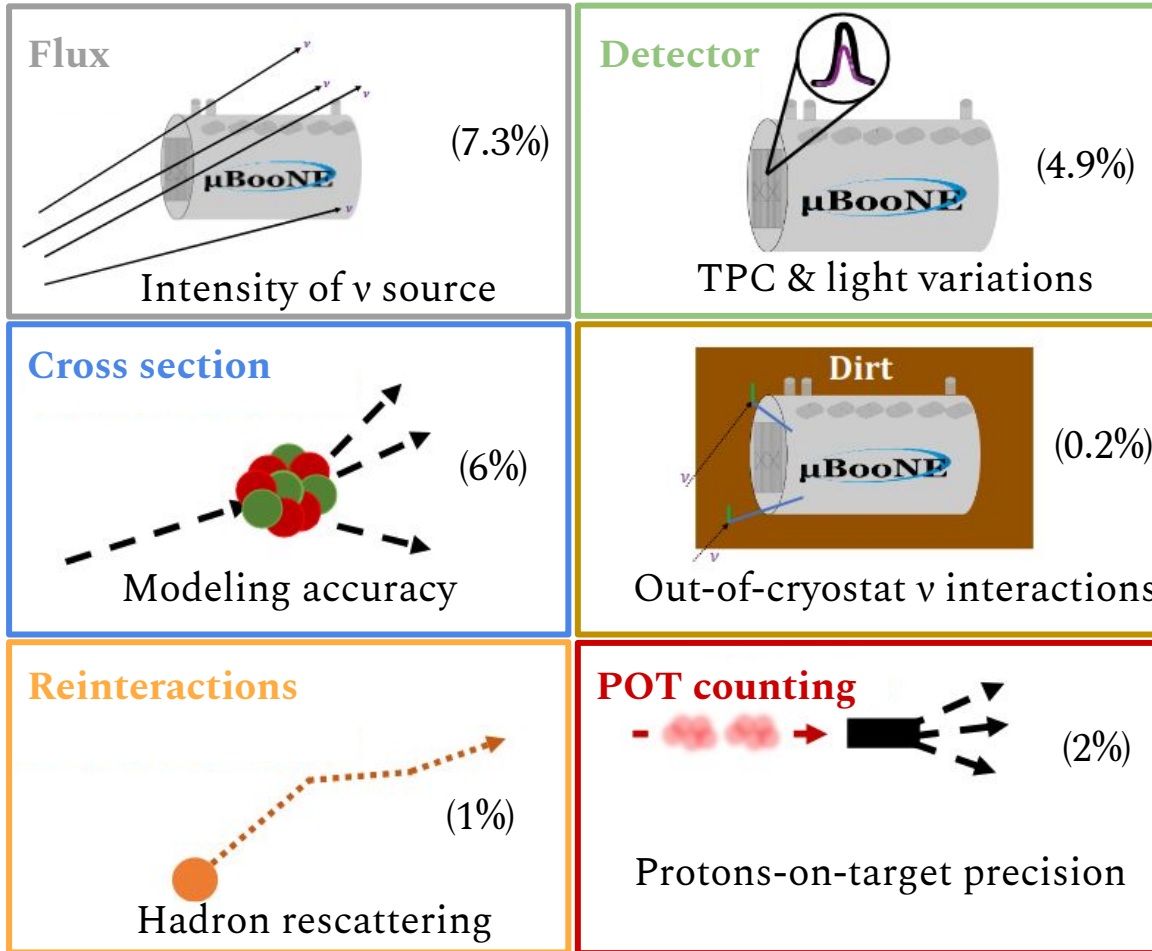
Input Quantities

- Measurement (Data)
- Background (MC)
- Response Matrix (MC)
- Total Covariance Matrix (MC)

Includes information on statistical
and systematic uncertainties



Uncertainties



- + Statistical (1.5%)
- + Number of argon targets (1%)

Total (11%)

Systematics-dominated analysis

Cross Section Extraction with Wiener SVD Unfolding

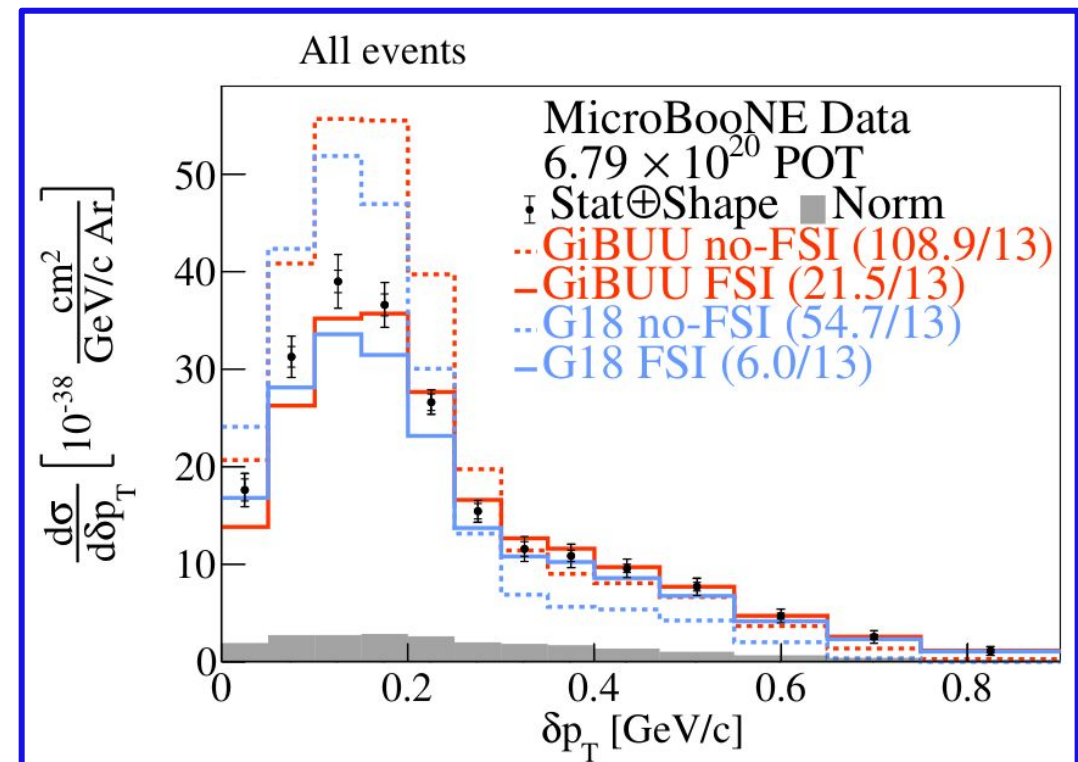
JINST 12 P10002 (2017)

Output quantities in
regularized space

- Unfolded data spectrum

- Smearing Matrix A_C

*Applied on theory predictions
and included in data release



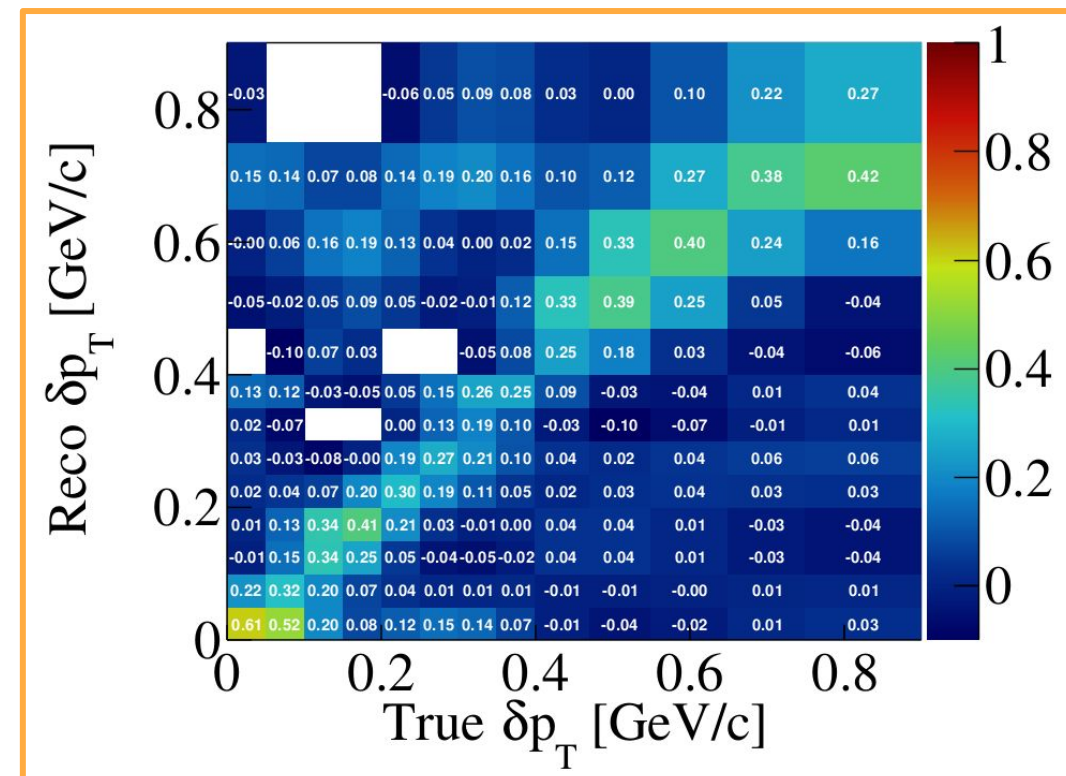
Cross Section Extraction with Wiener SVD Unfolding

JINST 12 P10002 (2017)

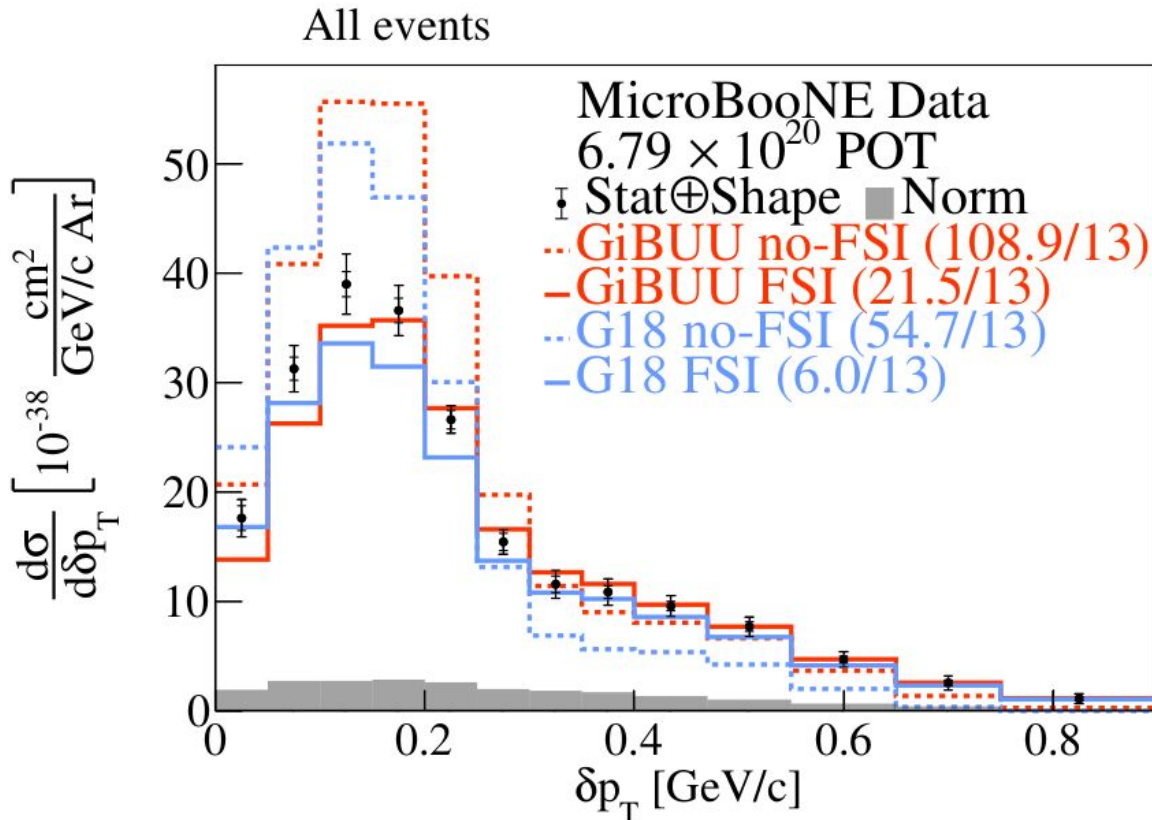
Output quantities in
regularized space

- Unfolded data spectrum
- Smearing Matrix A_C

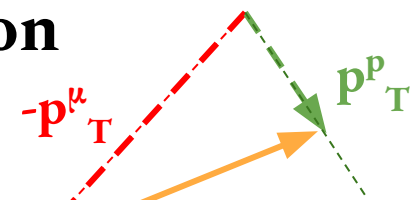
*Applied on theory predictions
and included in data release



Transverse Missing Momentum δp_T Cross Section



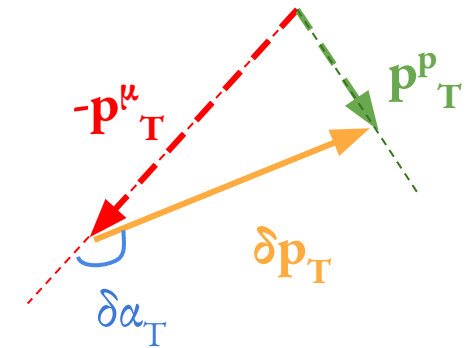
- First neutrino-argon differential cross section in δp_T
- FSI reduces strength of the peak
- Small changes in the tail
- Data favors FSI addition



G18 = GENIE v3.0.6 G18_10a_02_11b + tune*
 GiBUU = GiBUU 2021

High Statistics→Into the Multiverse!

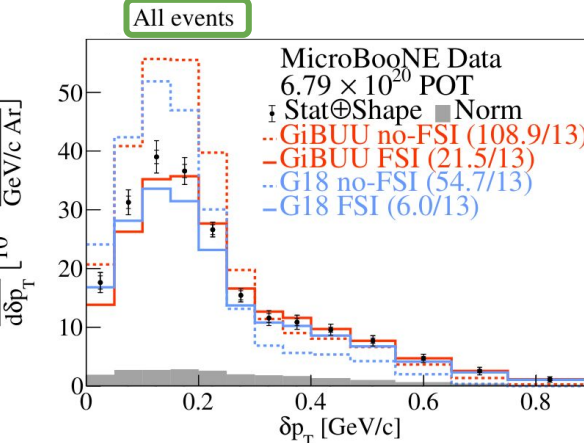
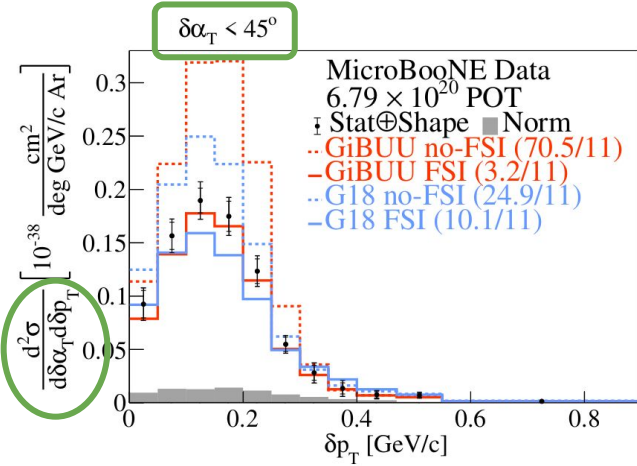
- Extension to 2D for the first time on argon
- Probe regions with greater model discrimination power



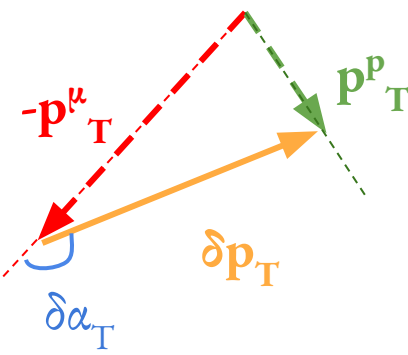
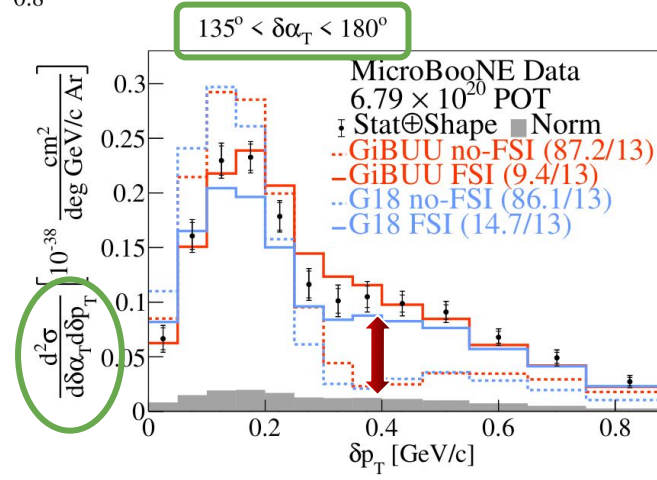
High Statistics → Into the Multiverse!

- Extension to 2D for the first time on argon
- Probe regions with greater model discrimination power

QE-dominated

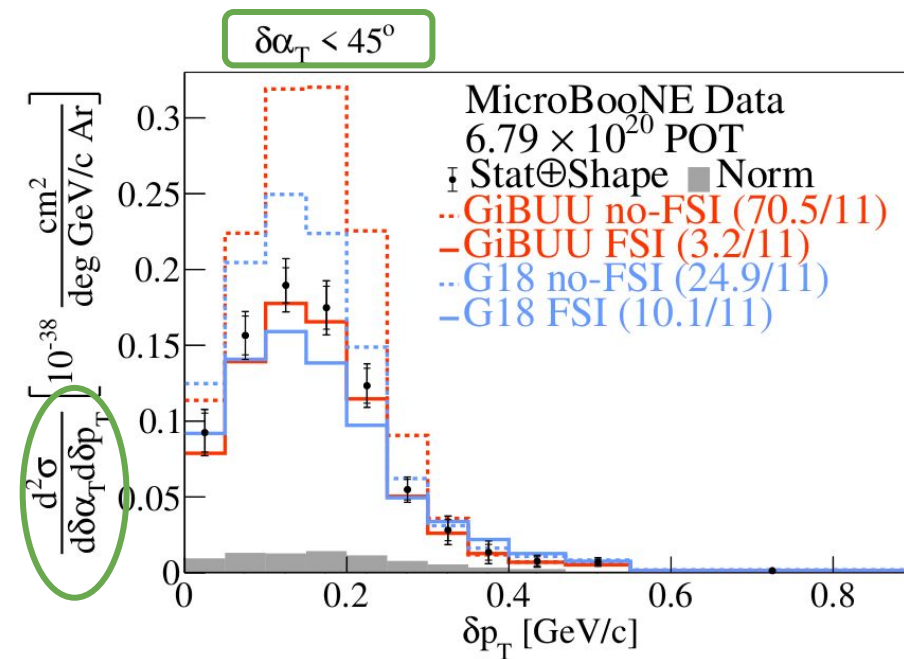
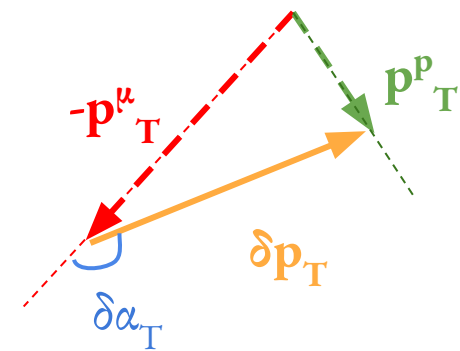


MEC/RES/FSI-dominated



High Statistics → Into the Multiverse!

QE-dominated region



- Addition of FSI reduces peak strength
- No high transverse missing momentum tail
- Ideal part of phase-space to study Fermi motion
- Results consistent with local Fermi gas distribution

[arXiv:2301.03706](https://arxiv.org/abs/2301.03706)

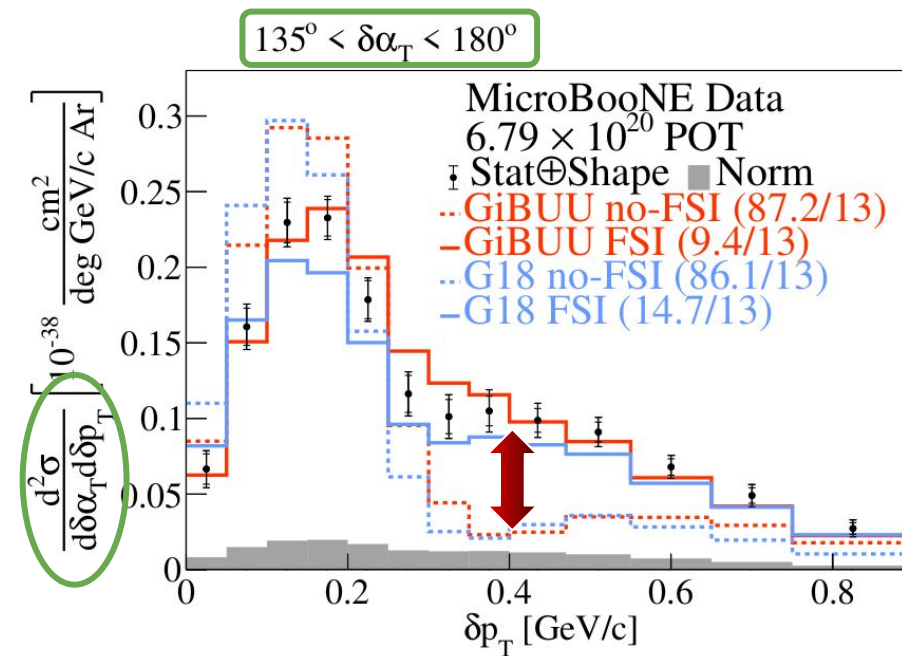
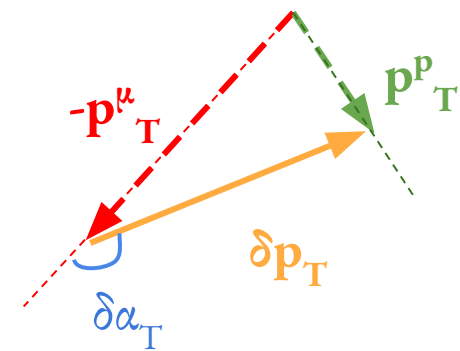
* Phys. Rev. D 105, 072001 (2022)

G18 = GENIE v3.0.6 G18_10a_02_11b + tune*

GiBUU = GiBUU 2021

High Statistics → Into the Multiverse!

MEC/RES/FSI-dominated



- FSI predictions in good agreement with data
- Minimal no-FSI contributions at high δp_T
- High δα_T & high δp_T part of phase-space ideal to test FSI / multinucleon effects

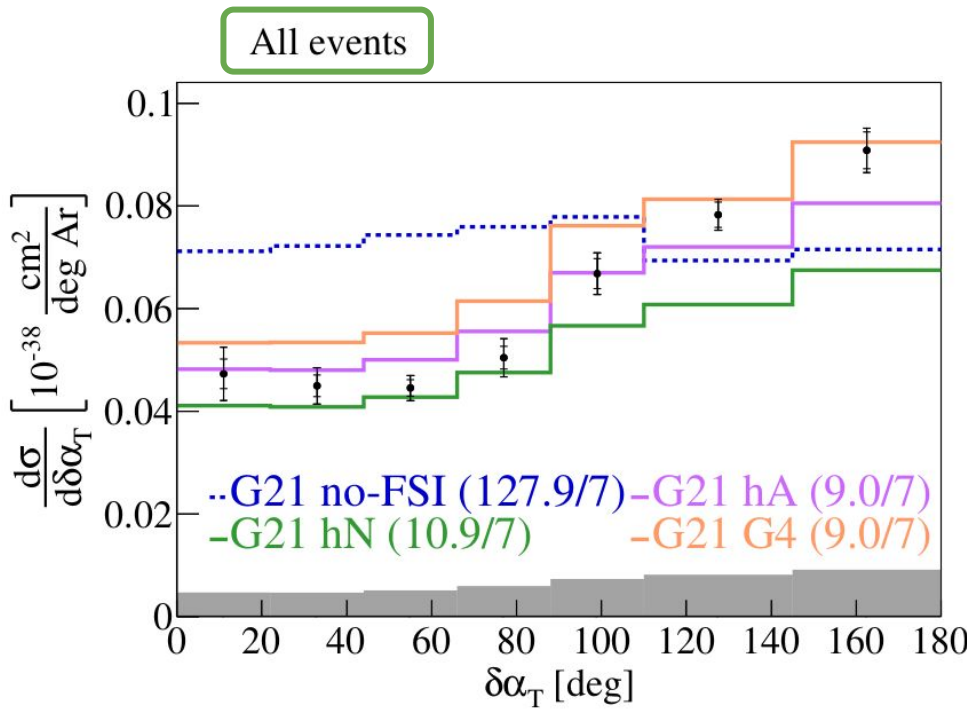
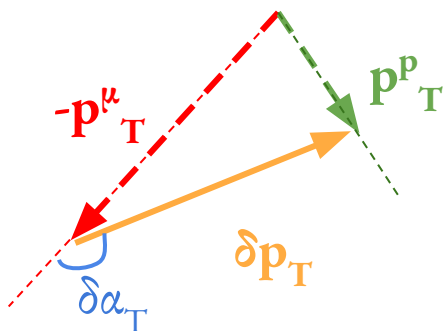
[arXiv:2301.03706](https://arxiv.org/abs/2301.03706)

* Phys. Rev. D 105, 072001 (2022)

G18 = GENIE v3.0.6 G18_10a_02_11b + tune*

GiBUU = GiBUU 2021

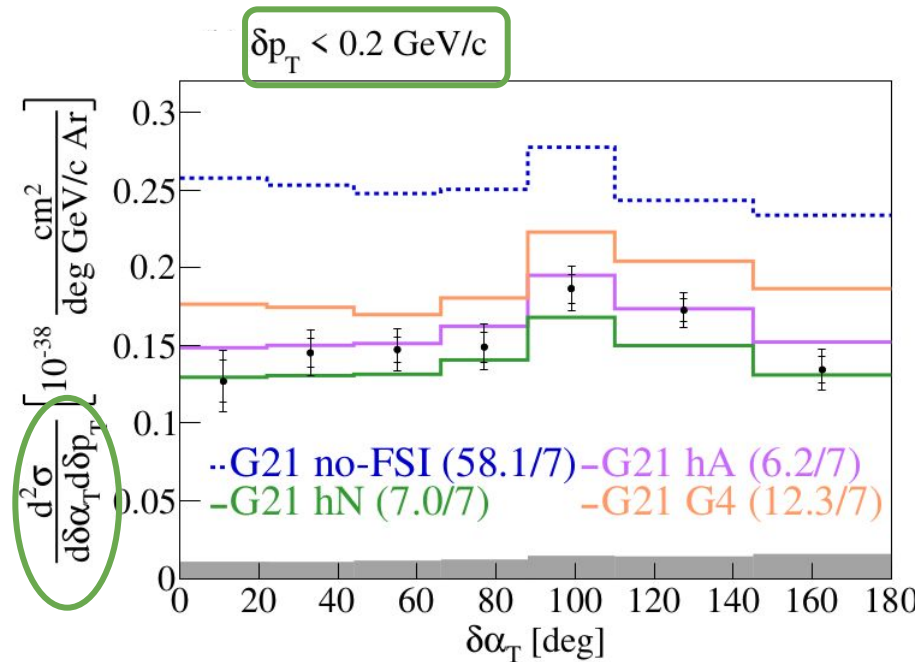
Transverse Orientation $\delta\alpha_T$ Cross Section



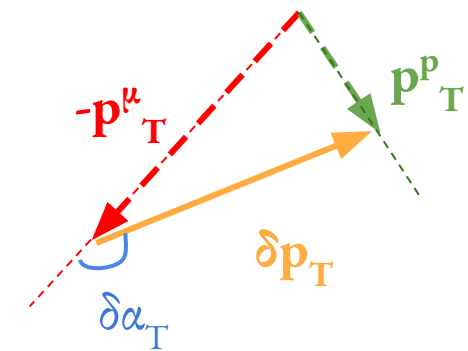
- First neutrino-argon differential cross section in $\delta\alpha_T$
- Sensitive to proton FSI modeling
- Data favors FSI addition
- Shape differences observed

High Statistics → Into the Multiverse!

QE-dominated region

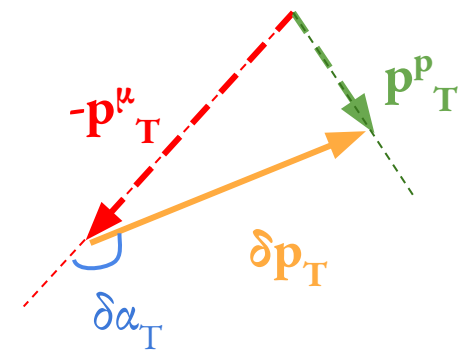
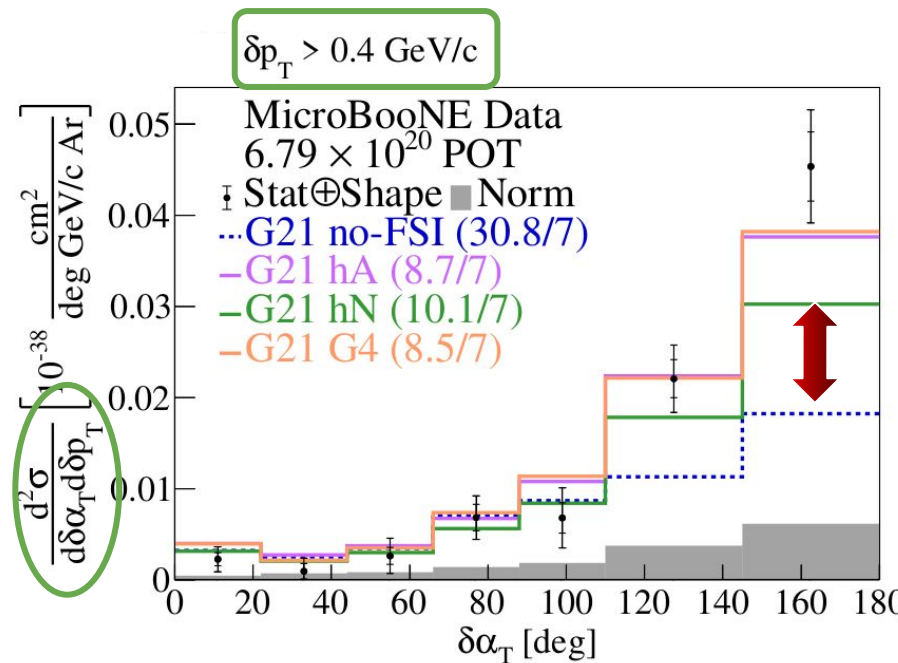


- Flat distribution indicative of absence of proton FSI
- Shape and normalization differences across FSI models



High Statistics → Into the Multiverse!

MEC/RES/FSI-dominated



- Primarily contributions from MEC/RES & QE events undergoing FSI
- More asymmetric behavior compared to 1D result
- No-FSI contribution lower than FSI ones
- High $\delta\alpha_T$ & high δp_T part of phase-space ideal to test FSI / multinucleon effect sensitivity

[arXiv:2301.03706](https://arxiv.org/abs/2301.03706)

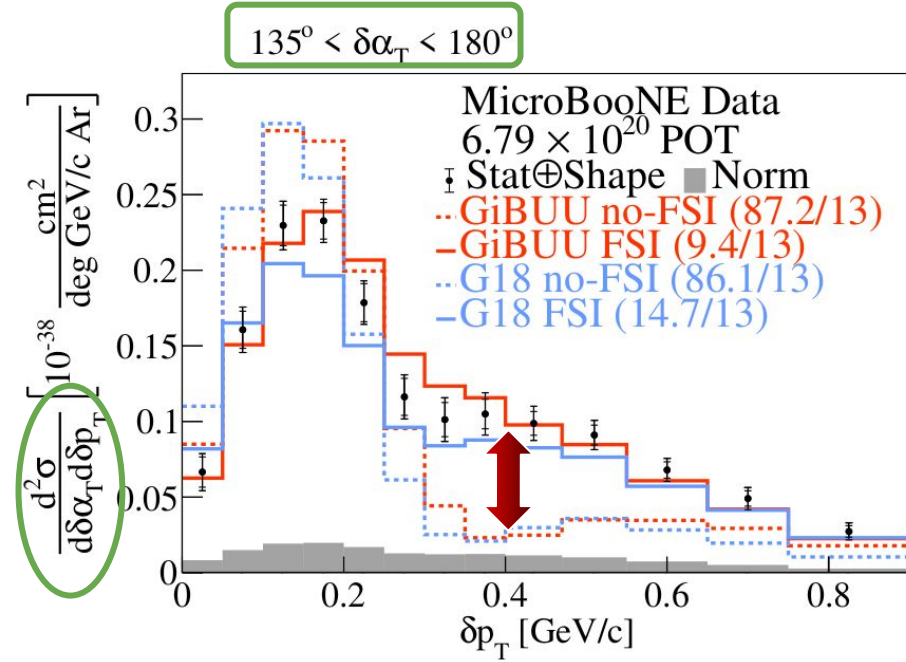
* [Phys. Rev. D 101, 033003 \(2020\)](https://doi.org/10.1103/PhysRevD.101.033003)

G21 = GENIE v3.0.6 G21_11b_00_000

SuSAv2 QE & MEC*, hA/hN/G4 = FSI modeling options

CC1p0 π TKI Summary

- First single- and double- differential neutrino-argon cross section measurements in TKI
- Fermi motion studied with 2D measurement in δp_T with $\delta\alpha_T < 45^\circ$
- FSI & multinucleon effects studied with 2D measurement in δp_T with $135^\circ < \delta\alpha_T < 180^\circ$
- Way more single- and double-differential results in [arXiv:2301.03700](https://arxiv.org/abs/2301.03700) and [arXiv:2301.03706](https://arxiv.org/abs/2301.03706)!



Wealth Of Cross Section Results To Follow!



CC inclusive

- ν_μ CC inclusive @ NuMI
- ν_e/ν_μ ratios @ BNB, NuMI
- 3D E_ν , E_μ , hadronic energy @ NuMI & BNB
- anti- ν_e @ NuMI

CC0π

- 2D ν_μ CC1p0π Generalized Kinematic Imbalance @ BNB
- ν_μ CC0π inclusive @ BNB
- 2D ν_μ CCNp0π @ BNB
- 1D ν_e CC0πNp @ NuMI
- 1D ν_μ NC1p0π @ BNB

Pion production

- ν_μ CC1π⁺ @ BNB, NuMI
- ν_μ CCNπ @ NuMI
- 1D ν_μ CCπ⁰ @ BNB
- 2D ν_μ CC/NC π⁰ @ BNB
- 2D $\nu_{e,\mu}$ NCπ⁰ @ BNB

Rare & novel channels

- ν_μ CC Kaon @ BNB, NuMI
- MeV-scale Physics in MicroBooNE
- Neutrons @ BNB



Thank you!

Backup Slides

3.6.3 Effect of Variation in Uncertainty

Figure 3.23 shows DUNE sensitivity to determination of neutrino mass hierarchy and discovery of CP violation as a function of exposure for several levels of signal normalization uncertainty. As seen in Figure 3.23, for early phases of DUNE with exposures less than $100 \text{ kt} \cdot \text{MW} \cdot \text{year}$, the experiment will be statistically limited. The impact of systematic uncertainty on the CP-violation sensitivity for large exposure is obvious in Figure 3.23; the ν_e signal normalization uncertainty must be understood at the level of $5\% \oplus 2\%$ in order to reach 5σ sensitivity for 75% of δ_{CP} values with exposures less than $\sim 900 \text{ kt} \cdot \text{MW} \cdot \text{year}$ in the case of the Optimized Design. Specifically, the absolute normalization of the ν_μ sample must be known to $\sim 5\%$ and the normalization of the ν_e sample, relative to the $\bar{\nu}_e$, ν_μ , and $\bar{\nu}_\mu$ samples after all constraints from external, near detector, and far detector data have been applied, must be determined at the few-percent level. This level of systematic uncertainty sets the capability and design requirements for all components of the experiment, including the beam design and the near and far detectors.

Volume 2: The Physics Program for DUNE at LBNF

LBNF/DUNE Conceptual Design Report

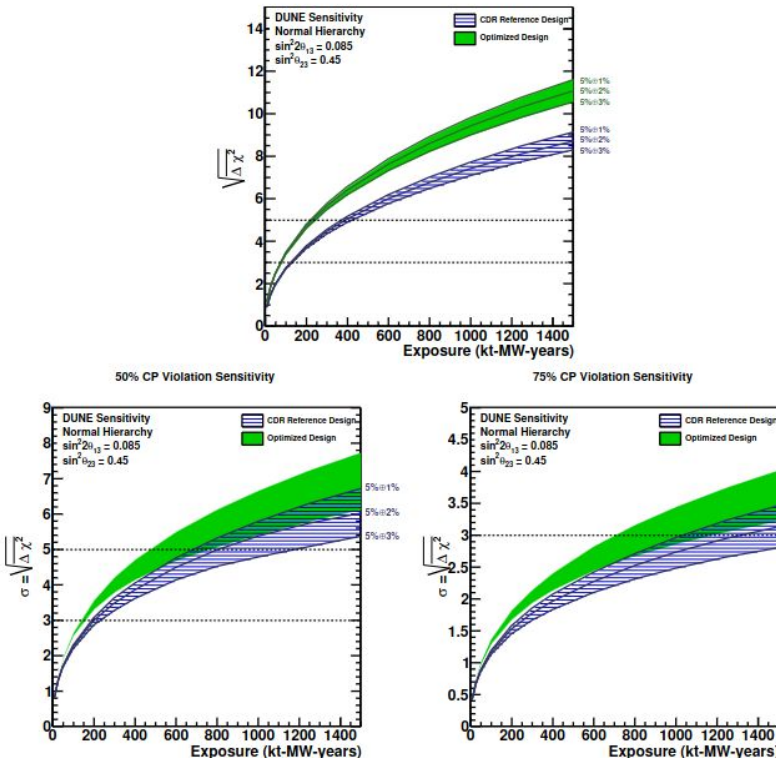
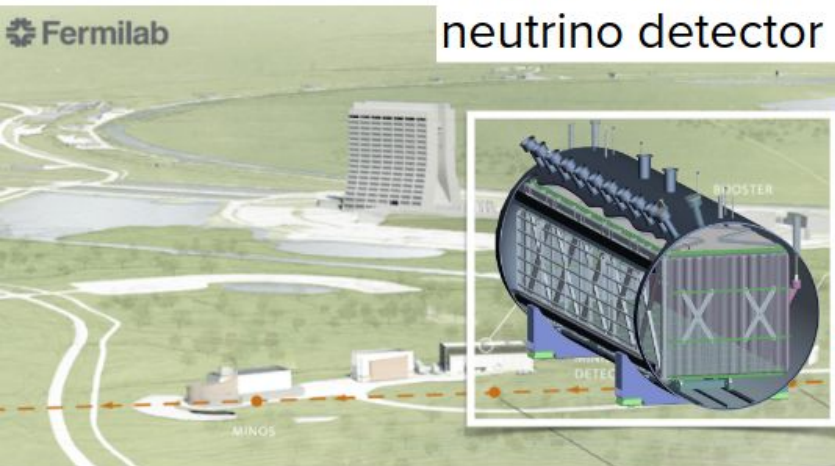
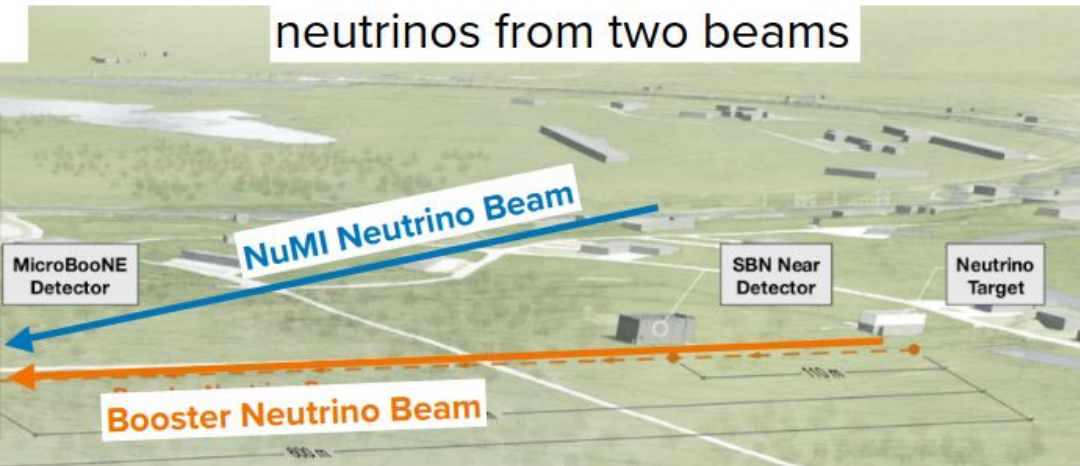


Figure 3.23: Expected sensitivity of DUNE to determination of the neutrino mass hierarchy (top) and discovery of CP violation, i.e., $\delta_{CP} \neq 0$ or π , (bottom) as a function of exposure in $\text{kt} \cdot \text{MW} \cdot \text{year}$, assuming equal running in neutrino and antineutrino mode, for a range of values for the ν_e and $\bar{\nu}_e$ signal normalization uncertainties from $5\% \oplus 3\%$ to $5\% \oplus 1\%$. The sensitivities quoted are the minimum sensitivity for 100% of δ_{CP} values in the case of mass hierarchy and 50% (bottom left) or 75% (bottom right) of δ_{CP} values in the case of CP violation. The two bands on each plot represent a range of potential beam designs: the blue hashed band is for the CDR Reference Design and the solid green band is for the Optimized Design. Sensitivities are for true normal hierarchy; neutrino mass hierarchy and θ_{23} octant are assumed to be unknown.

A short baseline neutrino detector



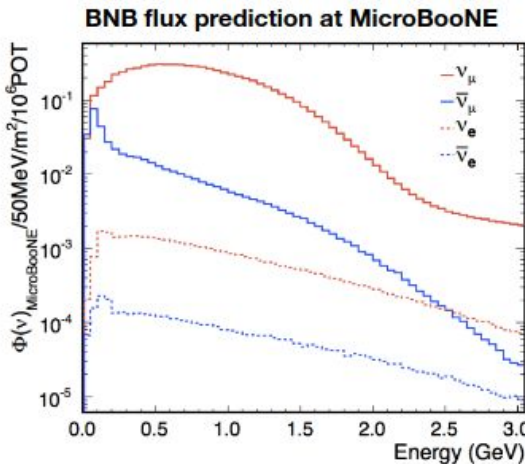
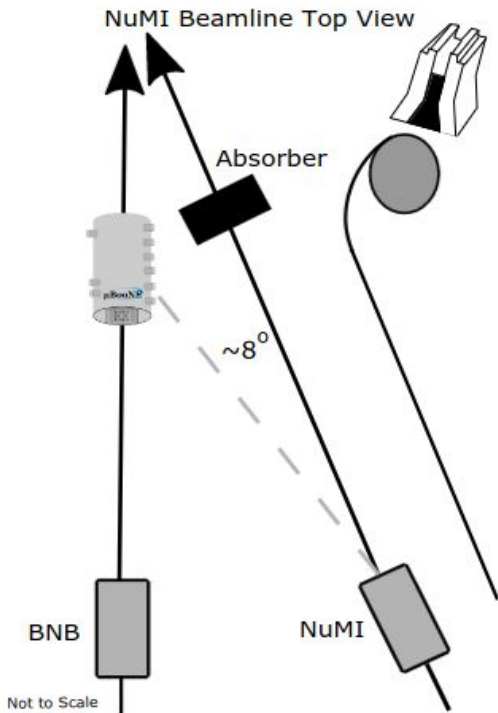
Studying accelerator neutrinos from two beams



MicroBooNE's physics program

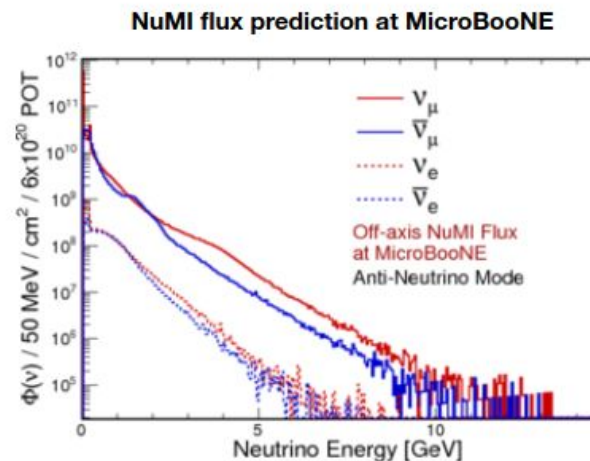
Non-standard neutrino oscillations	Cross-section measurements	Detector physics, R&D
---------------------------------------	-------------------------------	--------------------------

Beyond Standard Model physics!

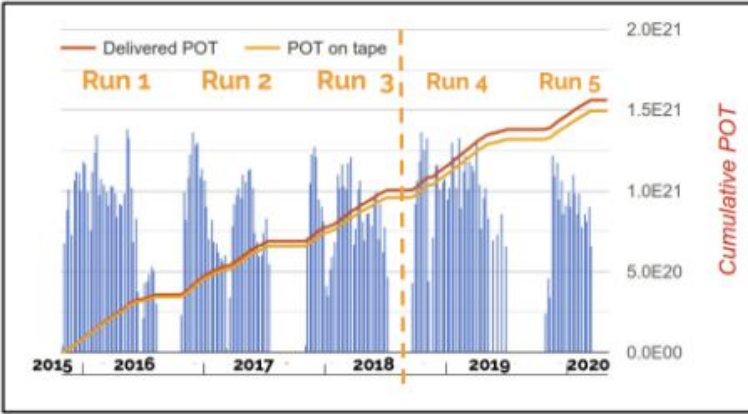


- 8 GeV protons
- ~ 470 m from MicroBooNE
- On-axis

- 120 GeV protons
- ~ 680 m from MicroBooNE
- $\sim 8^\circ$ off-axis from MicroBooNE



- MicroBooNE collected BNB and NuMI data between 2015 and 2020
- ~50% of the dataset (Runs 1-3) used in first wave of results



First results

POT: Protons on Target

From raw hits to
particle reconstruction

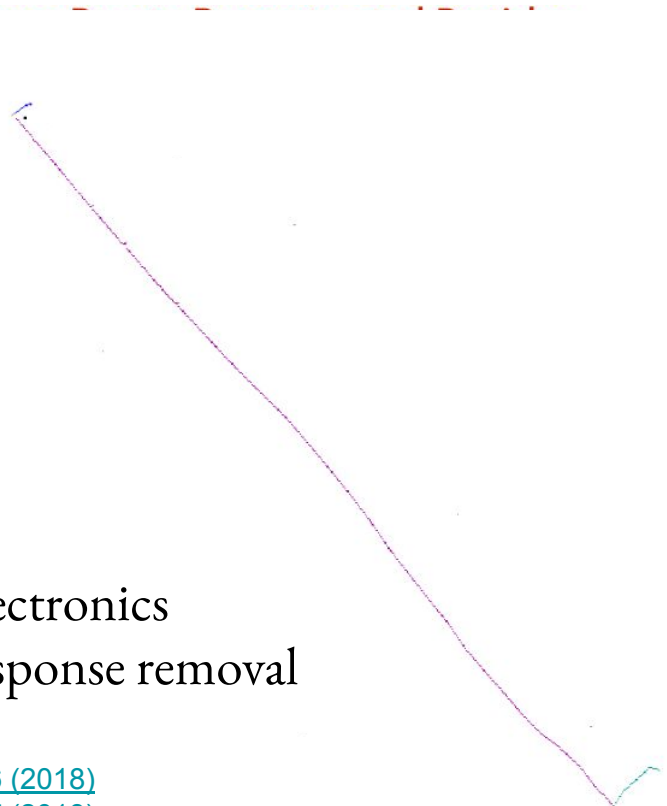
Pandora Pattern Recognition

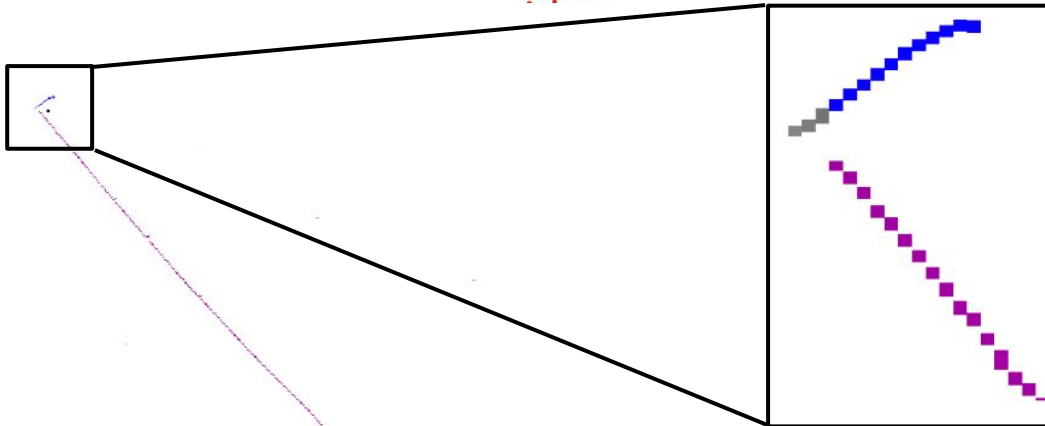
• Eur. Phys. J. C78, 1, 82 (2018)

Readout electronics
and field response removal

[JINST 13, P07006 \(2018\)](#)

[JINST 13, P07007 \(2018\)](#)



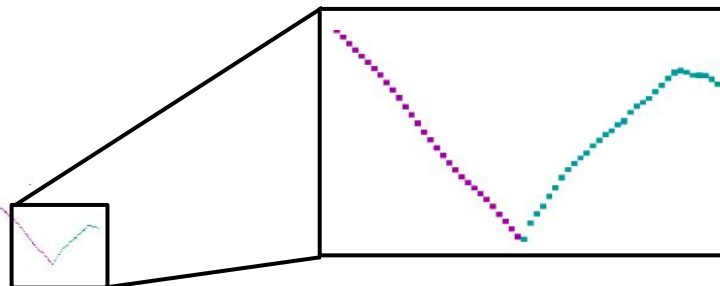


From raw hits to
particle reconstruction

Pandora Pattern Recognition

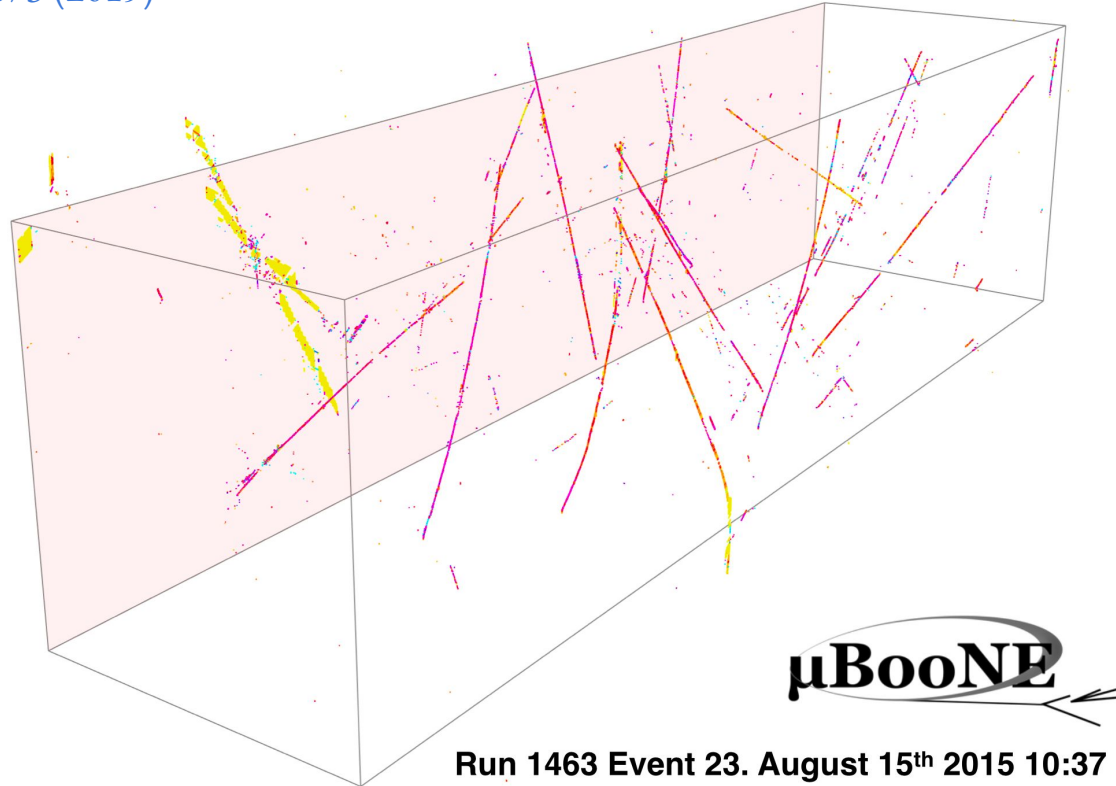
Eur. Phys. J. C78, 1, 82 (2018)

Readout electronics
and field response removal



[JINST 13, P07006 \(2018\)](#)
[JINST 13, P07007 \(2018\)](#)

Eur. Phys. J. C 79 673 (2019)



Readout window of 2.3 ms

- ~20 cosmic interactions
- ~0.0017 ν interactions

Significant reduction using optical information
to 1 ν interaction in ~10 events

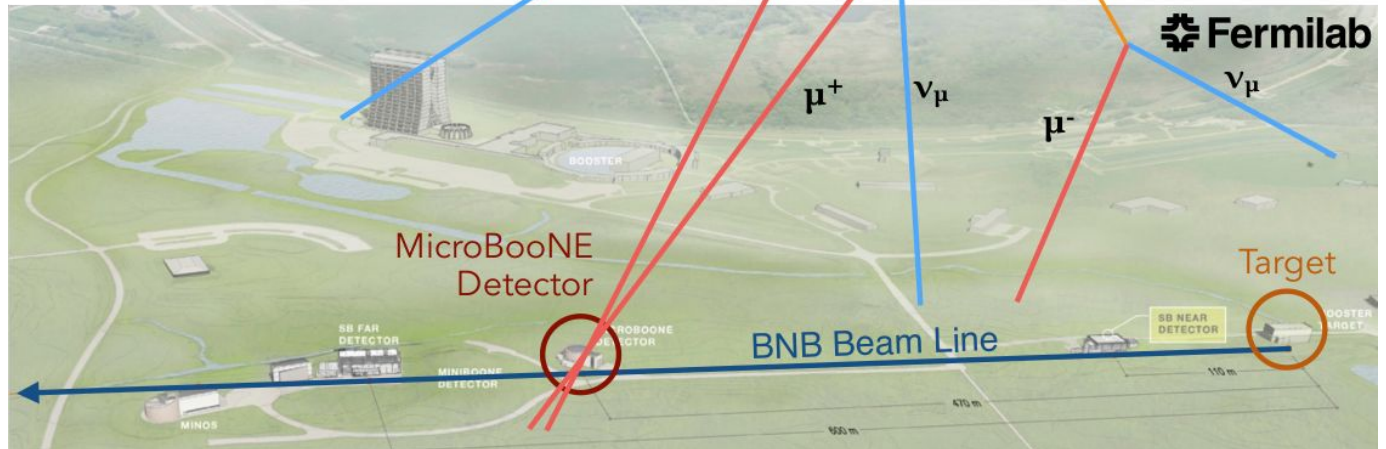
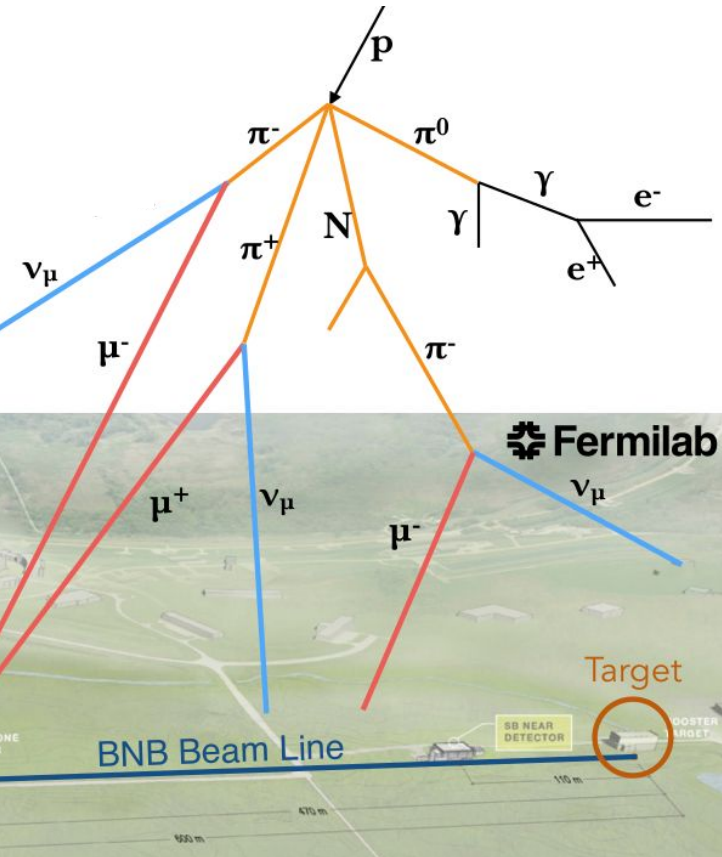


TABLE IV. Tuned parameter values and uncertainties after fitting to T2K CC0 π data for the nominal simulation and three tunes that build to the final four parameter tune. Note that postfit χ^2 values are quoted here only for the 58 bins included in the fit (excluding the highest muon momentum bin in each $\cos \theta$ bin), and using diagonal elements of the covariance matrix only. In the text and figures, pre- and postfit χ^2 comparisons are also quoted for the full T2K dataset of 67 bins. “Norm.” is an abbreviation for normalization.

	MaCCQE fitted value	CC2p2h Norm. fitted value	CCQE RPA Strength fitted value	CC2p2h Shape fitted value	T2K $\chi^2_{\text{diag}}/\text{N}_{\text{bins}}$
Nominal (untuned)	0.961242 GeV	1	100%	0	106.7/58
Fit MaCCQE + CC2p2h Norm.	1.14 ± 0.07 GeV	1.61 ± 0.19	100% (fixed)	0 (fixed)	71.8/58
Fit MaCCQE + CC2p2h Norm + CCQE RPA Strength	1.18 ± 0.08 GeV	1.12 ± 0.38	$(64 \pm 23)\%$	0 (fixed)	69.7/58
Fit MaCCQE + CC2p2h Norm + CCQE RPA Strength + CC2p2h Shape	1.10 ± 0.07 GeV	1.66 ± 0.19	$(85 \pm 20)\%$	$1^{+0}_{-0.74}$	52.5/58

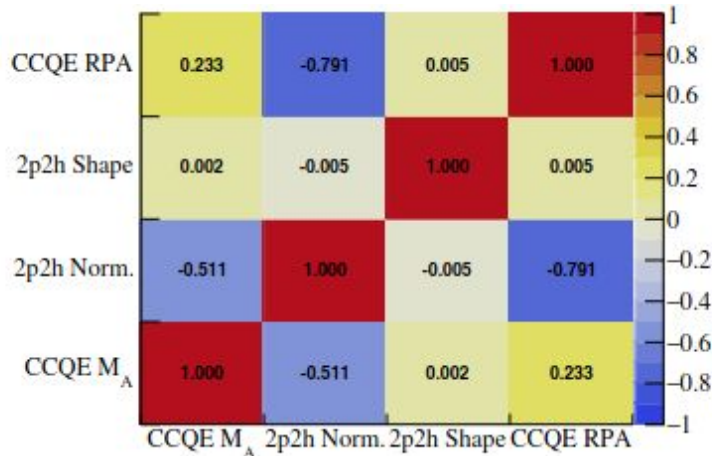
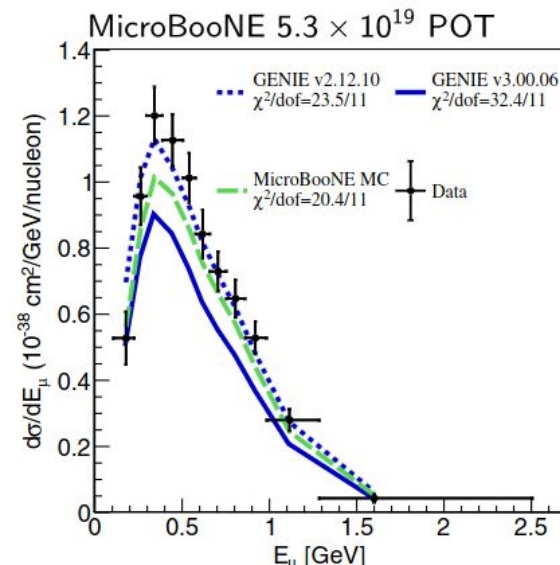


FIG. 7. Correlations between parameters after fitting to T2K CC0 π data.



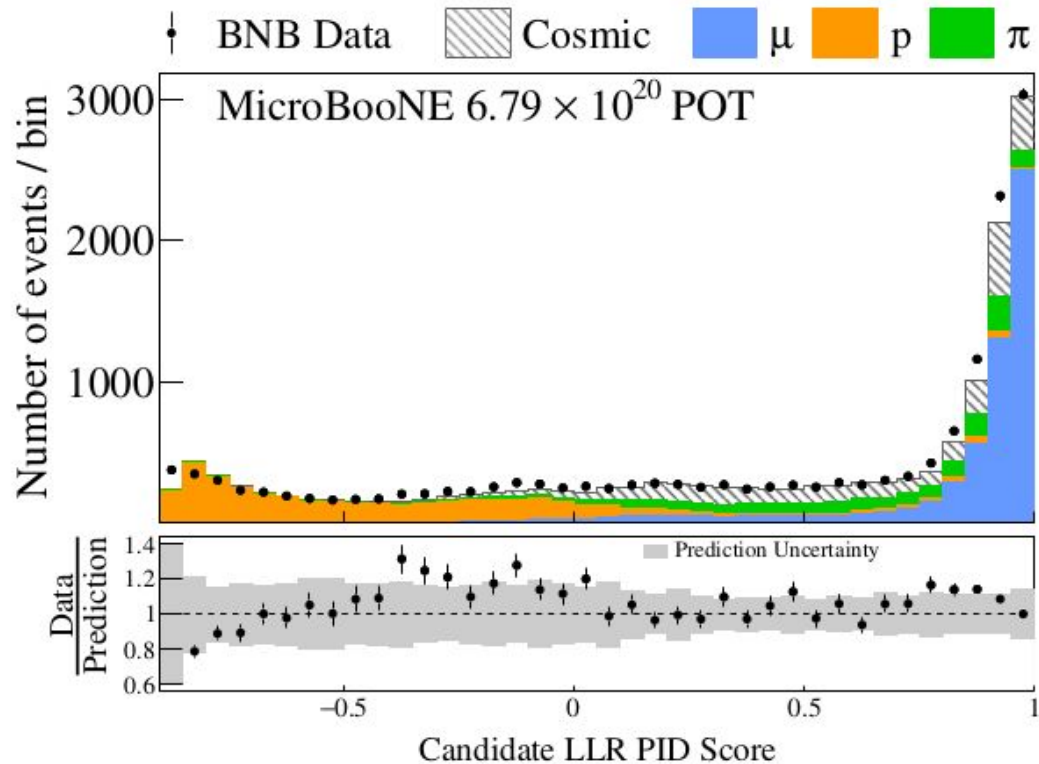


FIG. 1. The log-likelihood ratio (LLR) particle identification (PID) score distribution used to tag the muon and proton candidates.

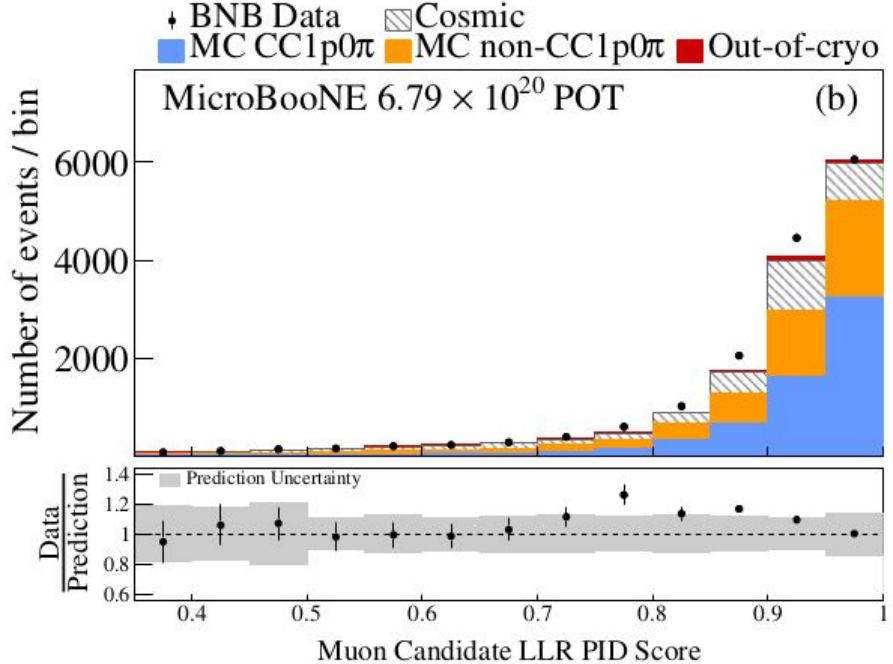
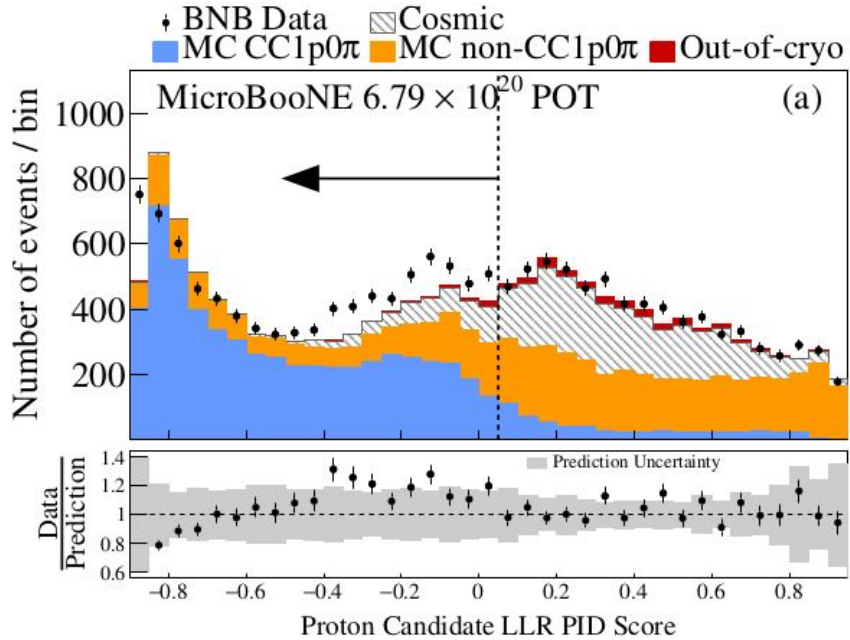


FIG. 2. (Top) the proton candidate LLR PID score distribution, illustrating the fitness of a cut at $\text{LLR PID} < 0.05$ to reject cosmic and non-CC1p0 π background events. (Bottom) the muon candidate LLR PID score distribution, illustrating a peak close to one. Only statistical uncertainties are shown on the data. The bottom panel shows the ratio of data to prediction.

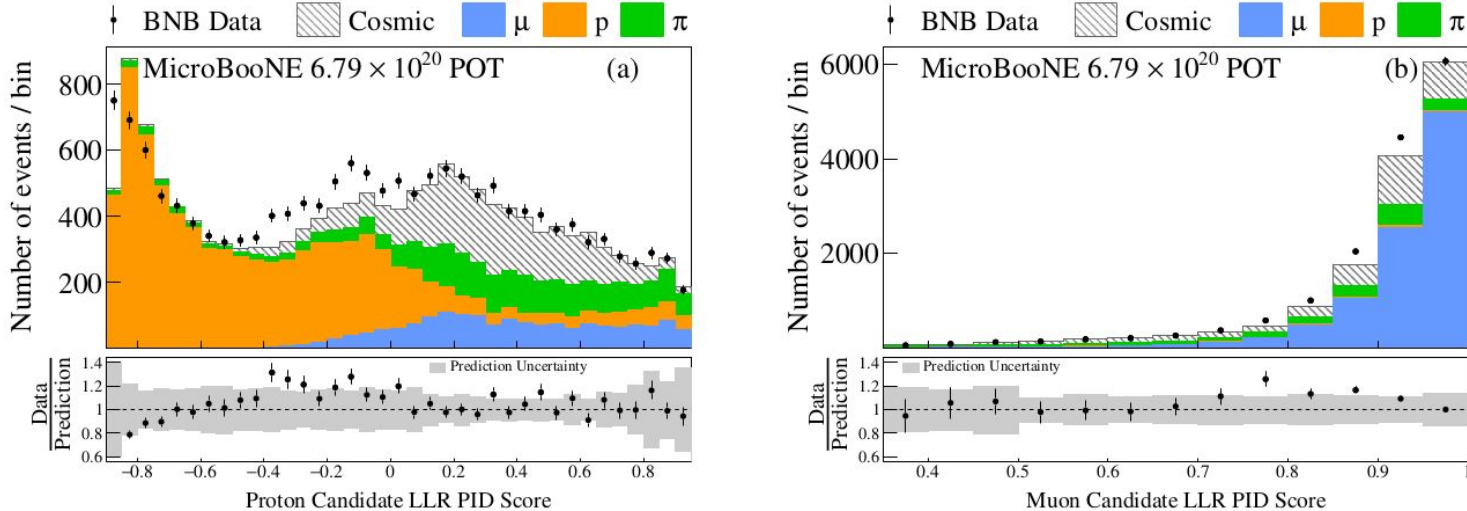


FIG. 1. (Left) the proton candidate LLR PID score distribution, illustrating the particle composition of the variable. (Right) the muon candidate LLR PID score distribution, illustrating a peak close to one. Only statistical uncertainties are shown on the data. The bottom panel shows the ratio of data to prediction.

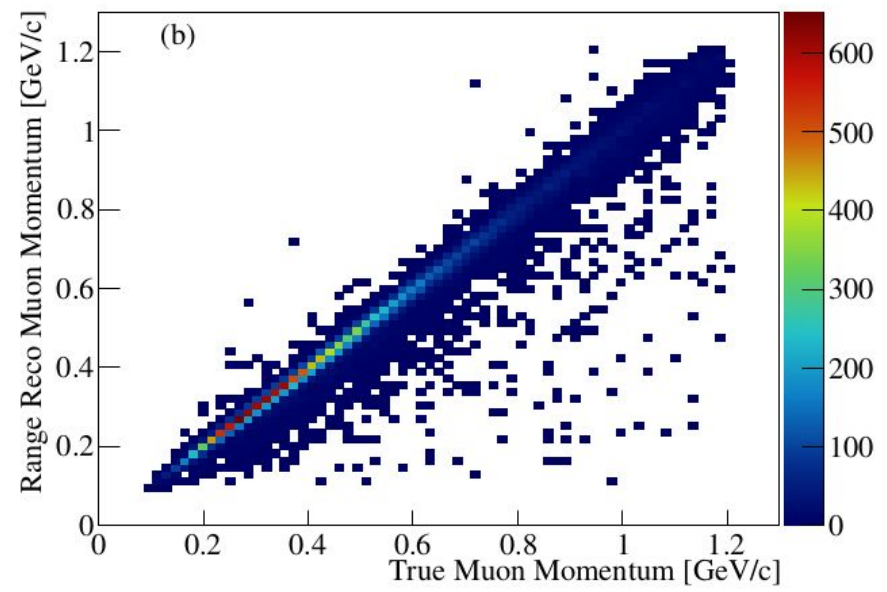
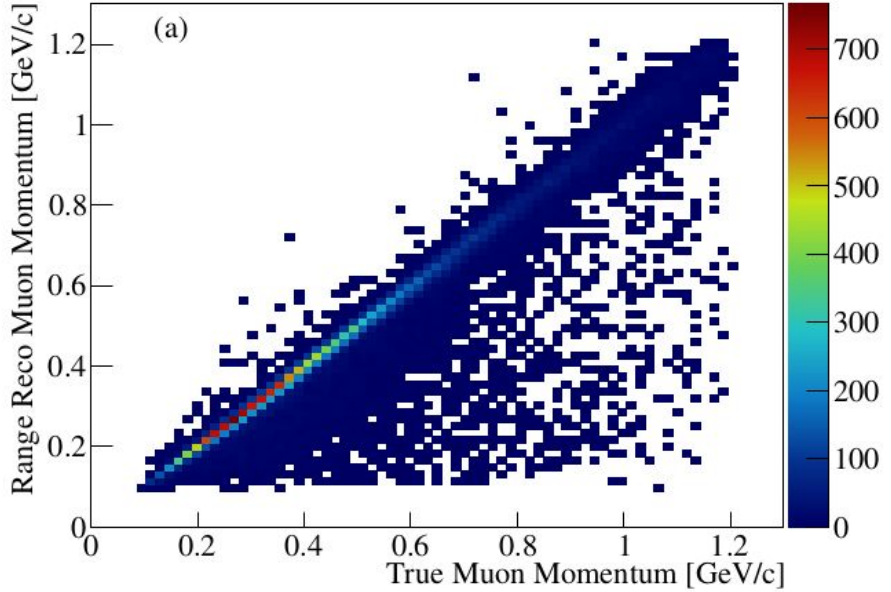
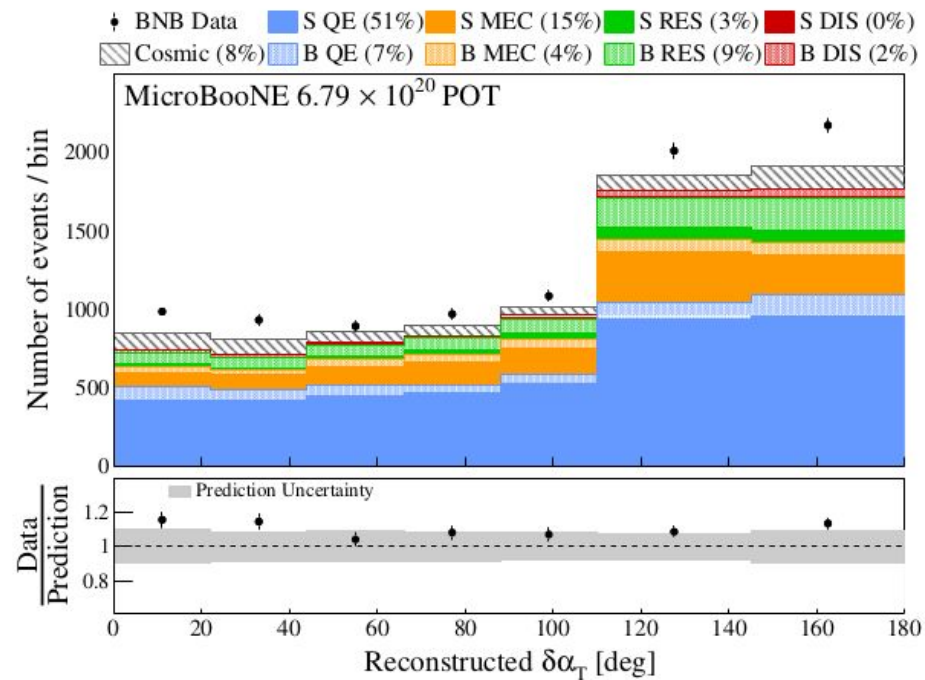
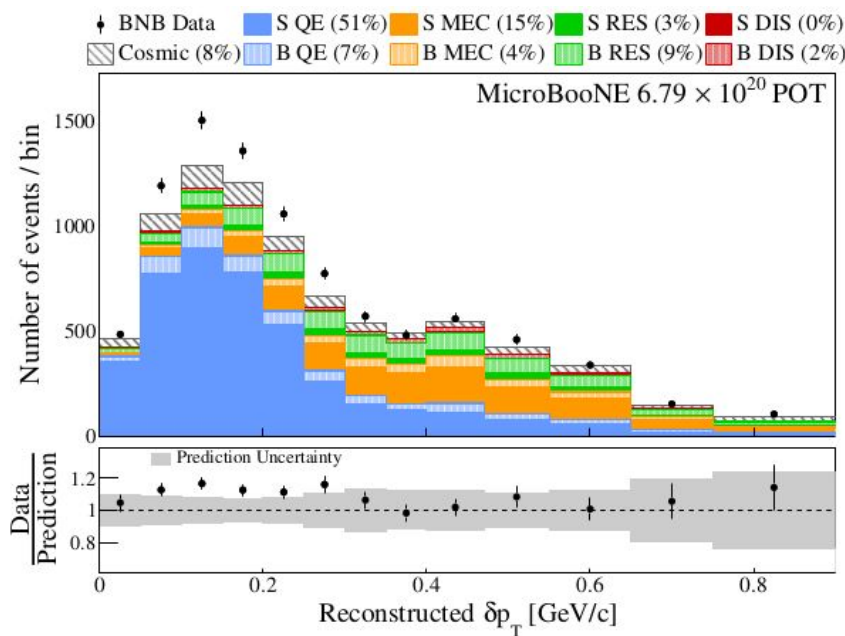
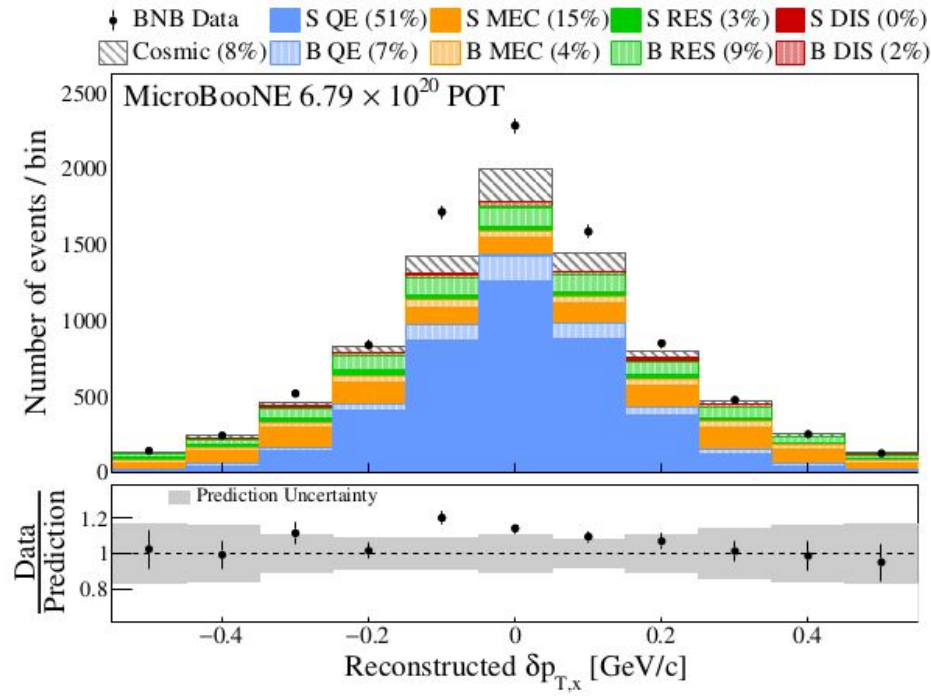
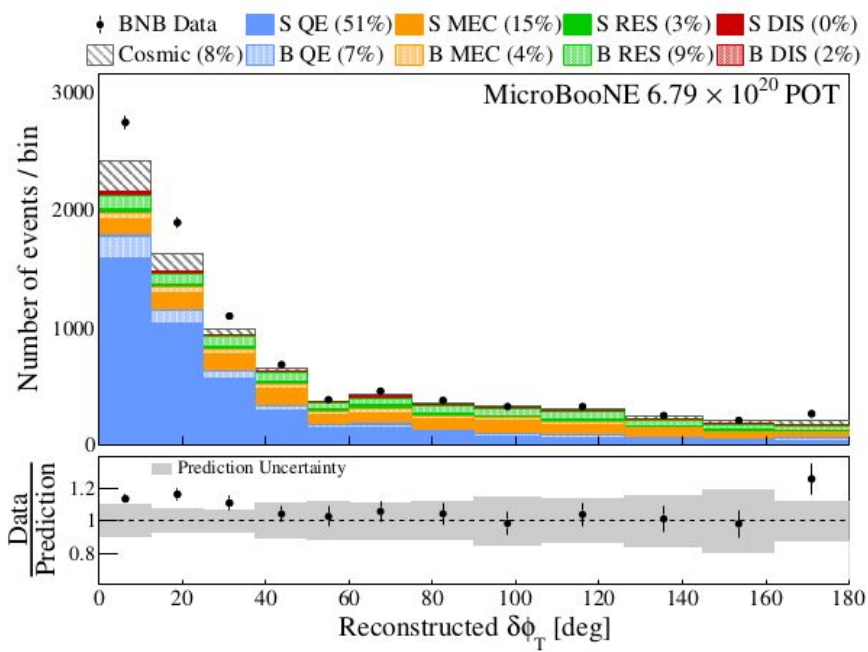
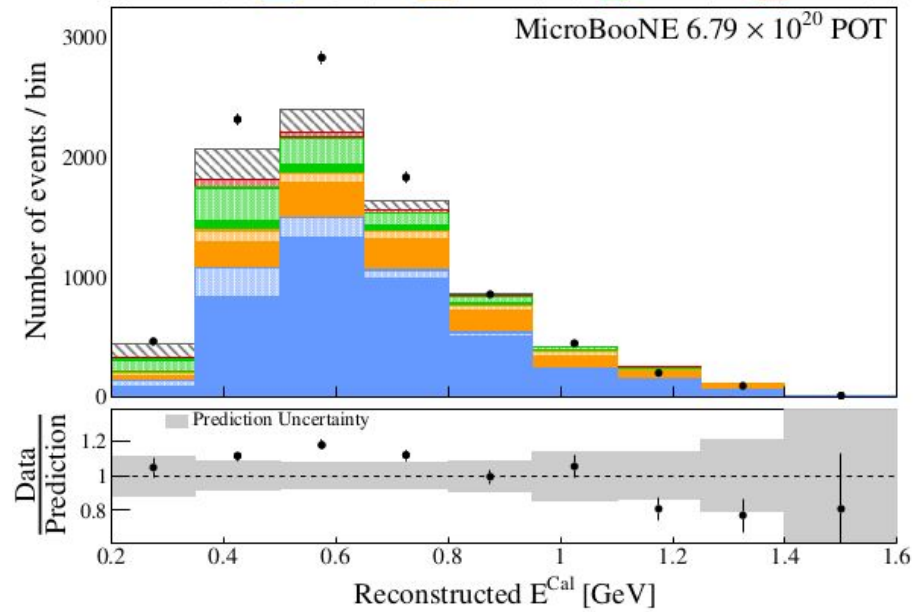
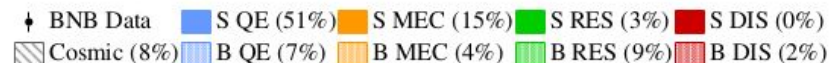
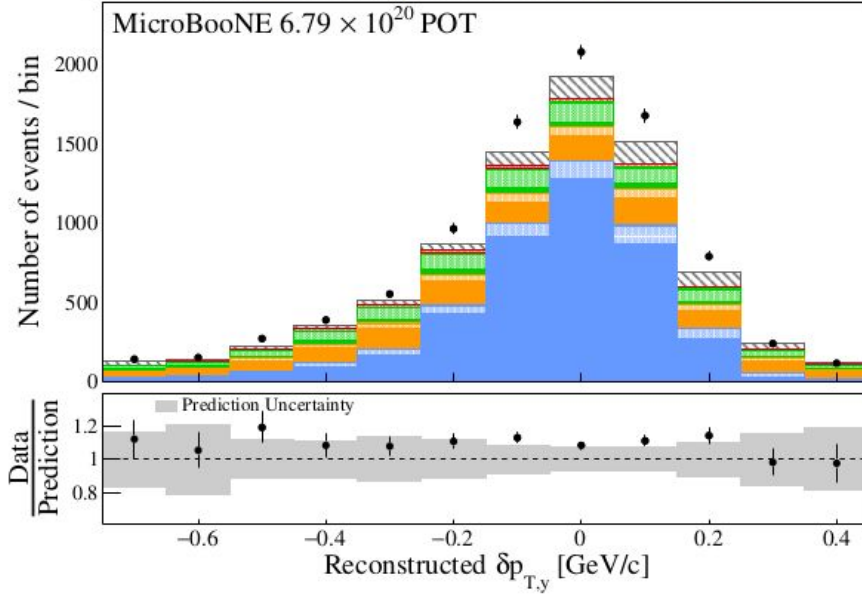
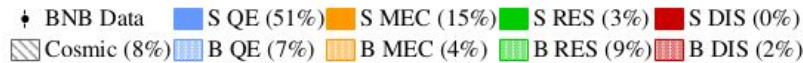


FIG. 3. Muon momentum reconstruction (top) before and (bottom) after the application of the muon momentum quality cut using contained muon tracks.







Unfolding problem

- In practice, the data unfolding problem starts with

$$\chi^2(s) = (\mathbf{m} - \mathbf{r} \cdot s)^T \text{Cov}^{-1}(\mathbf{m} - \mathbf{r} \cdot s)$$

- \mathbf{m} : measured spectrum, m -dimensional vector
- \mathbf{s} : unknown spectrum, to be unfolded, n -dimensional vector
- \mathbf{r} : smearing (response) matrix, $m \times n$ and $m \geq n$
- Cov : covariance matrix containing all statistical and systematic uncertainties associated with \mathbf{m} and \mathbf{r} .

- Cholesky decomposition: $\text{Cov}^{-1} = Q^T Q$, Q is a lower triangular matrix

$$\chi^2(s) = (M - R \cdot s)^T \cdot (M - R \cdot s)$$

Pre-scaling

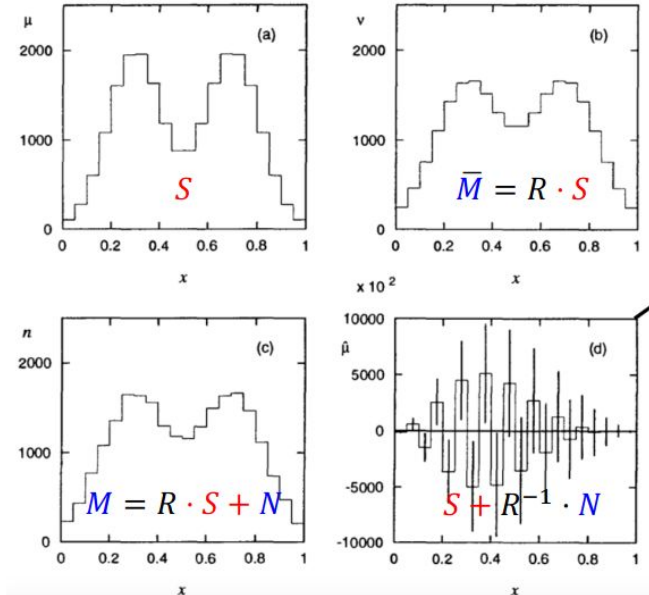
- $M := Q \cdot \mathbf{m}$
- $R := Q \cdot \mathbf{r}$

Solution (direct inversion)

$$\begin{aligned}\hat{s} &= (R^T R)^{-1} R^T M \\ \hat{s} &= (R^T R)^{-1} R^T (R \cdot s_{true} + N)\end{aligned}$$

The response matrix R is unnecessary to be a square matrix

Unfolding problem



This is one unbiased solution (direct inversion) to an unfolding problem. However, it has catastrophic oscillations, i.e. huge variance, in the unfolded spectrum.

- Decrease the number of bins to suppress the “oscillation” --> Nyquist theorem
- Trade-off **bias** and **variance** to suppress the “oscillation” --> e.g. **regularization [unfolding method]**

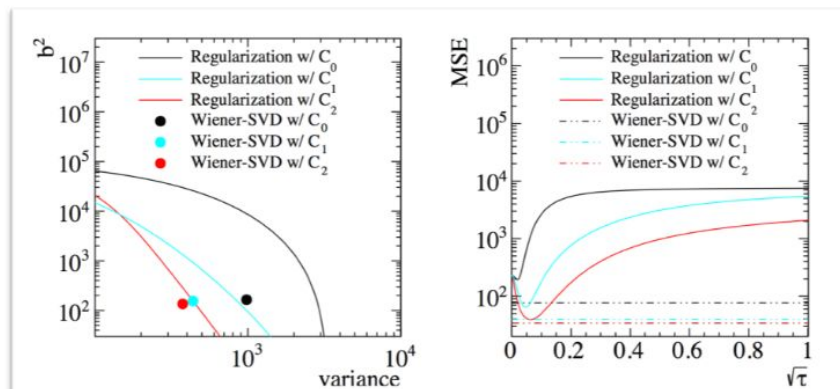
Wiener-SVD unfolding

- To automatically minimize the Mean Square Error (MSE) given a model S

$$\begin{aligned} MSE &= E \left[(\hat{S} - S)^2 \right] = E \left[\left(F \cdot \frac{M}{R} - S \right)^2 \right] = E \left[\left(F \cdot S + F \cdot \frac{N}{R} - S \right)^2 \right] \\ &= E \left[((\mathbf{F} - \mathbf{I}) \cdot \mathbf{S})^2 + \left(\mathbf{F} \cdot \frac{\mathbf{N}}{R} \right)^2 \right] \end{aligned}$$

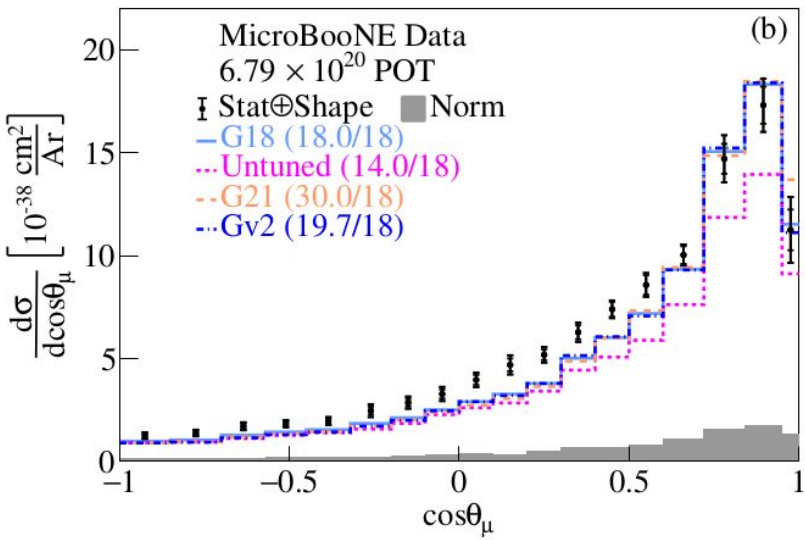
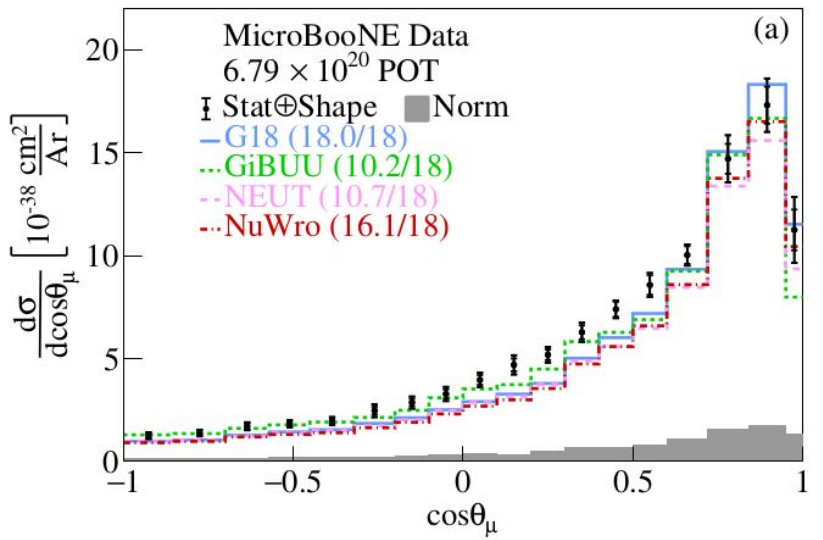
↑ Bias ↑ Variance

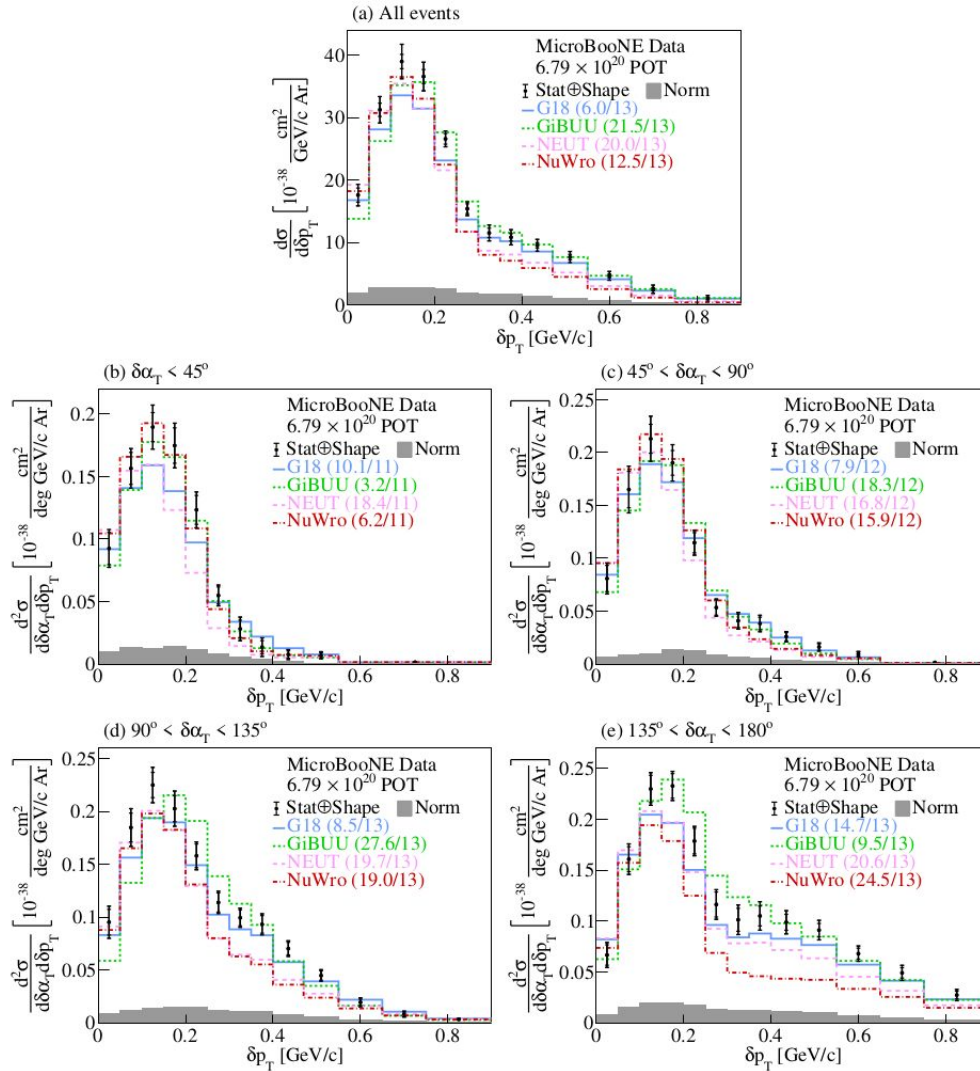
F = “filter” = additional smearing
matrix = regularization

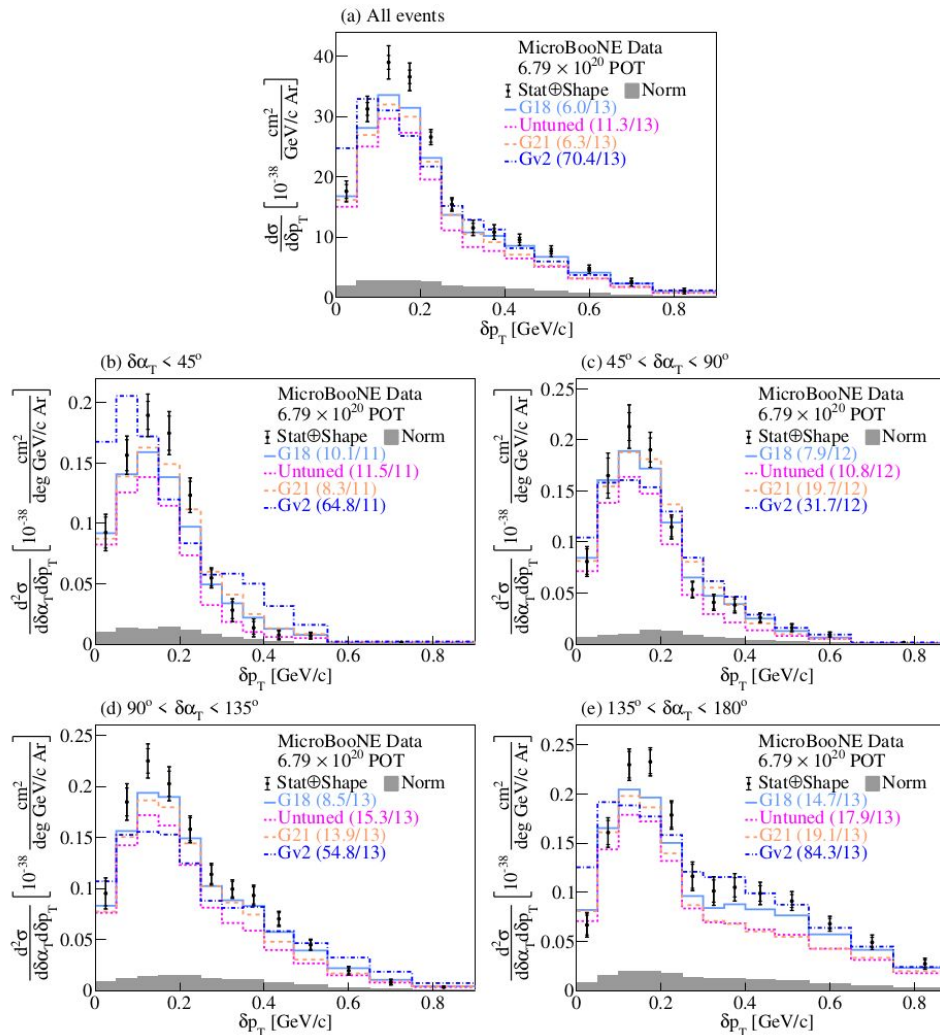


Given one model S

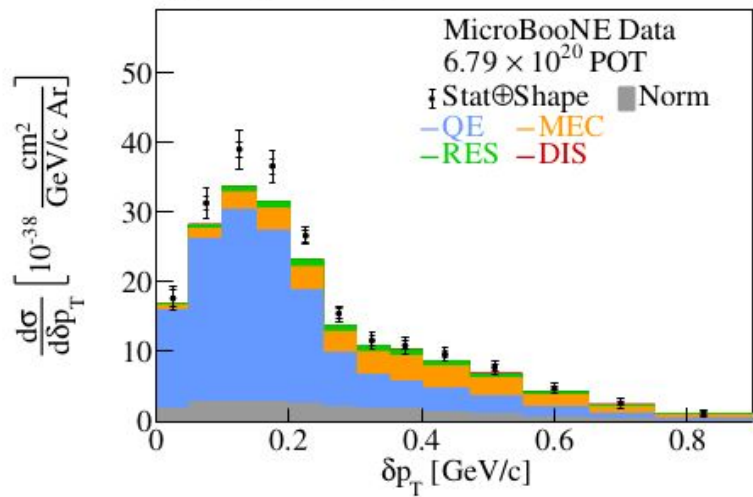
- General regularization, e.g. Tikhonov regularization, needs to “tune” a regularization strength parameter [curve in the left plot]
- Wiener-SVD regularization corresponds to a fixed point in the phase space of bias versus variance with **minimum MSE**



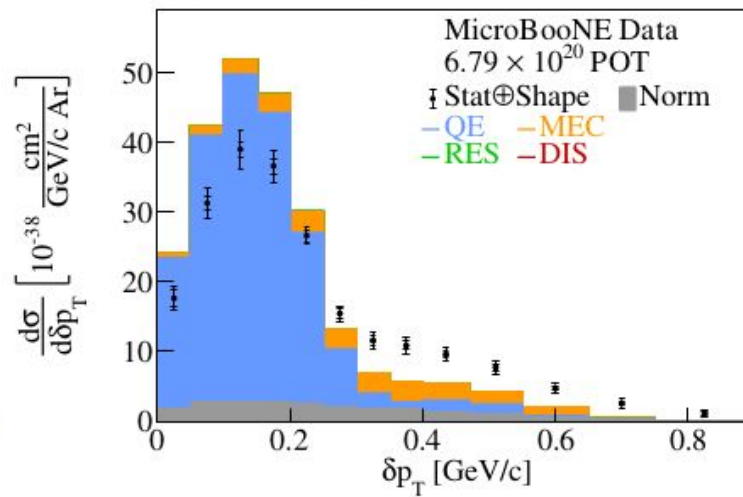


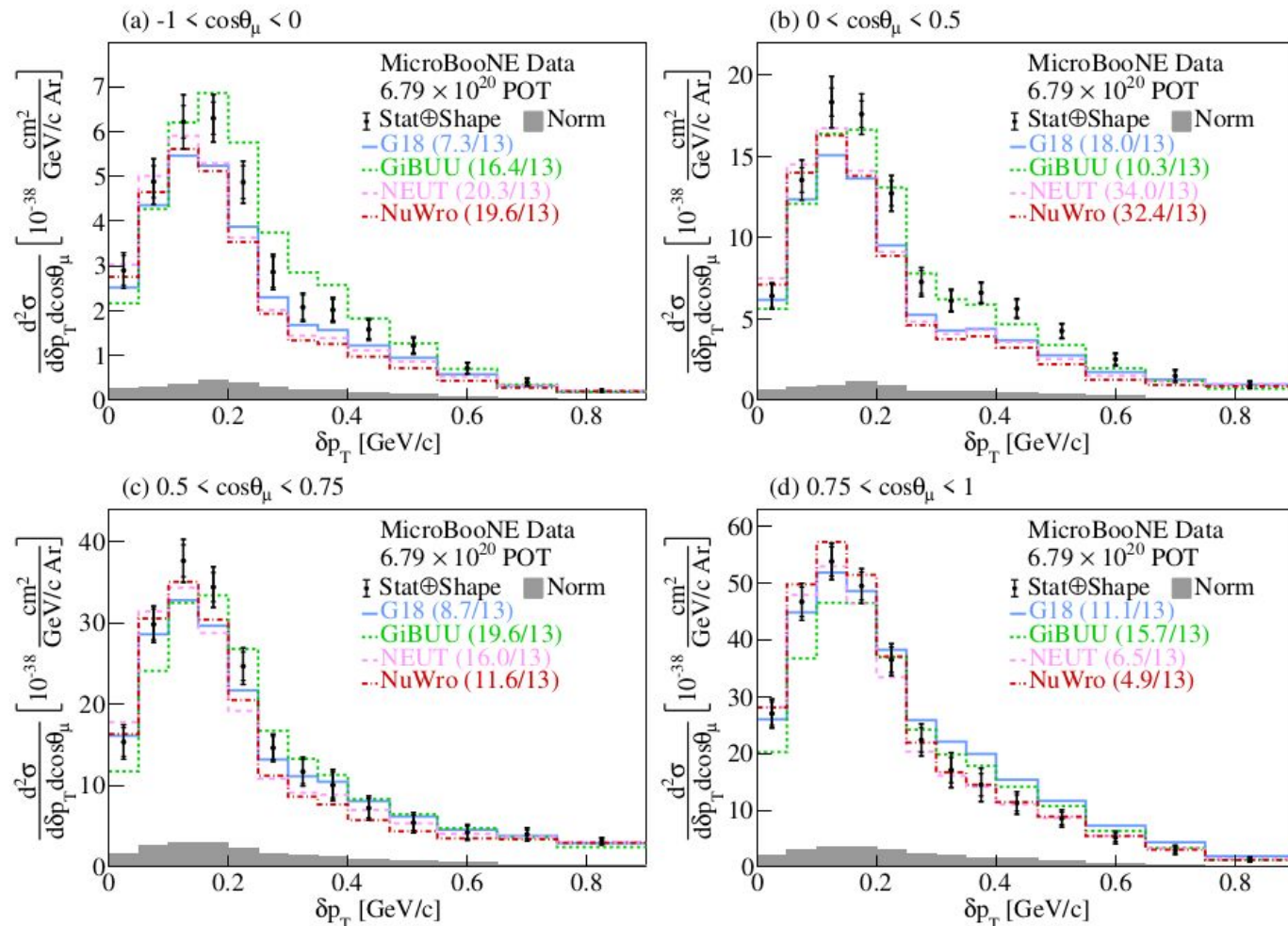


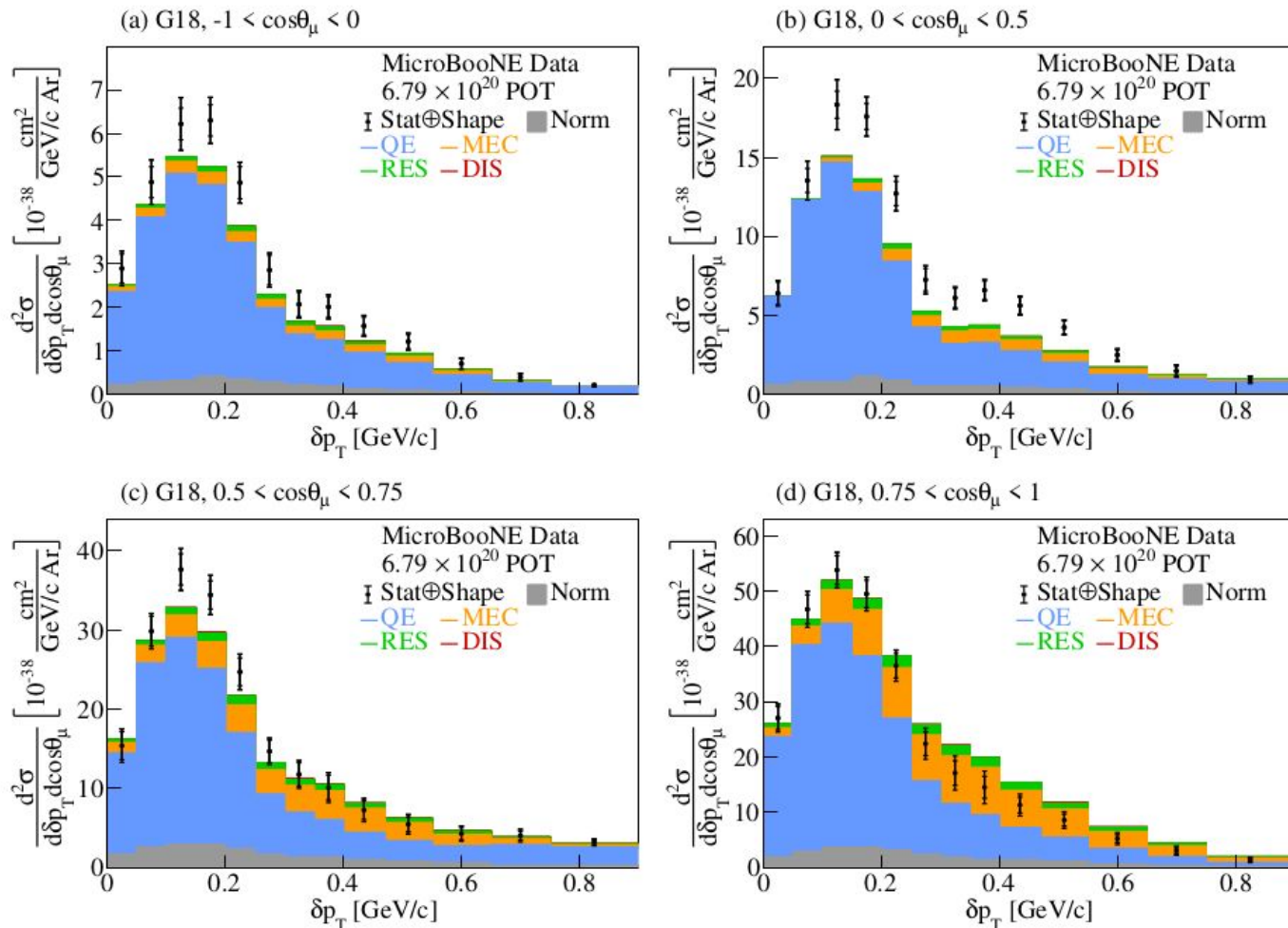
(a) G18, All events

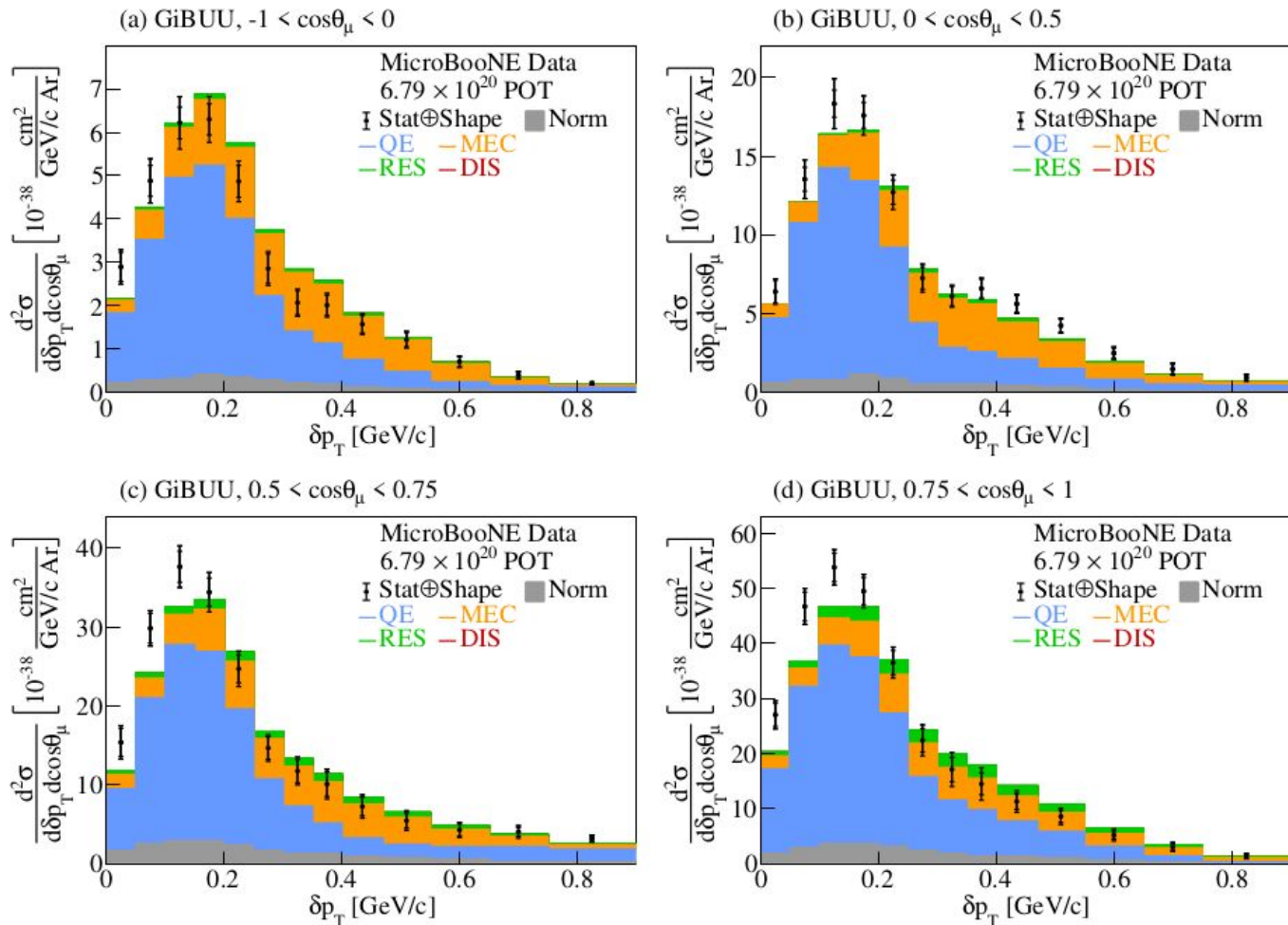


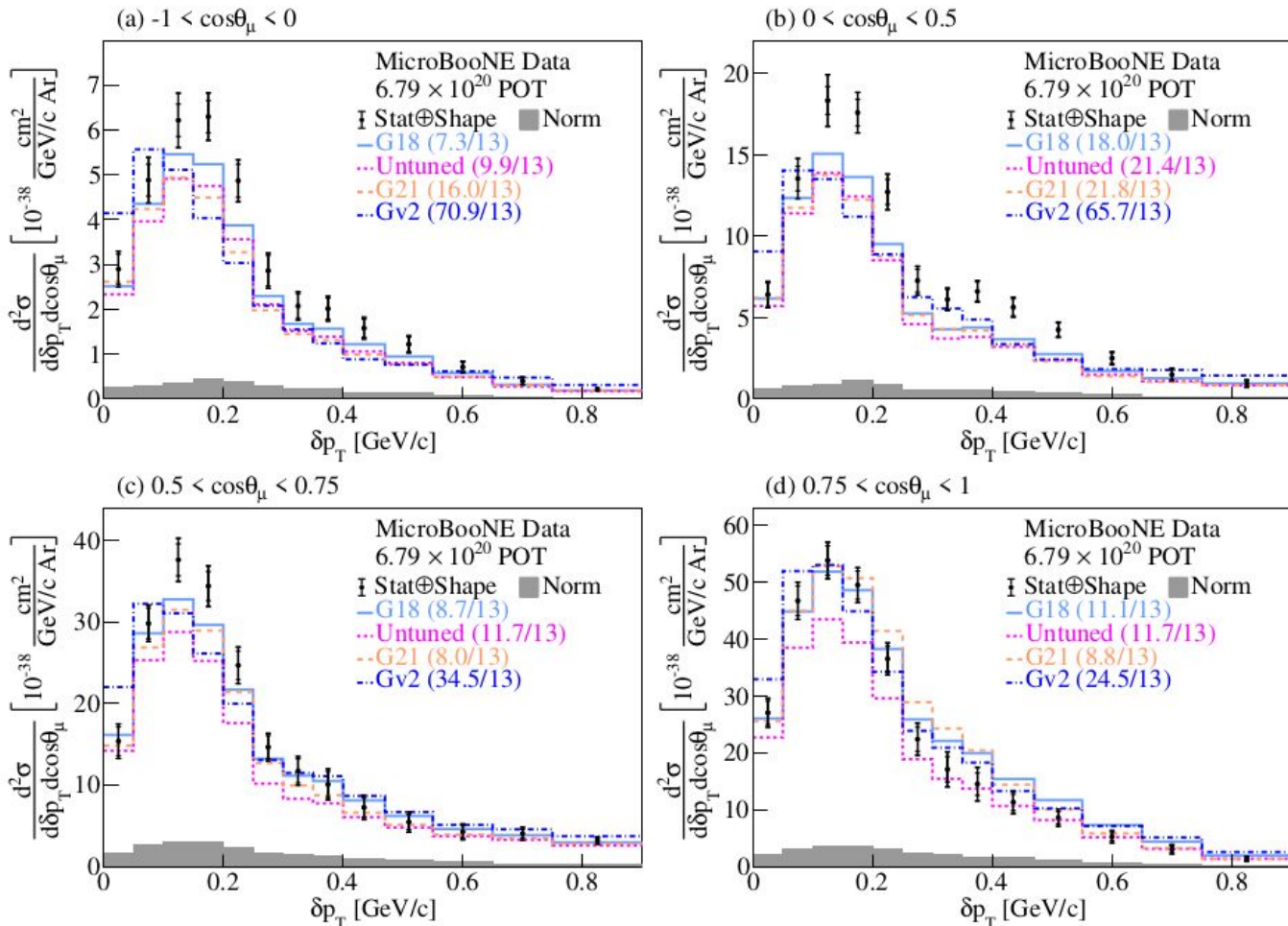
(b) G18 NoFSI, All events

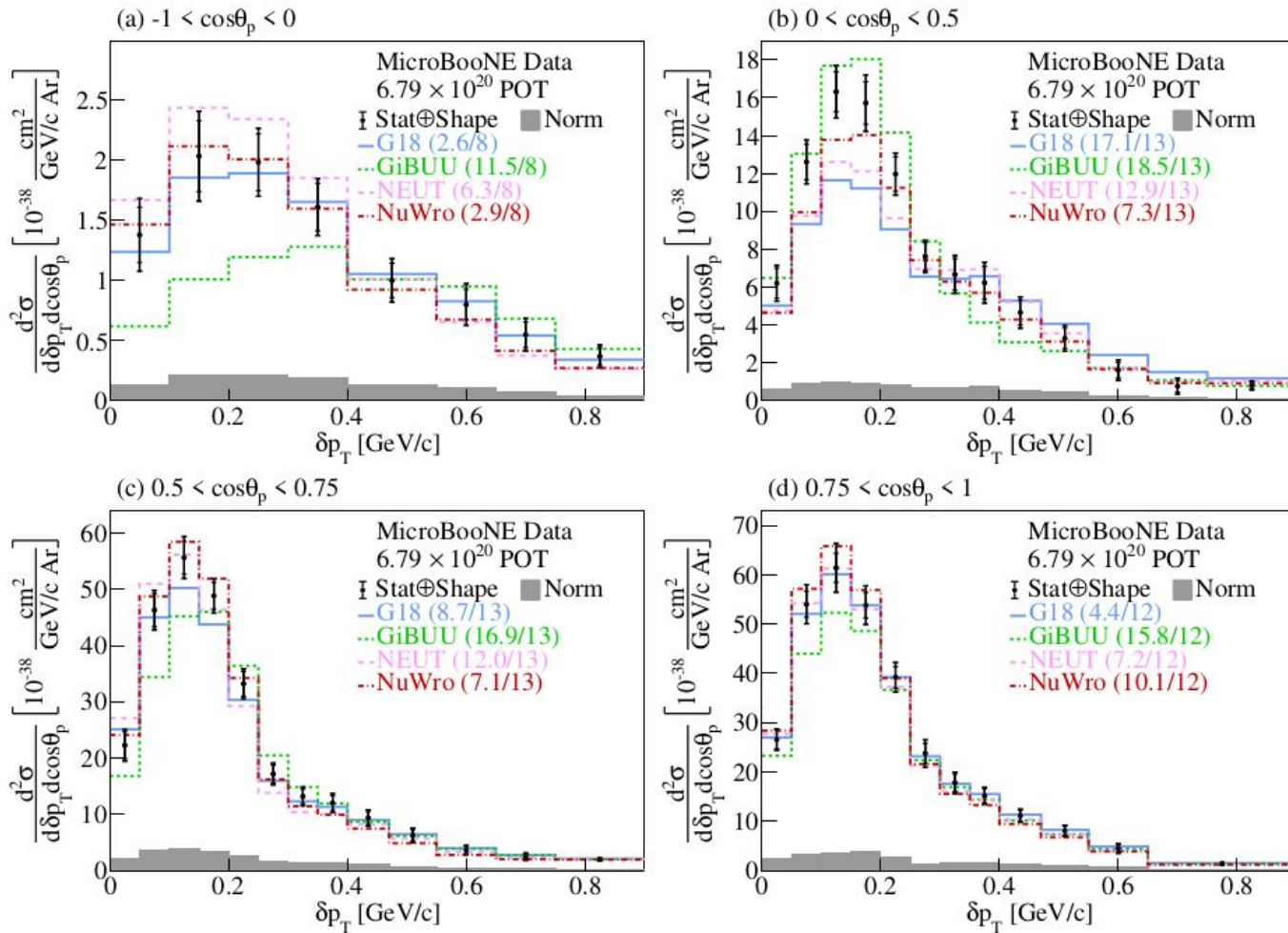


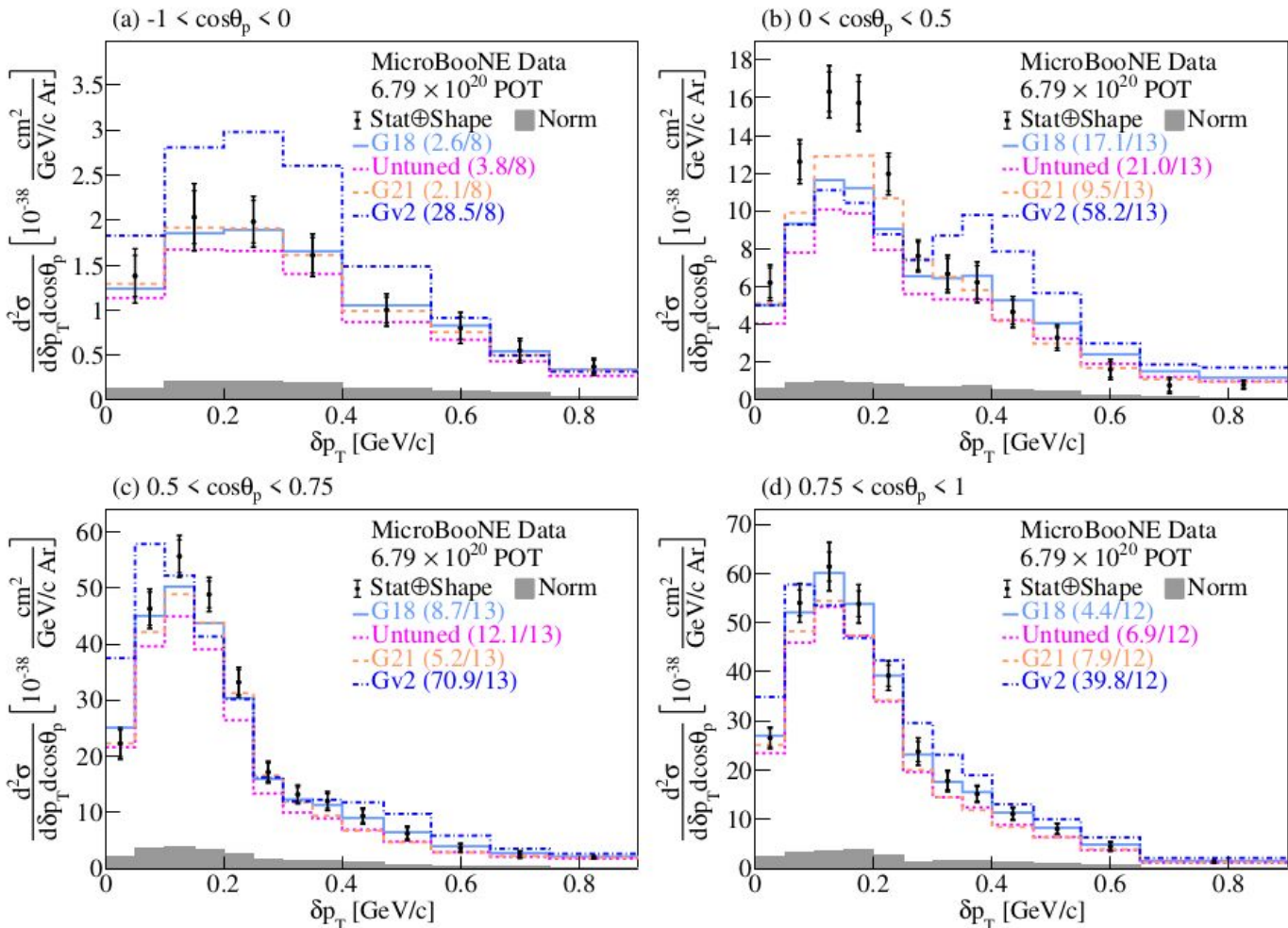


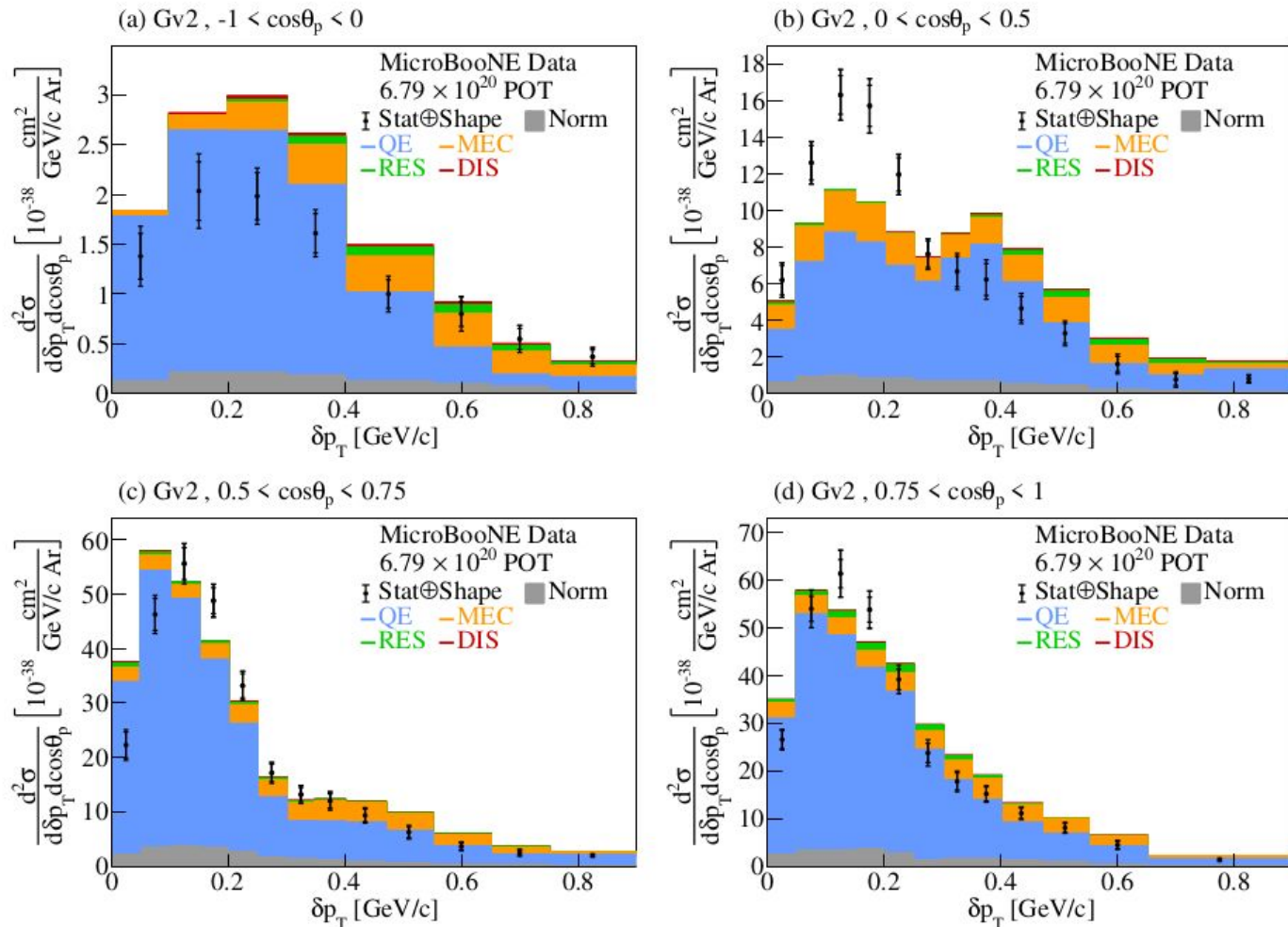


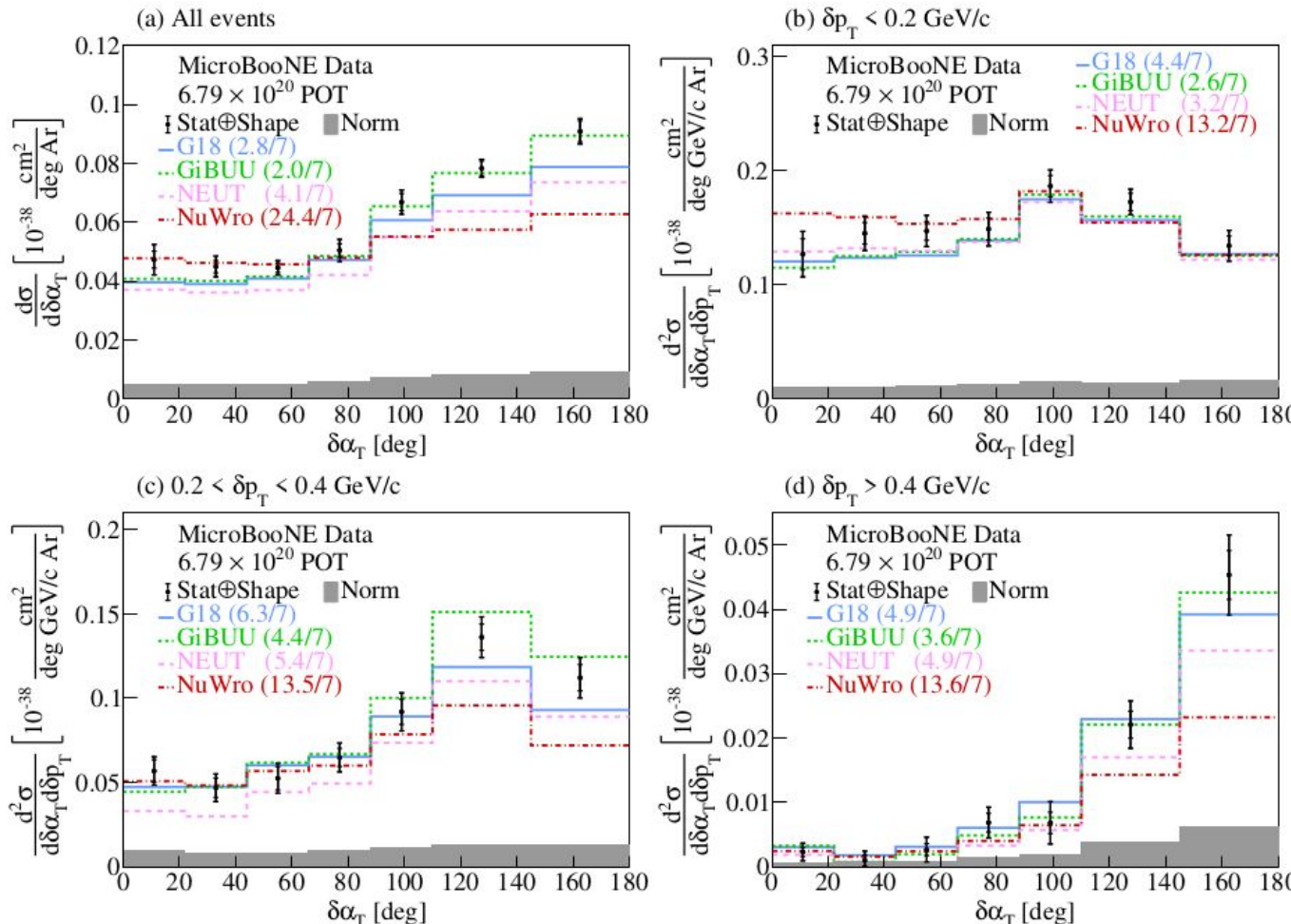


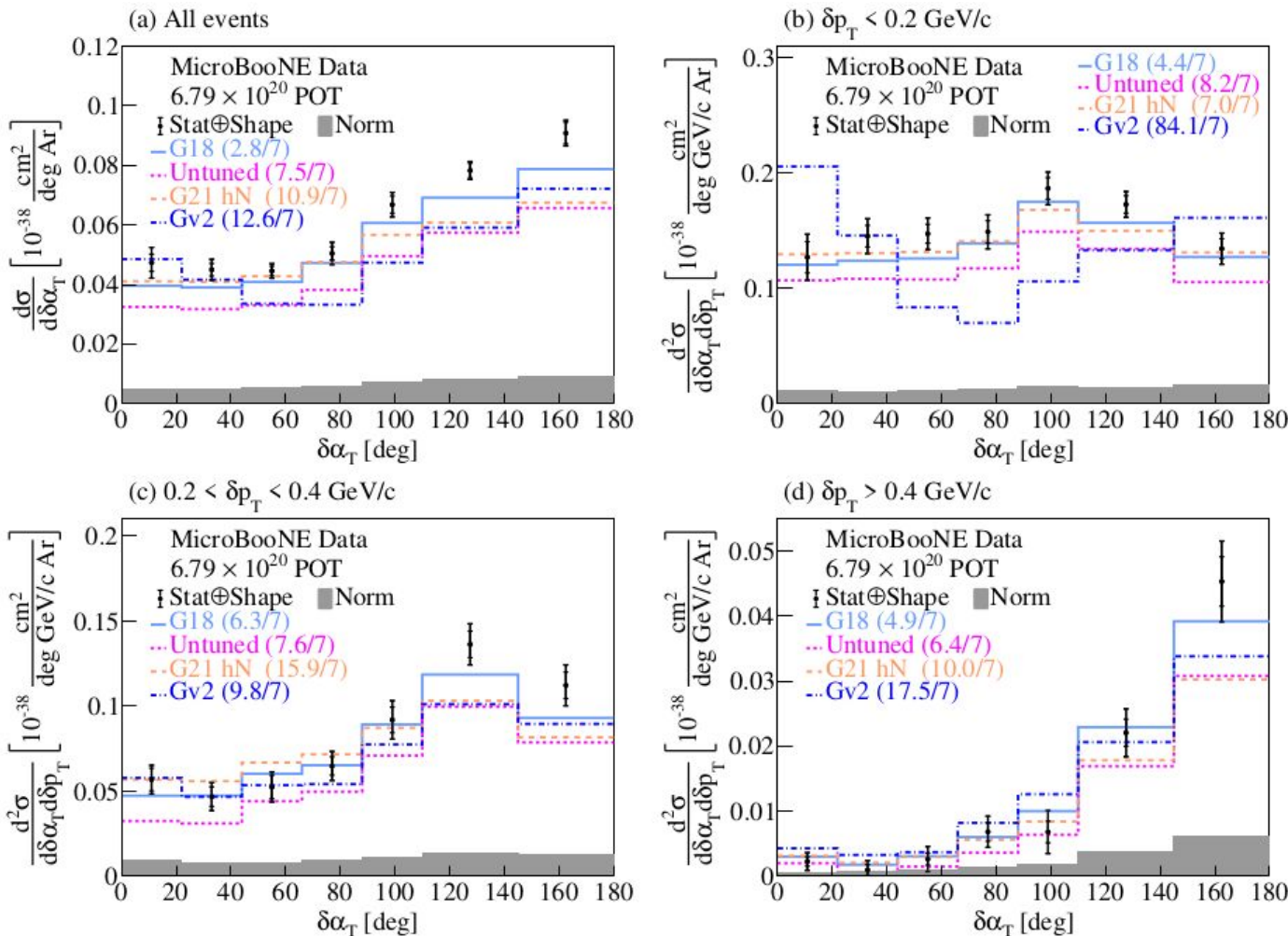


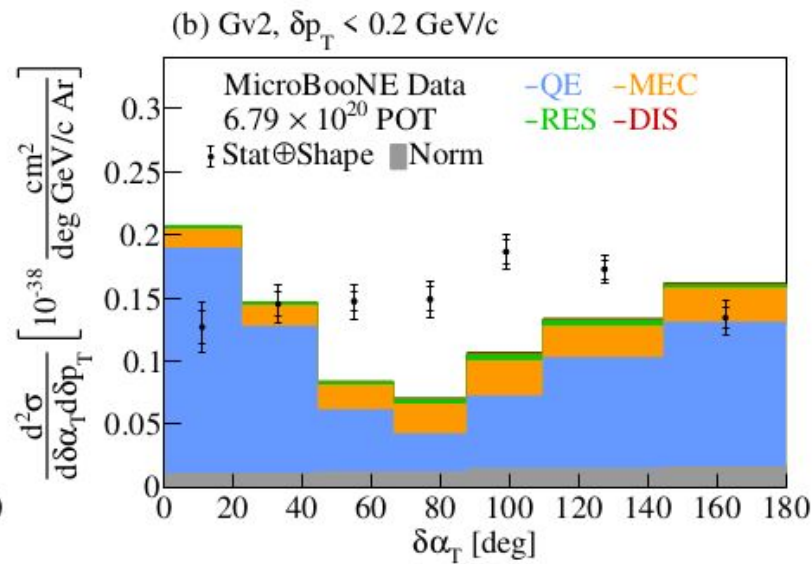
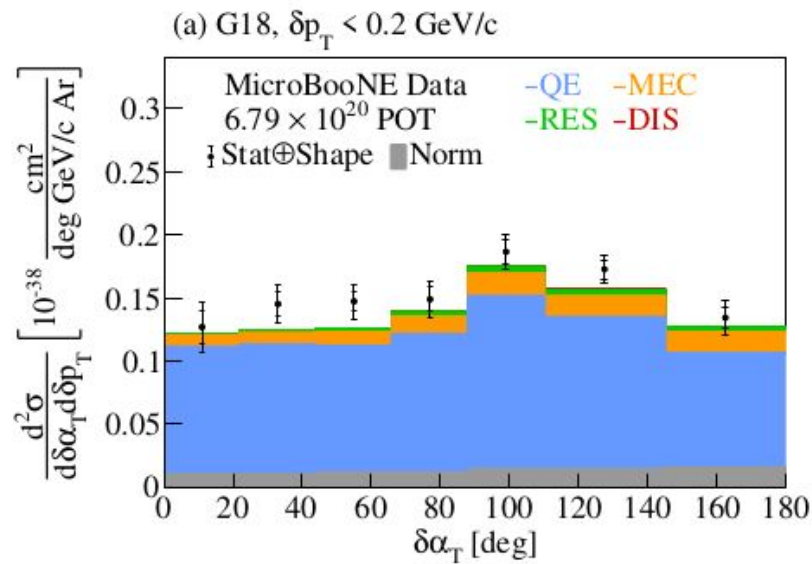


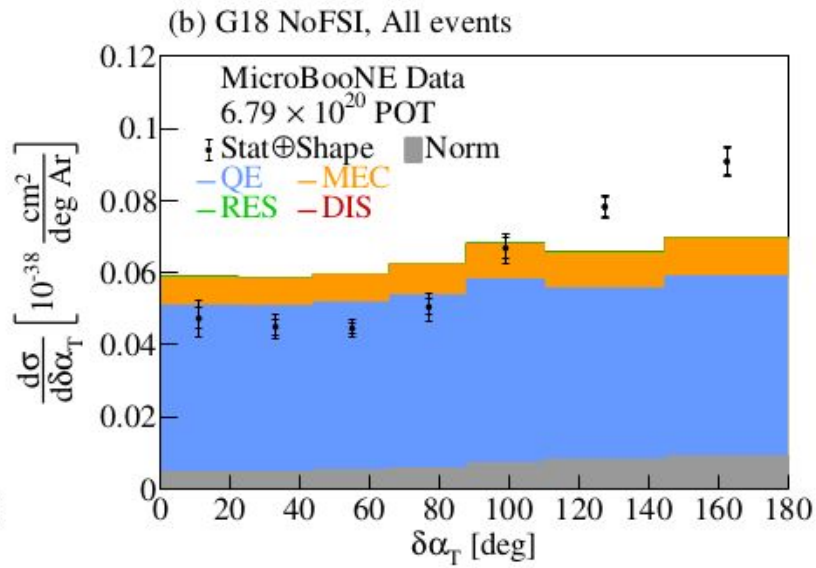
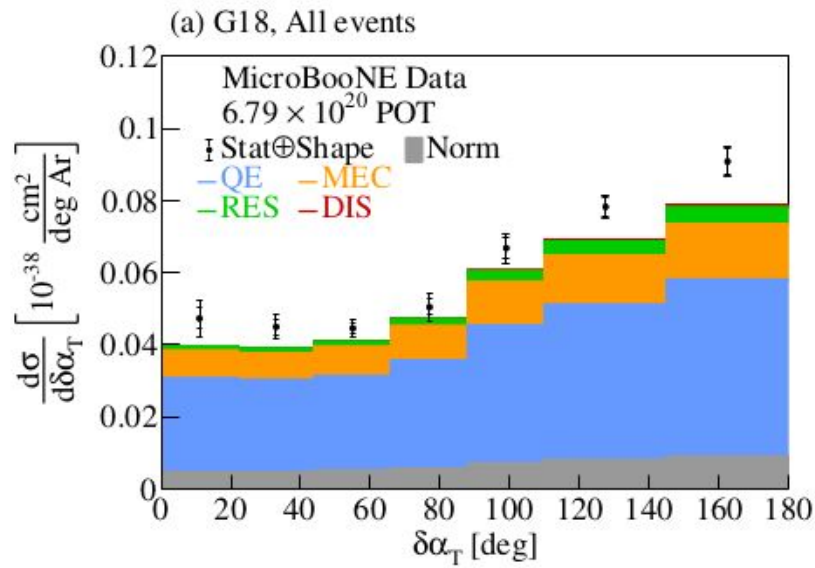


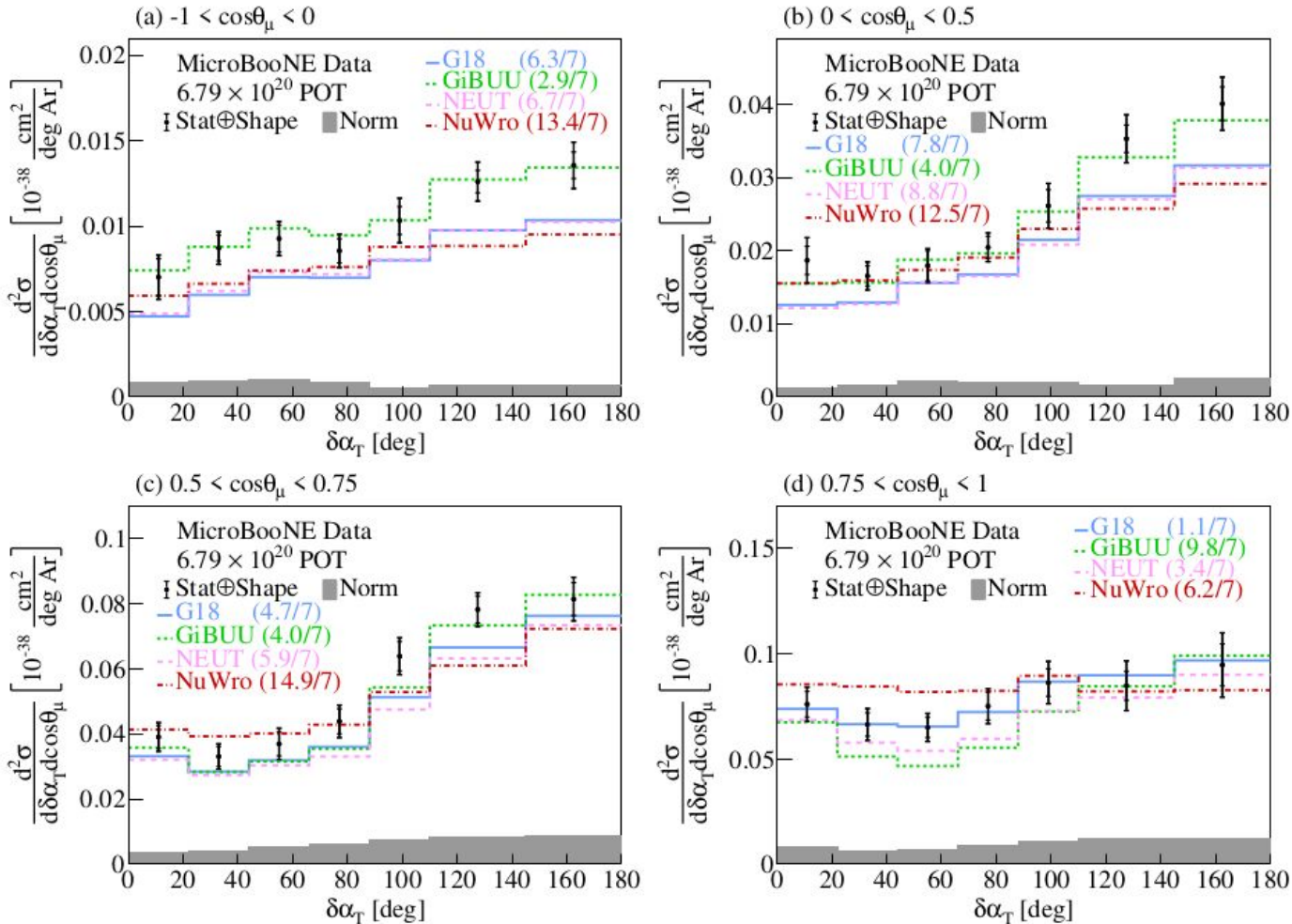


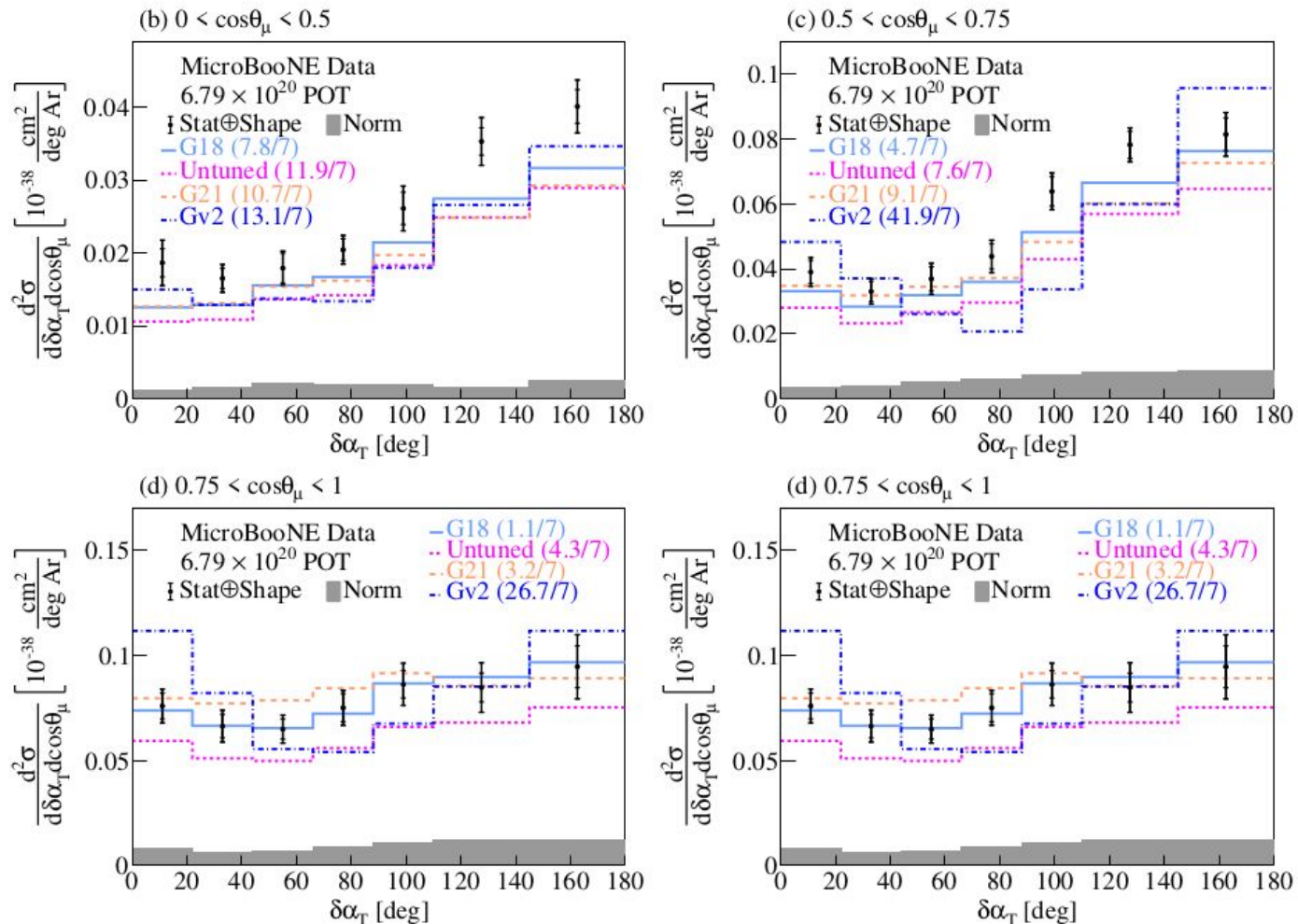


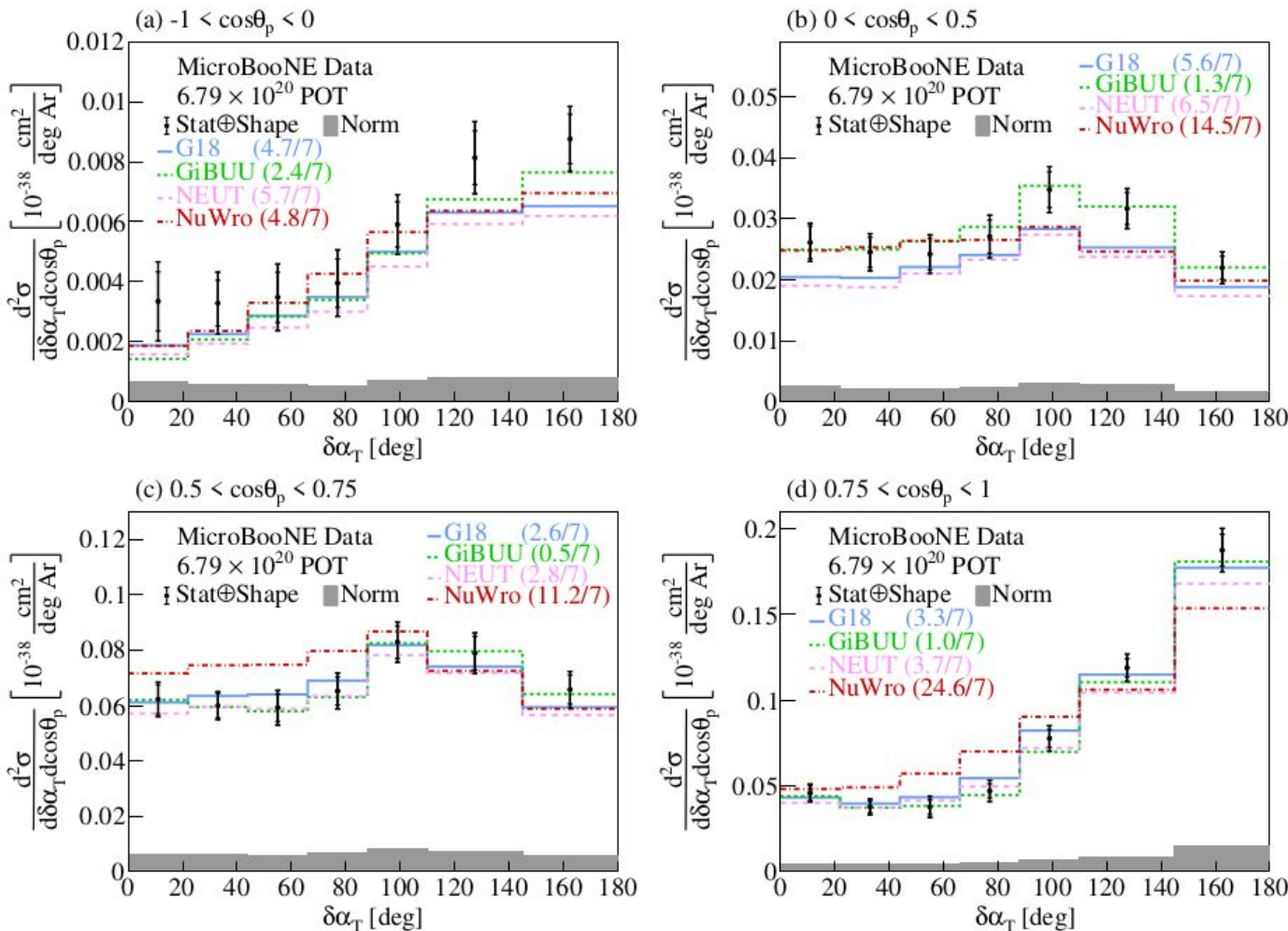


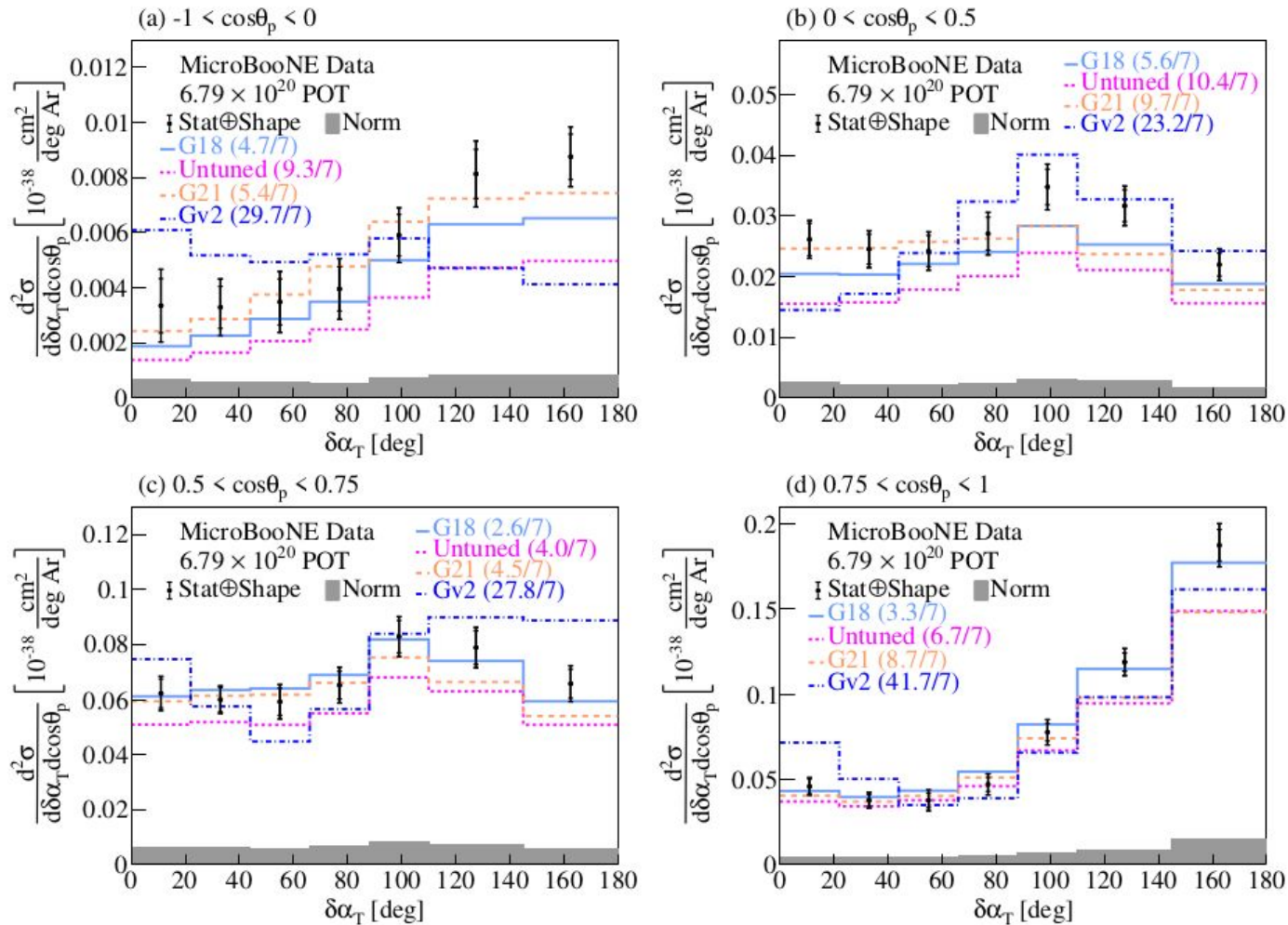


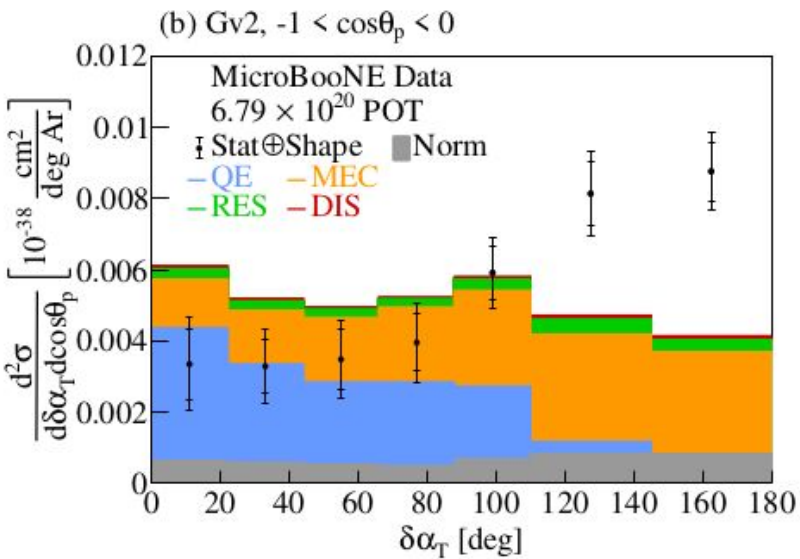
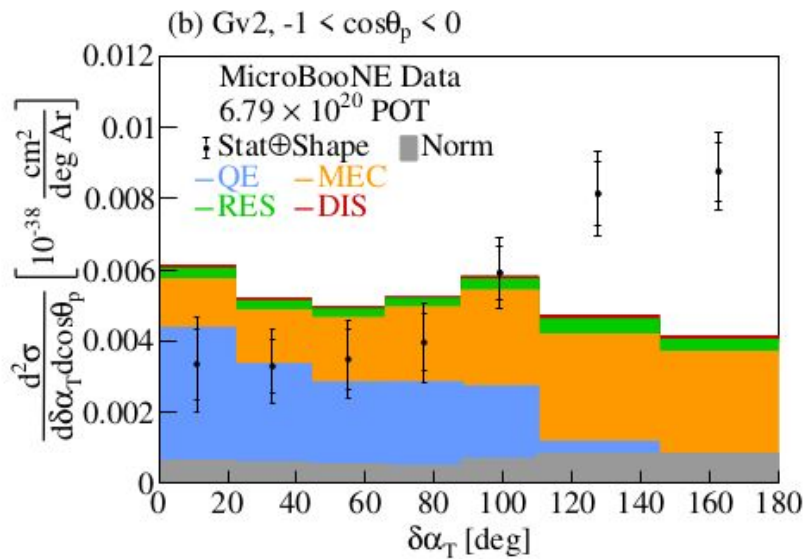


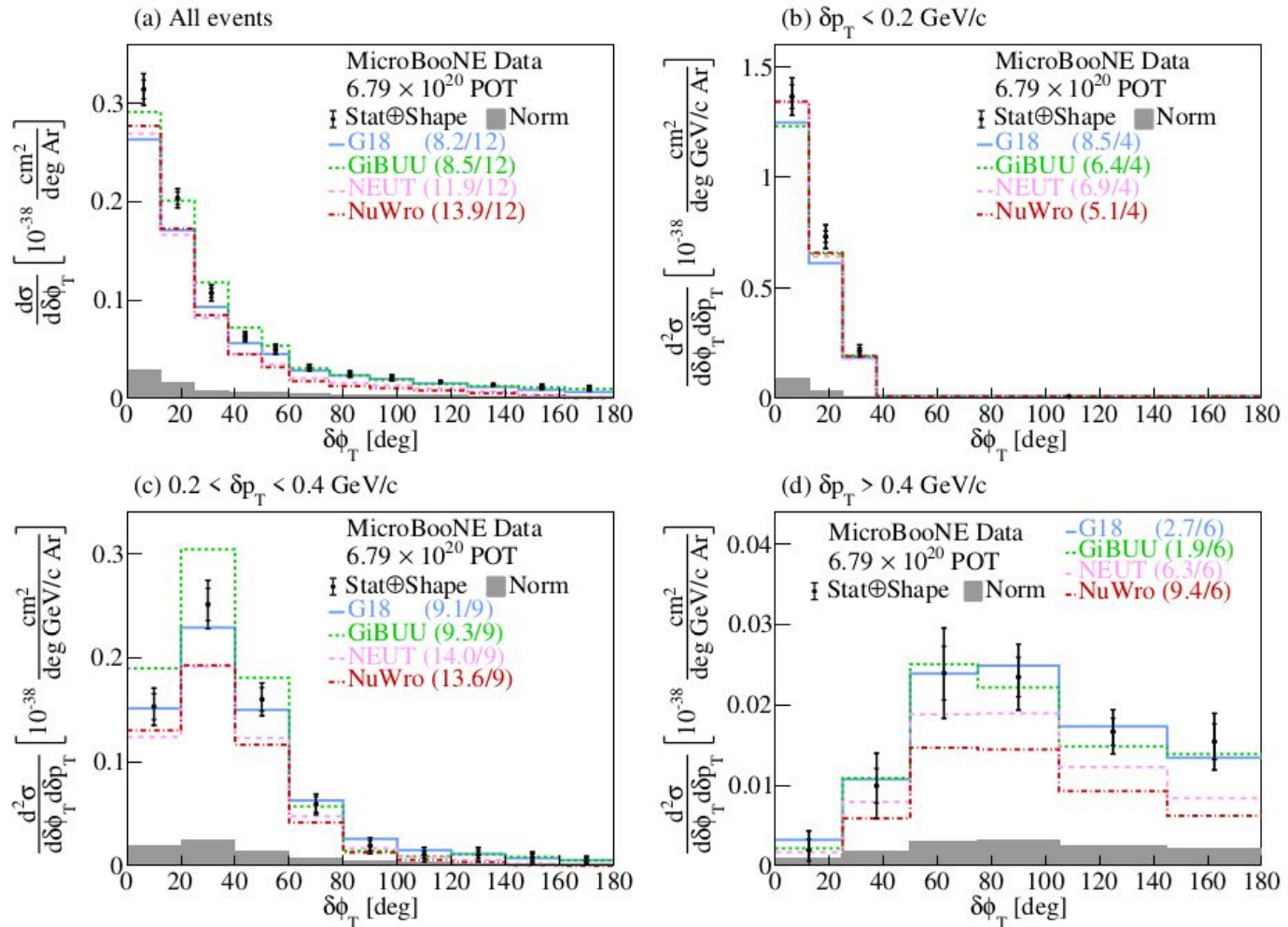


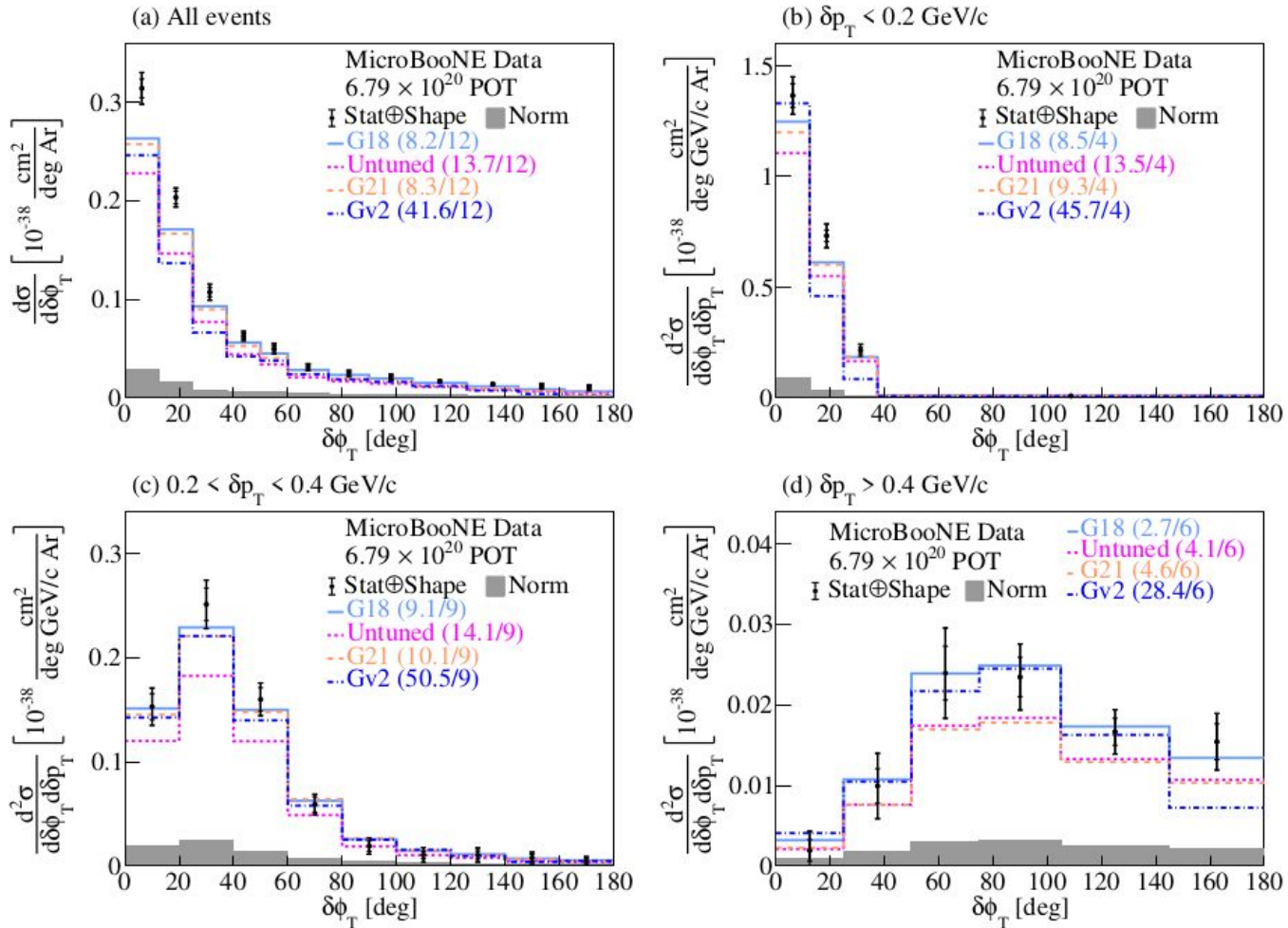


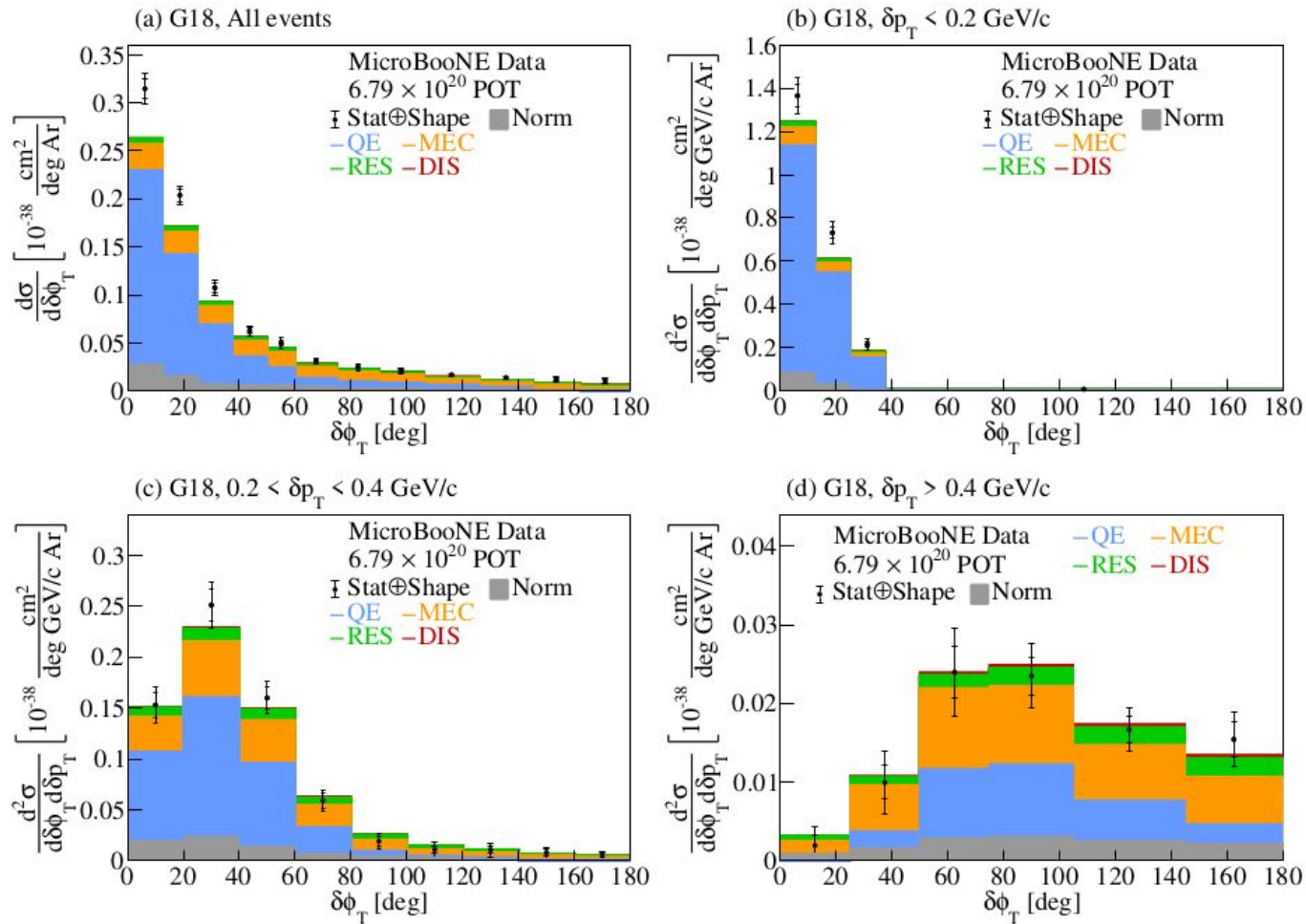


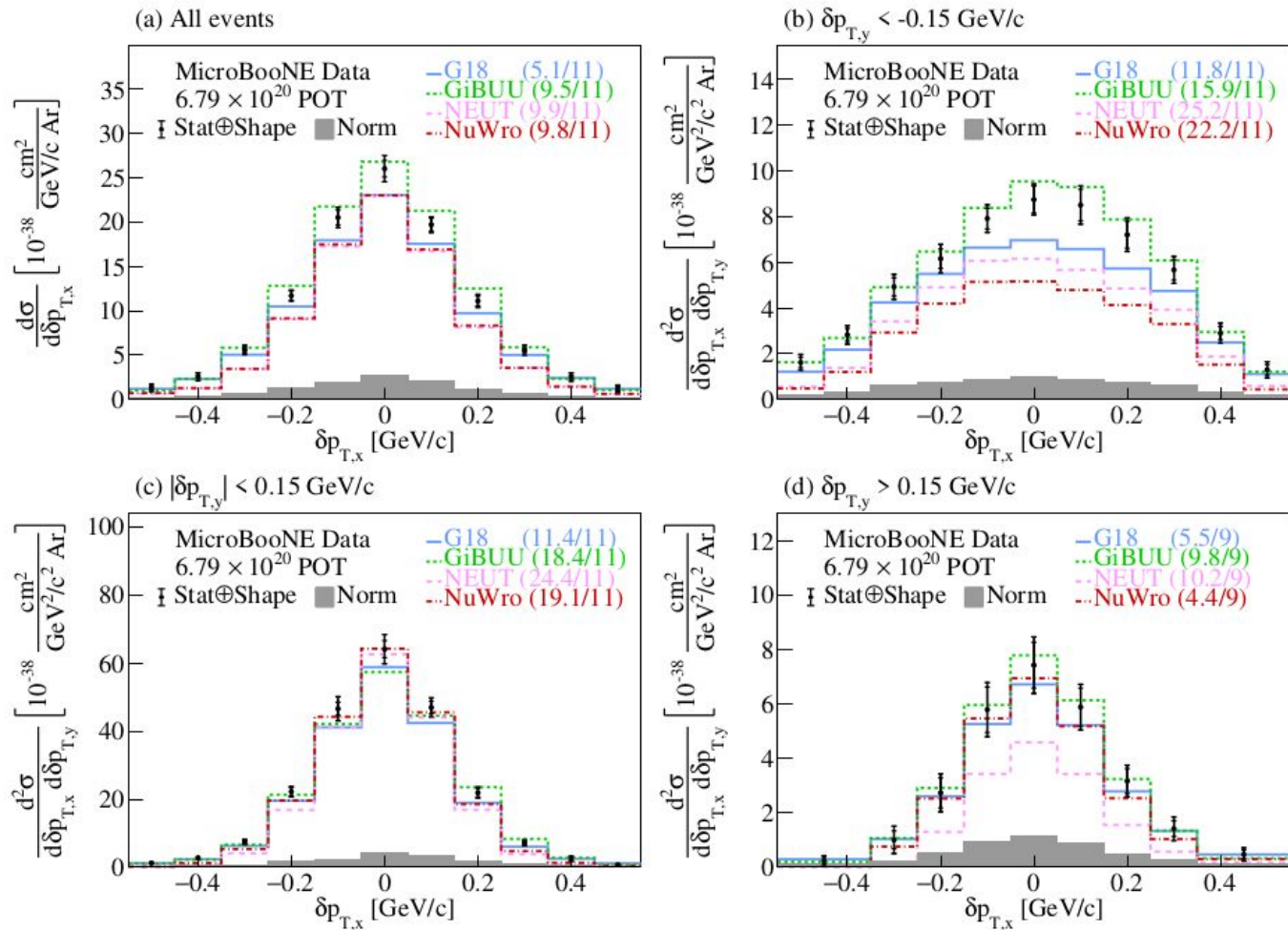


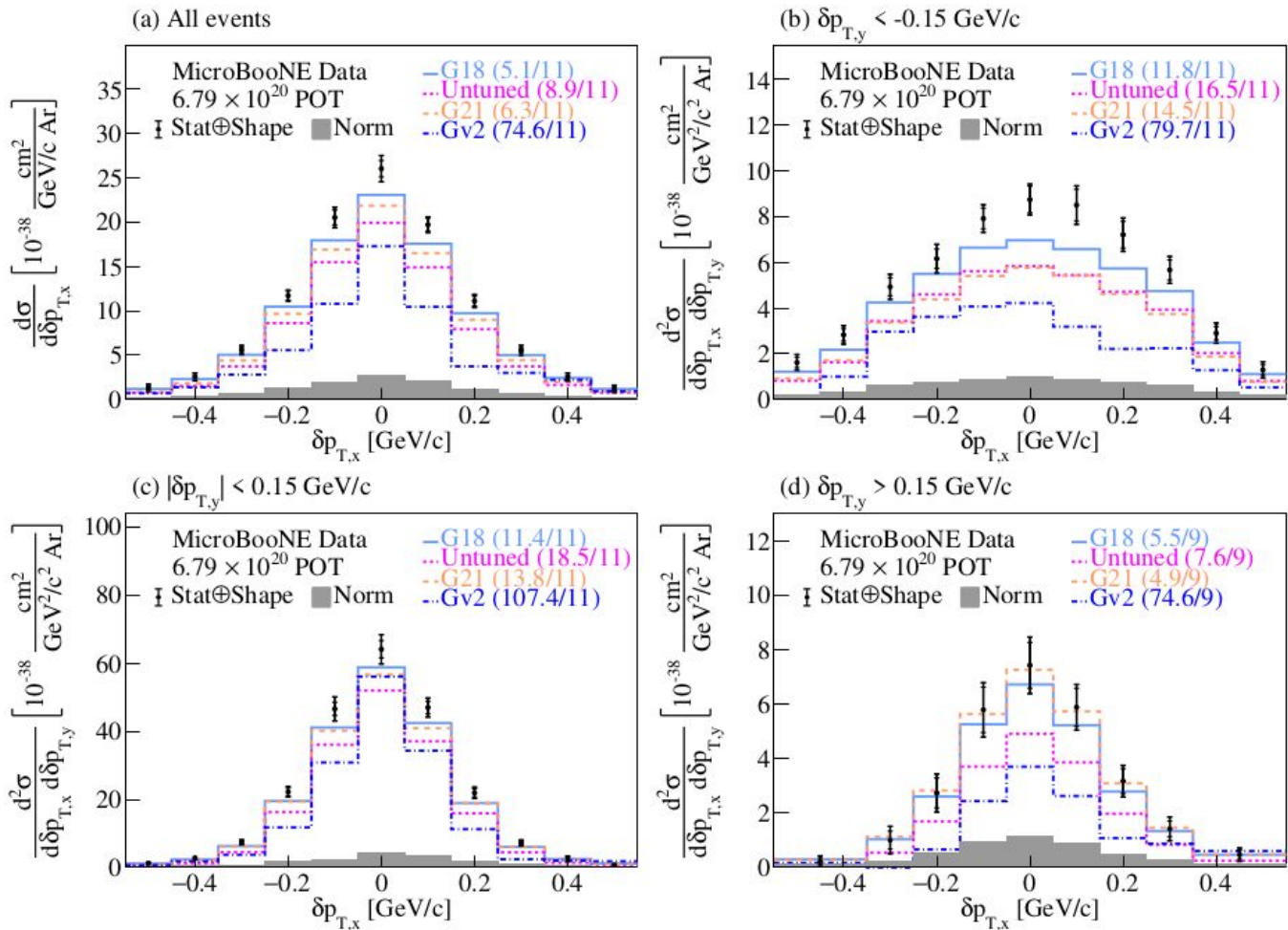


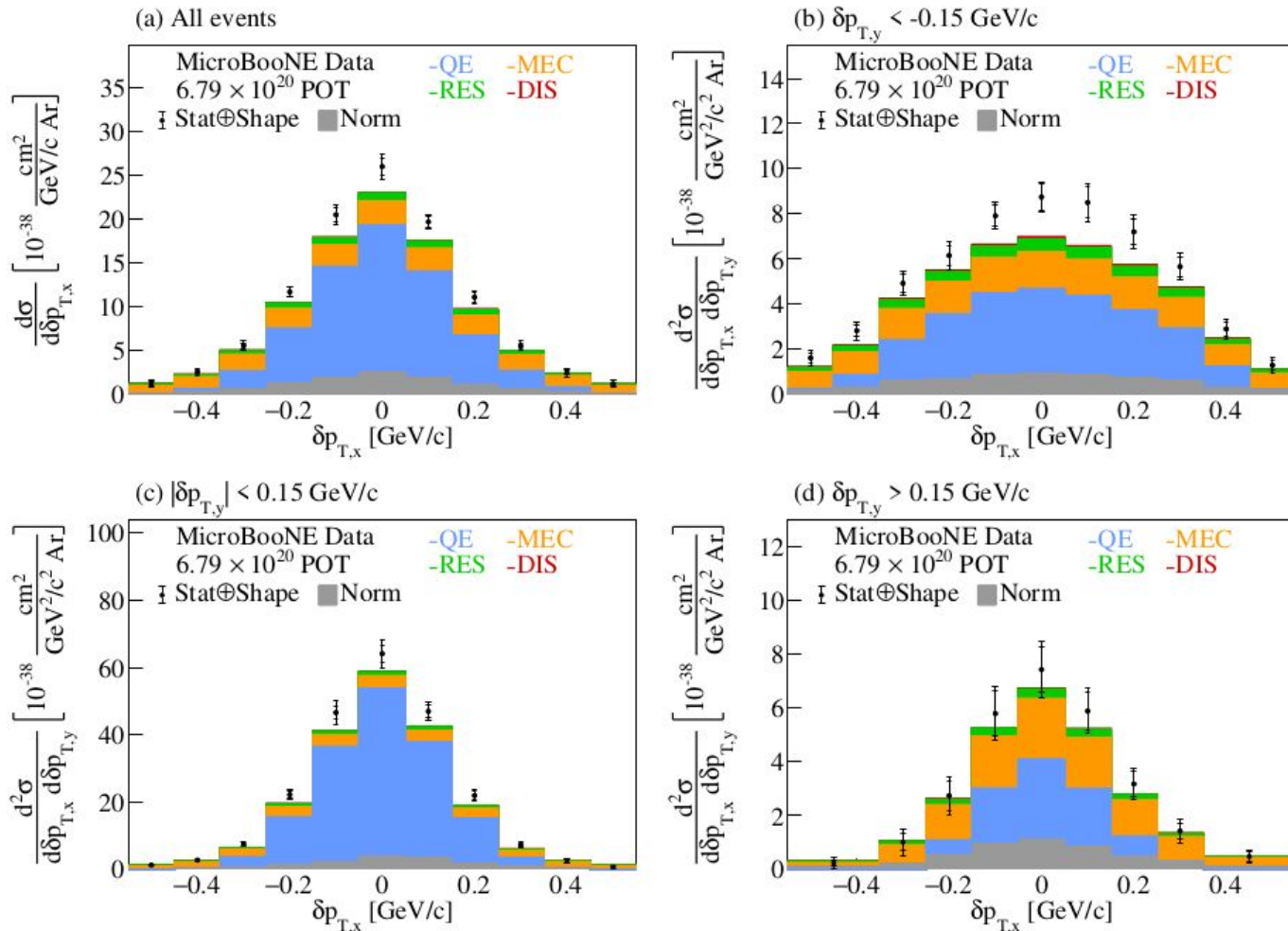


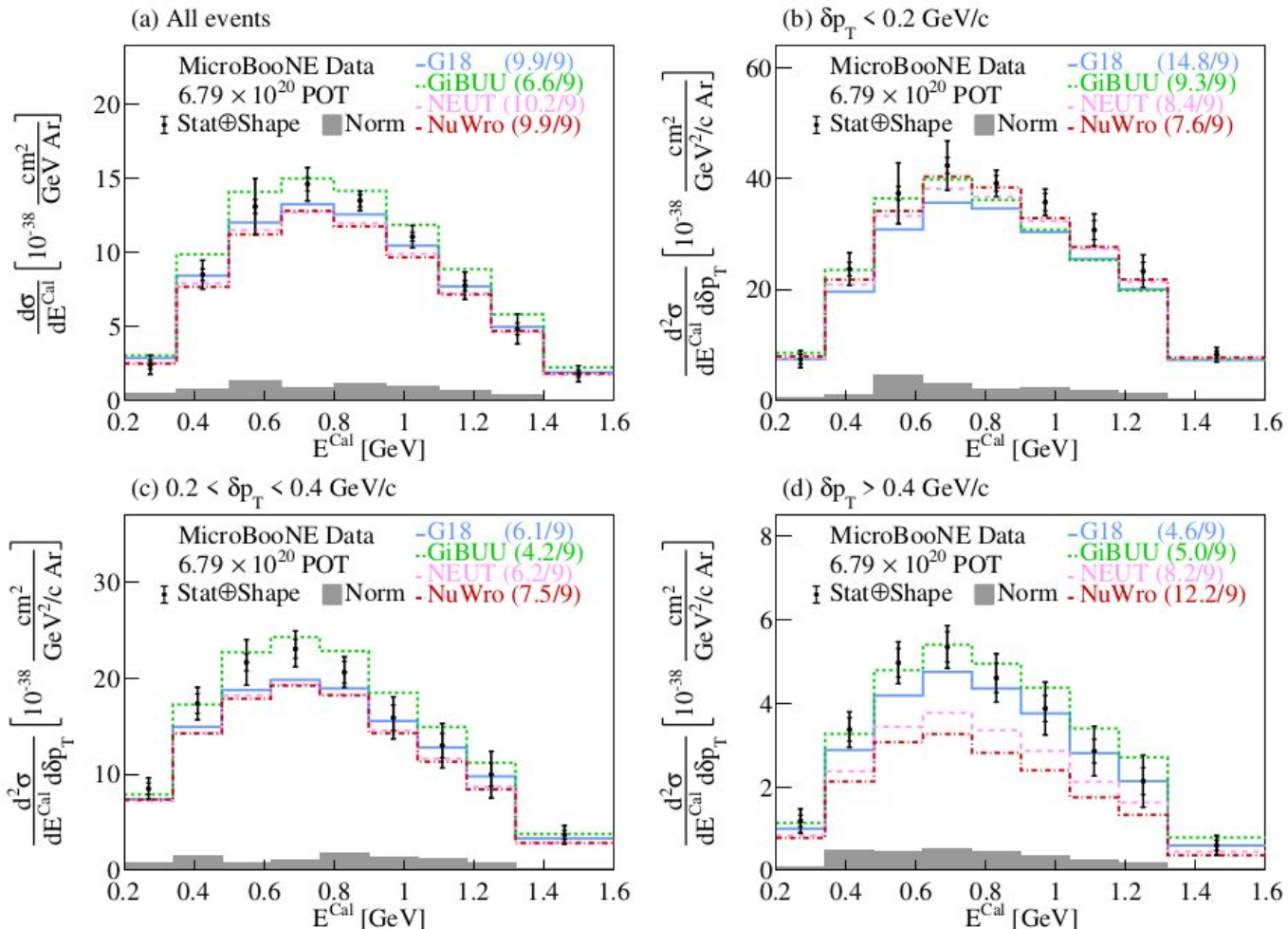


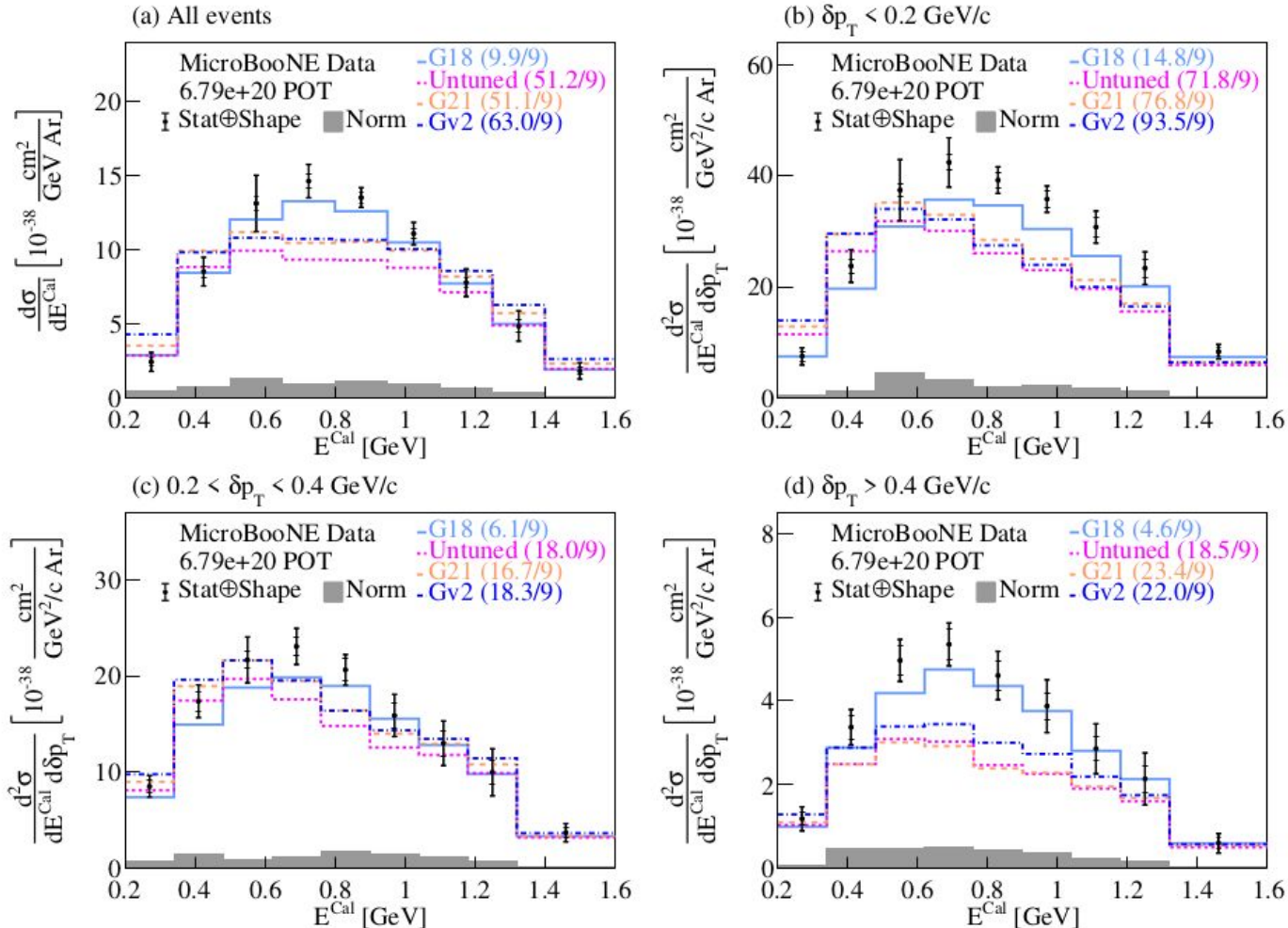


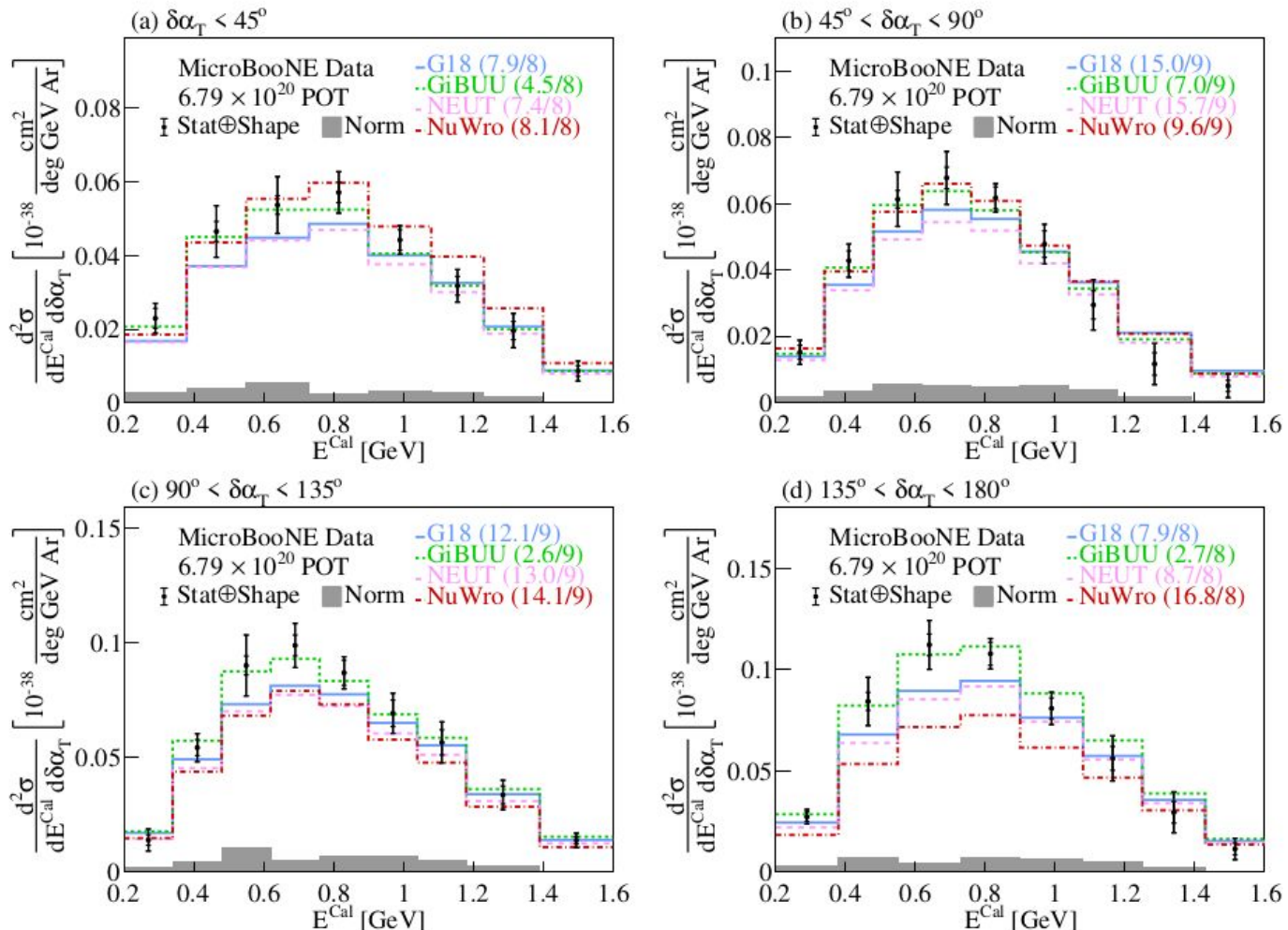


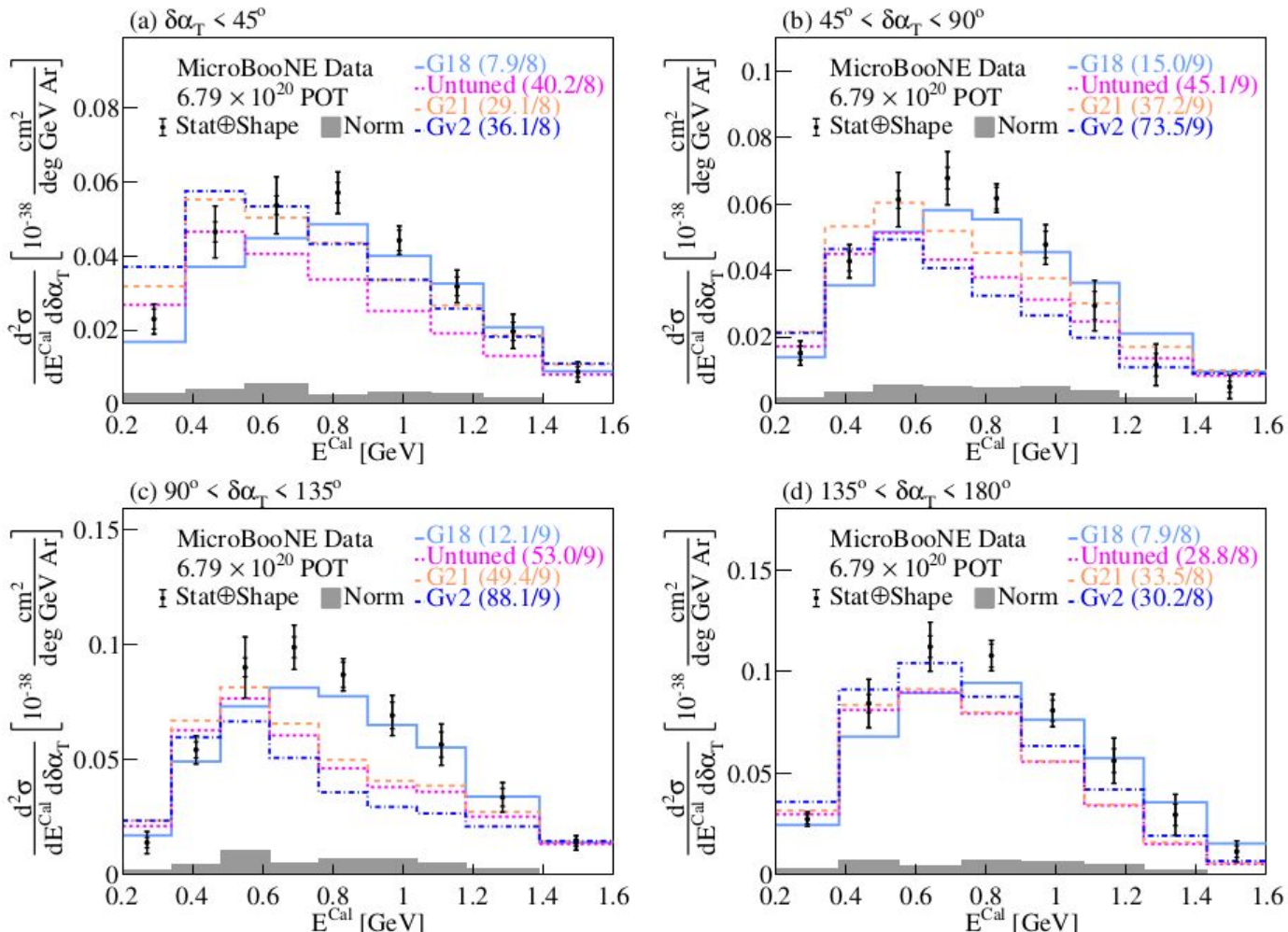


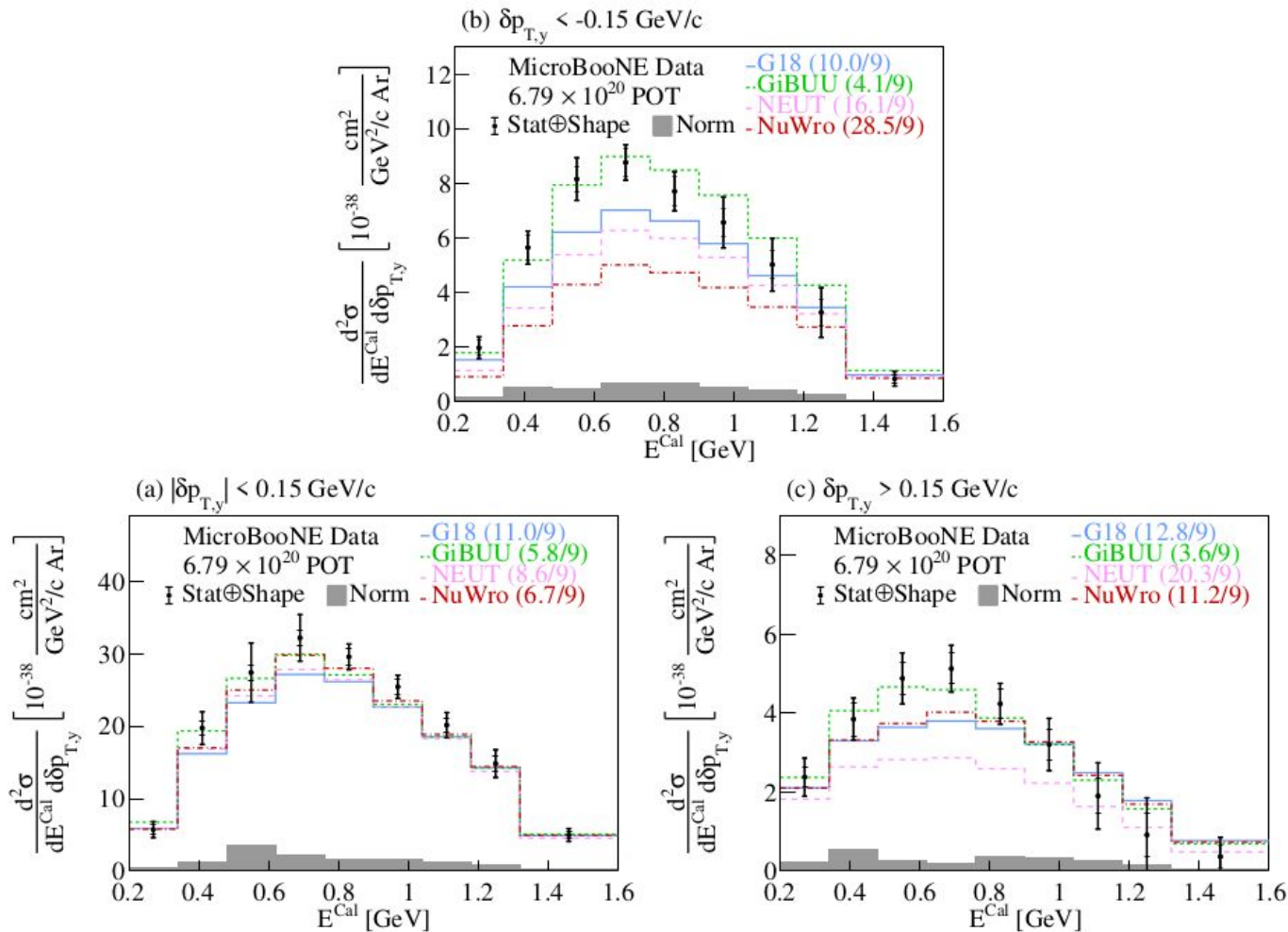


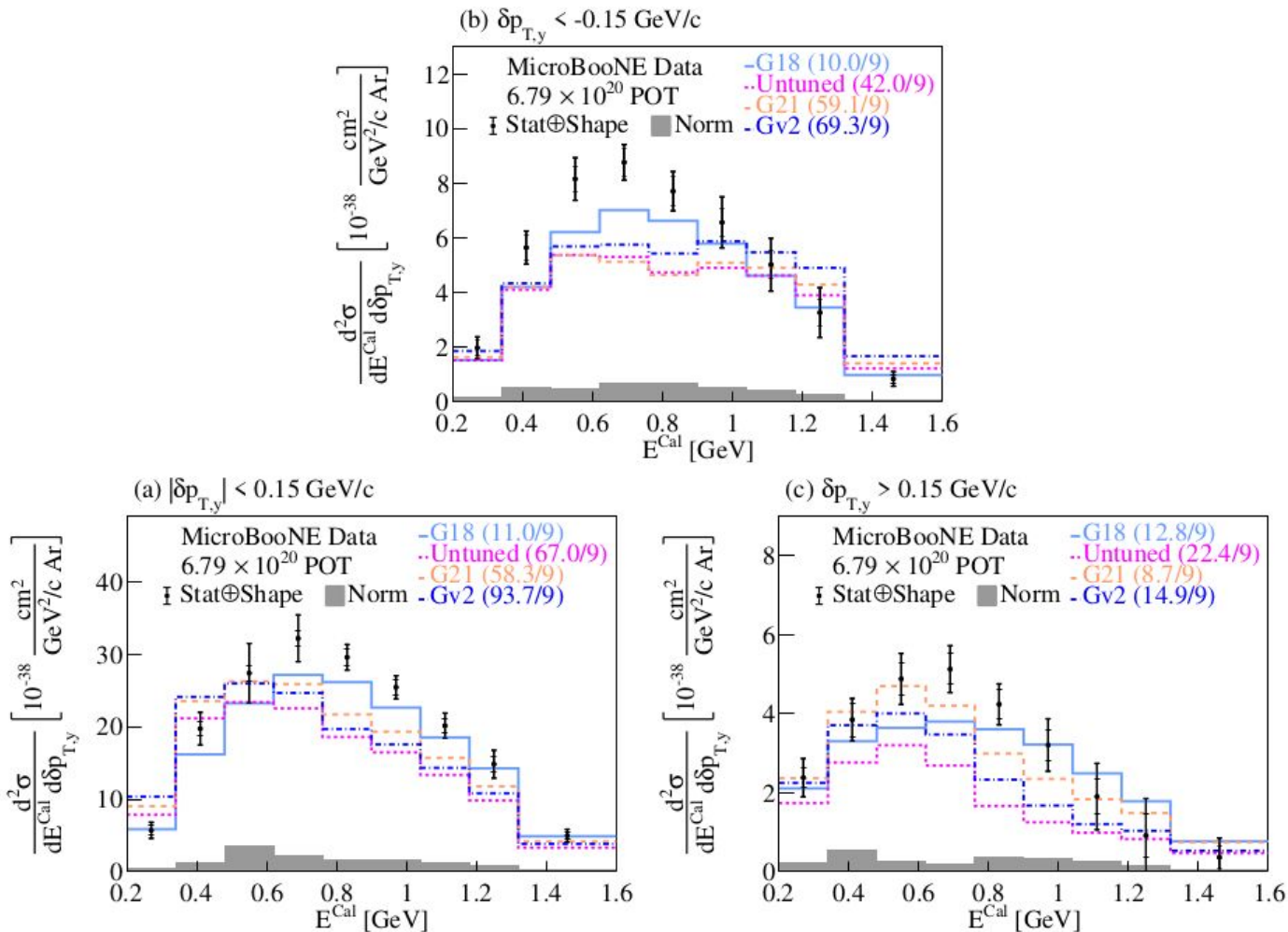




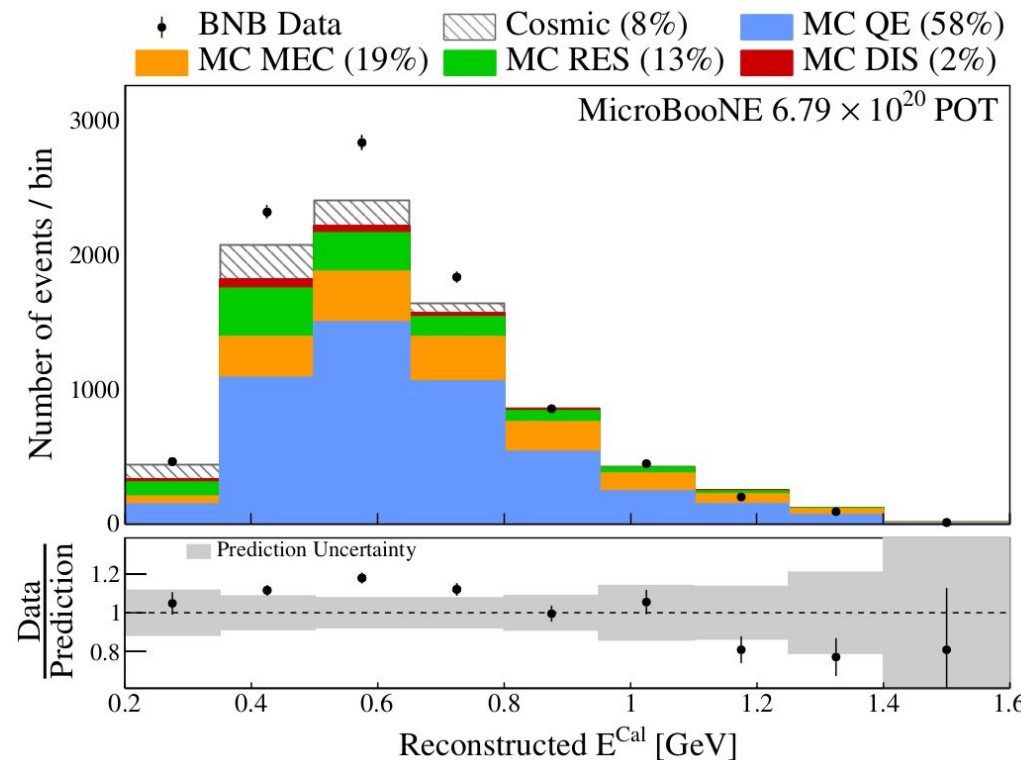








Calorimetric Energy

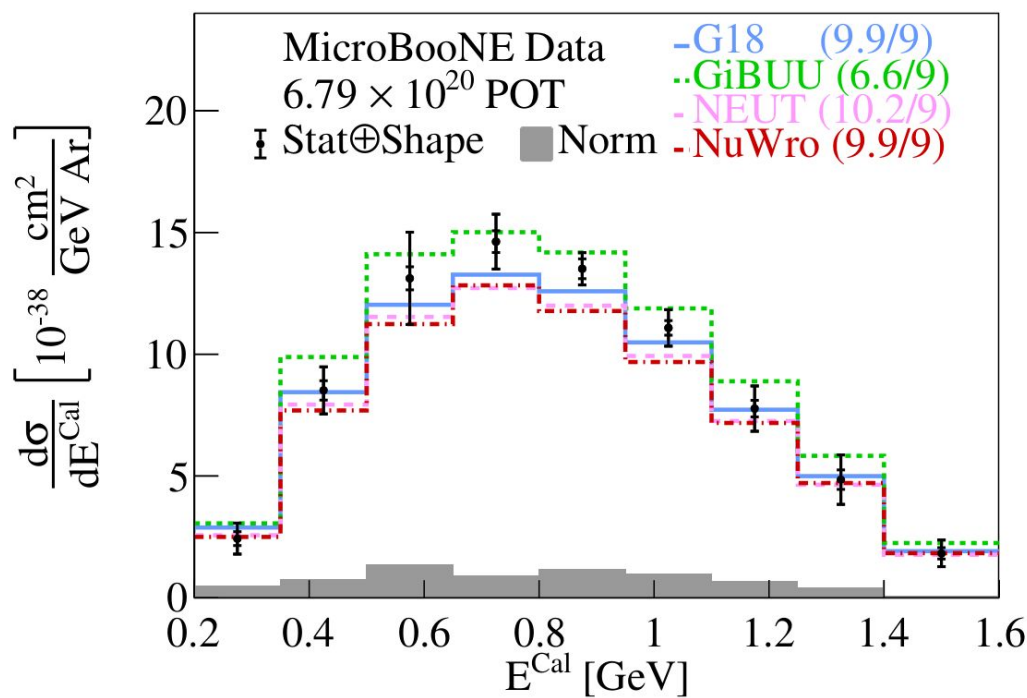


$$E^{Cal} = E_\mu + T_p + BE$$

- E_μ = muon energy
- T_p = proton kinetic energy
- $BE = 40$ MeV binding energy
- Peak at ~ 0.7 GeV

Calorimetric Energy Cross Section

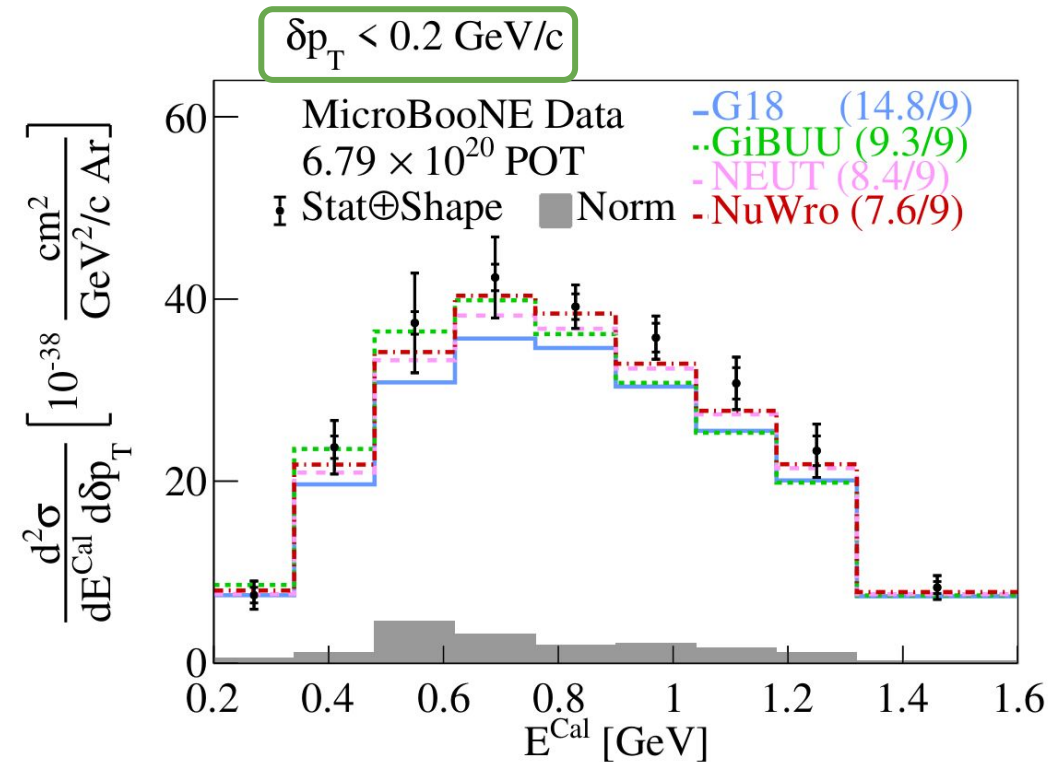
All events



$$E^{Cal} = E_\mu + T_p + BE$$

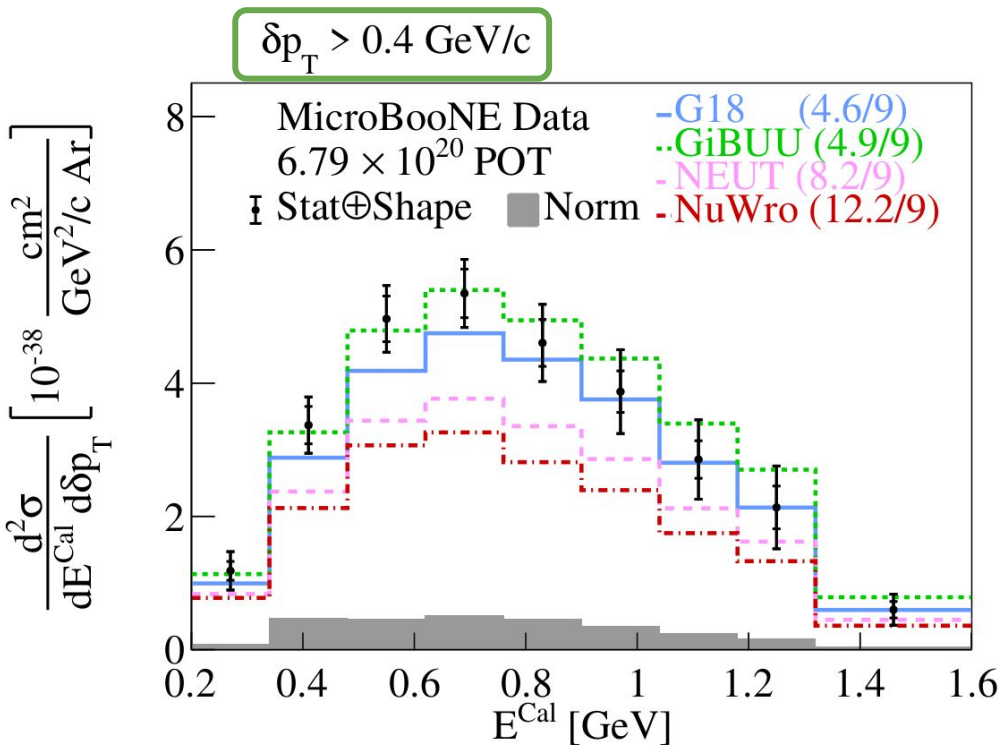
- E_μ = muon energy
- T_p = proton kinetic energy
- BE = 40 MeV binding energy
- All generators yield good agreement

High Statistics→Into the Multiverse!



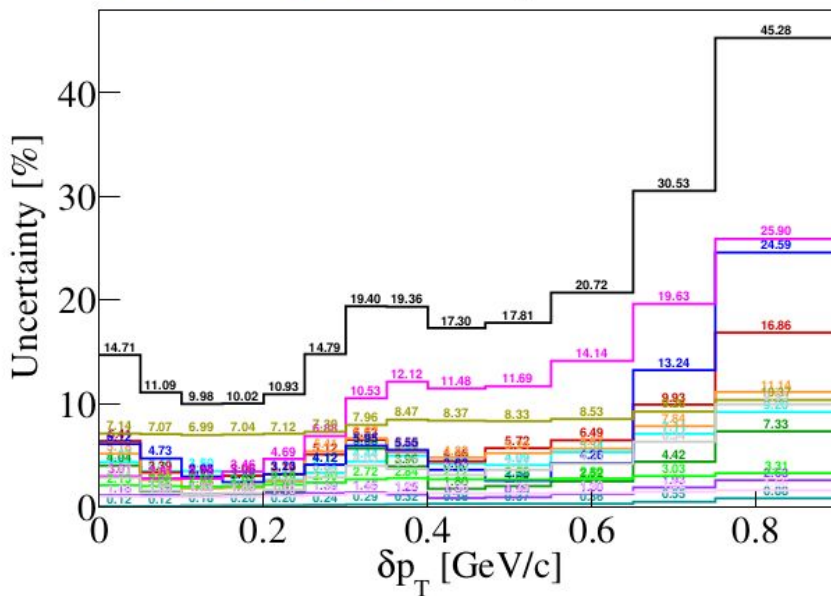
- QE dominated region
- All generators yield good agreement

High Statistics→Into the Multiverse!

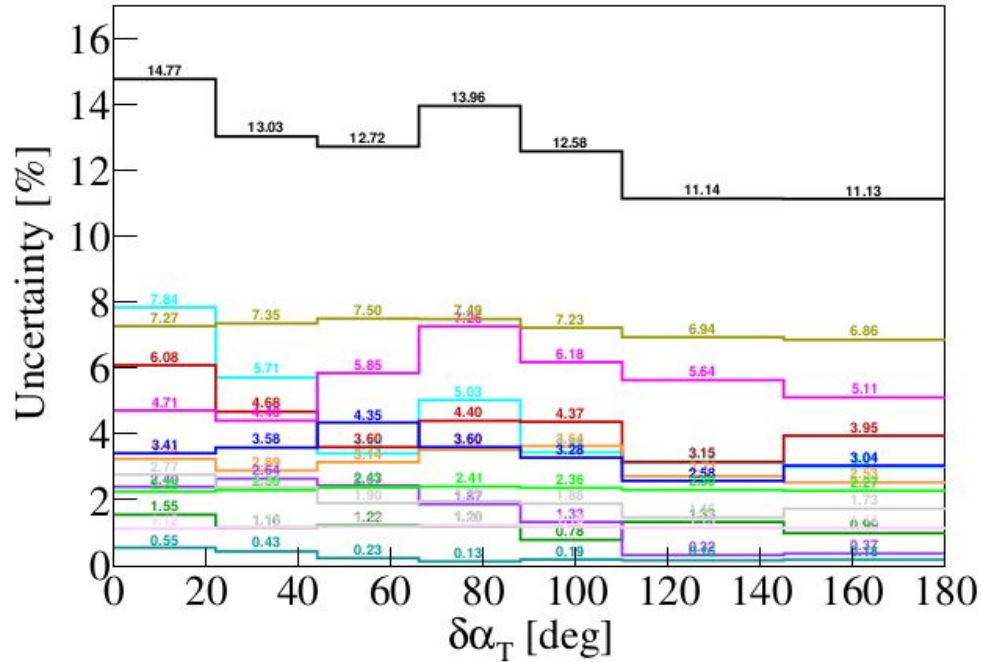


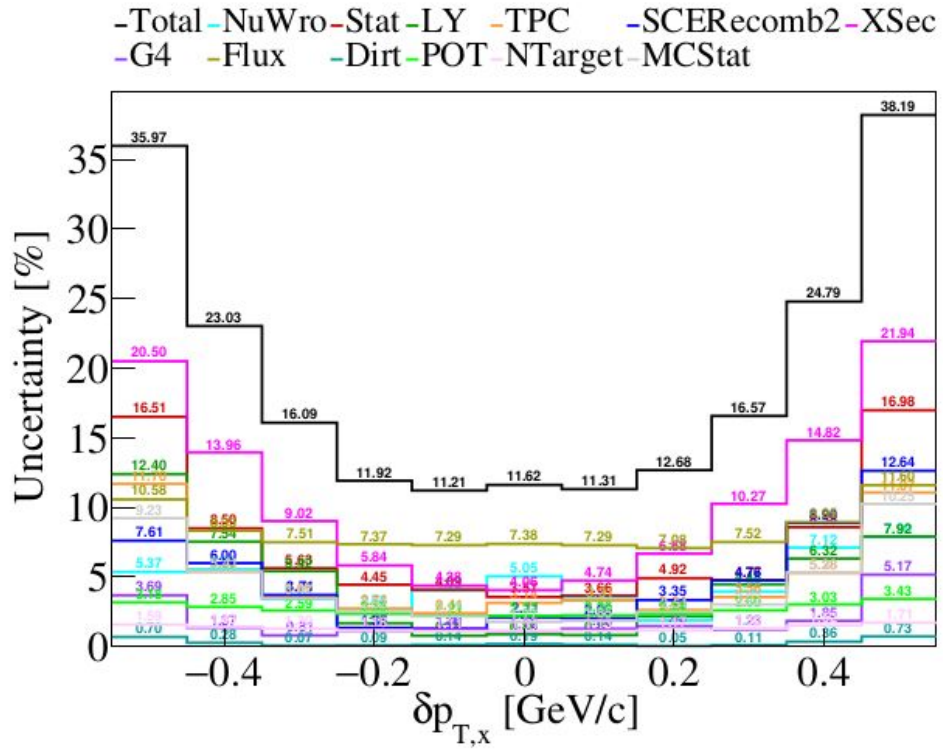
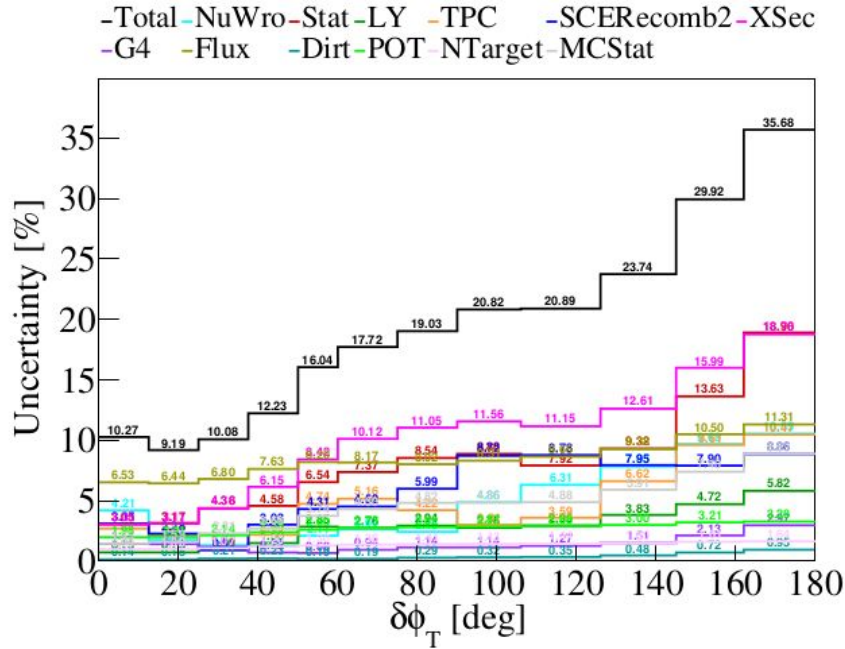
- MEC/RES dominated region
- Similar shapes
- Normalization differences
- Still reasonable χ^2 !

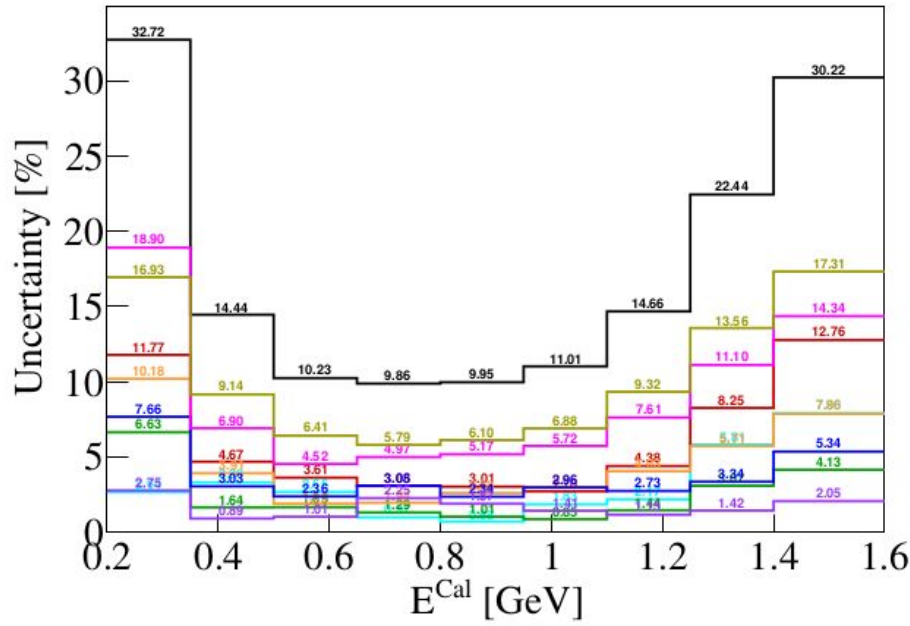
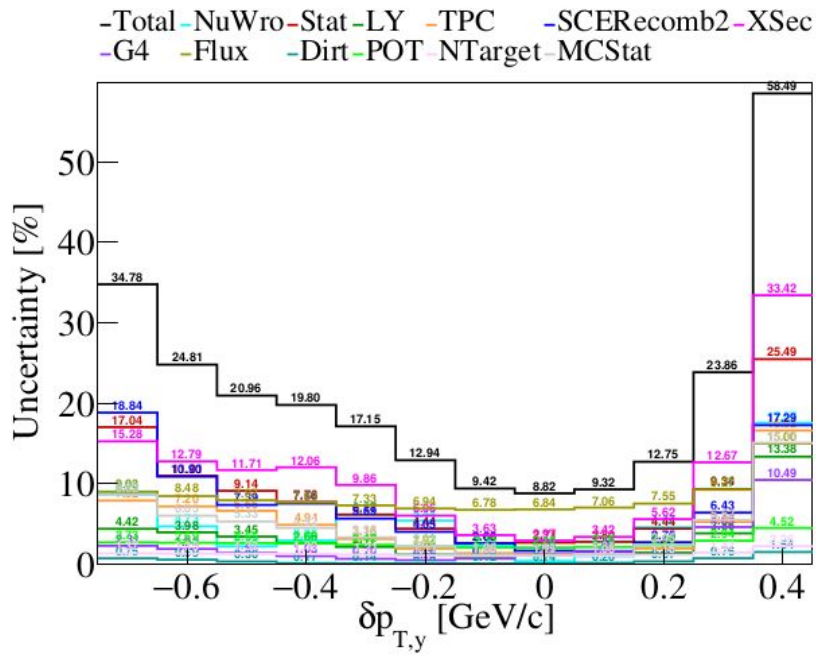
-Total -NuWro -Stat -LY -TPC -SCERecomb2 -XSec
 -G4 -Flux -Dirt -POT -NTarget -MCStat



-Total -NuWro -Stat -LY -TPC -SCERecomb2 -XSec
 -G4 -Flux -Dirt -POT -NTarget -MCStat







Parameter	Description	CV	1σ Uncertainty	Contributing Uncertainty (%)
Quasi-Elastic Parameters				
MaCCQE	CCQE axial mass	1.10 GeV	± 0.1 GeV	0.038
RPA CCQE	Strength of the RPA correction	0.151	± 0.4	2.094
MaNCEL	Axial mass for NCEL	0.961242 GeV	$\pm 25\%$	0.348
EtaNCEL	Empirical parameter used to account for sea quark contribution to NCEL form factor	0.12	$\pm 30\%$	0.010
AxFCCQEshape	Parametrisation of the nucleon axial form factor	Dipole	z-expansion	0.022
VecFCCQEshape	Parametrisation of the nucleon vector form factors	BBA07	Dipole	0.051
MEC Parameters				
NormCCMEC	Energy-independent normalization for CCMEC	1.66	± 0.5	1.832
NormNCMEC	Energy-independent normalization for NCMEC	1	$\pm 20\%$	0.129
FracPNCCMEC	Fraction of initial nucleon pairs that are pn (0 = Valencia)	0	$\pm 20\%$	0.041
FracDeltaCCMEC	Relative contribution of Δ diagrams to total MEC cross section (0 = Valencia)	0	$\pm 30\%$	0.124
XSecShape CCMEC	Changes shape of differential cross section	1.0	0.0	2.273
DecayAngMEC	Changes angular distribution of nucleon cluster	Isotropic	$\cos^2 \vartheta$ in rest frame	0.693
Resonant Parameters				
MaCCRES	CCRES axial mass	1.120 GeV	± 0.2	0.986
MvCCRES	Shape-only CCRES axial mass	0.840 GeV	± 0.1	0.775
MaNCRES	NCRES axial mass	1.120 GeV	± 0.2	0.969
MvNCRES	NCRES vector mass.	0.840 GeV	± 0.1	0.395
ThetaDelta2Npi	Interpolates angular distribution for $\Delta \rightarrow N + \pi$	Rein-Sehgal	Isotropic	1.533
ThetaDelta2NRad	Interpolates angular distribution for $\Delta \rightarrow N + \gamma$	Rein-Sehgal	$\cos^2 \vartheta$	0.016

Parameter	Description	CV	1σ Uncertainty	Contributing Uncertainty (%)
Non-Resonant Parameters				
NonRESBGvpNC1pi	Non-resonant background normalization for νp NC1 π	0.1	± 0.5	0.041
NonRESBGvpNC2pi	Non-resonant background normalization for νp NC2 π	1	± 0.5	0.096
NonRESBGvnNC1pi	Non-resonant background normalization for $\bar{\nu} n$ NC1 π	0.3	± 0.5	0.390
NonRESBGvnNC2pi	Non-resonant background normalization for $\bar{\nu} n$ NC2 π	1	± 0.5	0.022
NonRESBGvbarpNC1pi	Non-resonant background normalization for $\bar{\nu} p$ NC1 π	0.3	± 0.5	0.010
NonRESBGvbarpNC2pi	Non-resonant background normalization for $\bar{\nu} p$ NC2 π	1	± 0.5	0.010
NonRESBGvbarnNC1pi	Non-resonant background normalization for $\bar{\nu} n$ NC1 π	0.1	± 0.5	0.010
NonRESBGvbarnNC2pi	Non-resonant background normalization for $\bar{\nu} n$ NC2 π	1	± 0.5	0.010
NonRESBGvpCC1pi	Non-resonant background normalization for νp CC1 π	0.007713	± 0.5	0.014
NonRESBGvpCC2pi	Non-resonant background normalization for νp CC2 π	0.787999	± 0.5	0.059
NonRESBGvnCC1pi	Non-resonant background normalization for $\bar{\nu} n$ CC1 π	0.127858	± 0.5	0.217
NonRESBGvnCC2pi	Non-resonant background normalization for $\bar{\nu} n$ CC2 π	2.11523	± 0.5	0.079
NonRESBGvbarpCC1pi	Non-resonant background normalization for $\bar{\nu} p$ CC1 π	0.127858	± 0.5	0.013
NonRESBGvbarpCC2pi	Non-resonant background normalization for $\bar{\nu} p$ CC2 π	2.11523	± 0.5	0.010
NonRESBGvbarnCC1pi	Non-resonant background normalization for $\bar{\nu} n$ CC1 π	0.007713	± 0.5	0.010
NonRESBGvbarnCC2pi	Non-resonant background normalization for $\bar{\nu} n$ CC2 π	0.787999	± 0.5	0.010
AhtBY	A _{HT} higher-twist parameter in the Bodek-Yang model scaling variable ξ_w	0.538	± 0.25	0.010
BhtBY	BHT higher-twist parameter in the Bodek-Yang model scaling variable ξ_w	0.305	± 0.25	0.010
CV1uBY	CV1u valence GRV98 PDF correction parameter in the Bodek-Yang model	0.291	± 0.3	0.010
CV2uBY	CV2u valence GRV98 PDF correction parameter in the Bodek-Yang model	0.189	± 0.4	0.010

Hadronisation Parameters

AGKYxF1pi	Hadronization parameter, applicable to true DIS interactions only	-0.385	± 0.2	0.108
AGKYpT1pi	Hadronization parameter, applicable to true DIS interactions only	1/6.625	± 0.03	0.034

Final State Interaction Parameters

MFP _{π}	π mean free path	0	± 0.2	0.032
MFP _N	Nucleon mean free path	0	± 0.2	1.212
FrCEx _{π}	Fractional cross section for π charge exchange	0	± 0.5	0.159
FrInel _{π}	Fractional cross section for π inelastic scattering	0	± 0.4	0.133
FrAbs _{π}	Fractional cross section for π absorption	0	± 0.3	0.906
FrCEx _N	Fractional cross section for nucleon charge exchange	0	± 0.2	0.953
FrInel _N	Fractional cross section for nucleon inelastic scattering	0	± 0.5	0.289
FrAbs _N	Fractional cross section for nucleon absorption	0	± 0.4	0.906

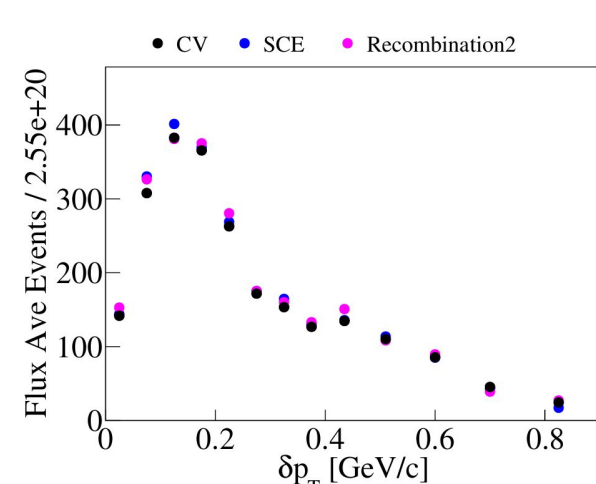
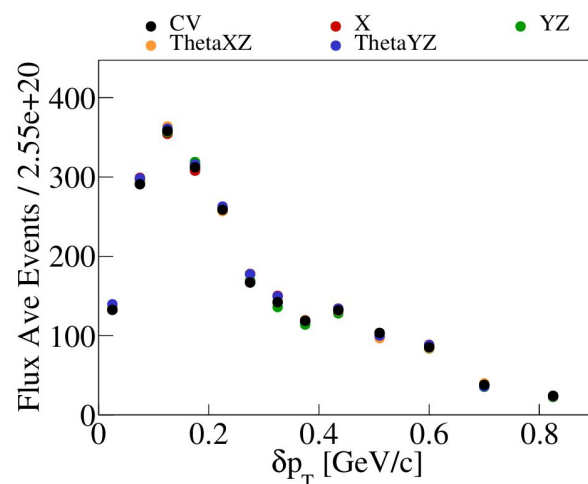
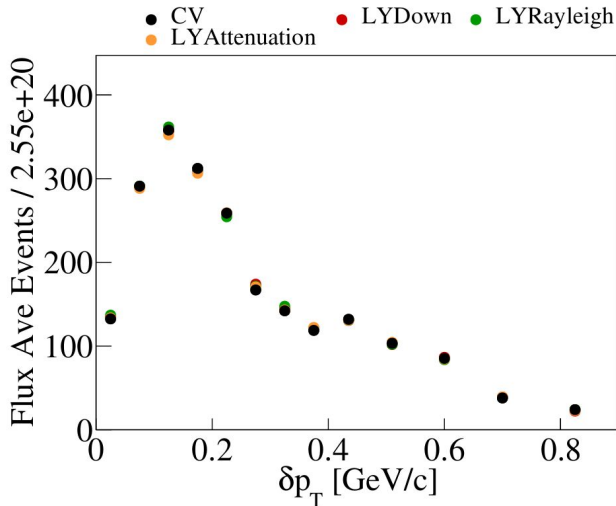
Delta Resonant Decay Parameters

RDecBRigamma	Normalization for $\Delta \rightarrow \gamma$ decays	Nominal BR	± 0.5	0.042
RDecBRIeta	Normalization for $\Delta \rightarrow \eta$ decays	Nominal BR	± 0.5	0.513

Coherent Parameters

NormCCCOH	Scaling factor for CCCOH π production total cross section	Nominal	100% increase	0.027
NormNCCOH	Scaling factor for NCCOH π production total cross section	Nominal	100% increase	0.016

Variation	Description
Wire Mod x position	Wire modification of x position
Wire Mod (y,z) position	Wire modification of (y,z) position
Wire Mod θ_{XZ}	Wire modification of angle in XZ plane
Wire Mod θ_{YZ}	Wire modification of angle in YZ plane
Light Yield Attenuation	Attenuation of LY response in detector over time
Light Yield Down	Turn down the light yield in the detector by 25%
Light Yield Rayleigh	Increase Rayleigh scattering length from 60 cm to 90 cm
Recombination	Reduce value of β' in the Modified Box Model
SCE	Use an alternative Space Charge Map



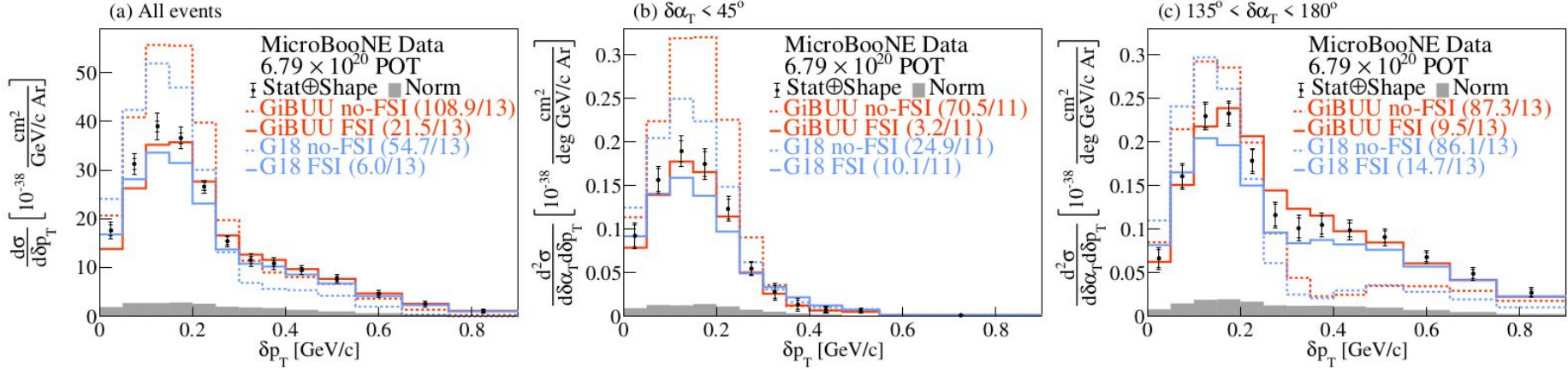


FIG. 1. The flux-integrated (a) single- and (b-c) double- (in $\delta\alpha_T$ bins) differential CC1p0 π cross sections as a function of the transverse missing momentum δp_T . Inner and outer error bars show the statistical and total (statistical and shape systematic) uncertainty at the 1σ , or 68%, confidence level. The gray band shows the separate normalization systematic uncertainty. Colored lines show the results of theoretical cross section calculations with (solid line) and without (dashed line) FSI based on the `GENIE` (blue) and `GiBUU` (orange) event generators.

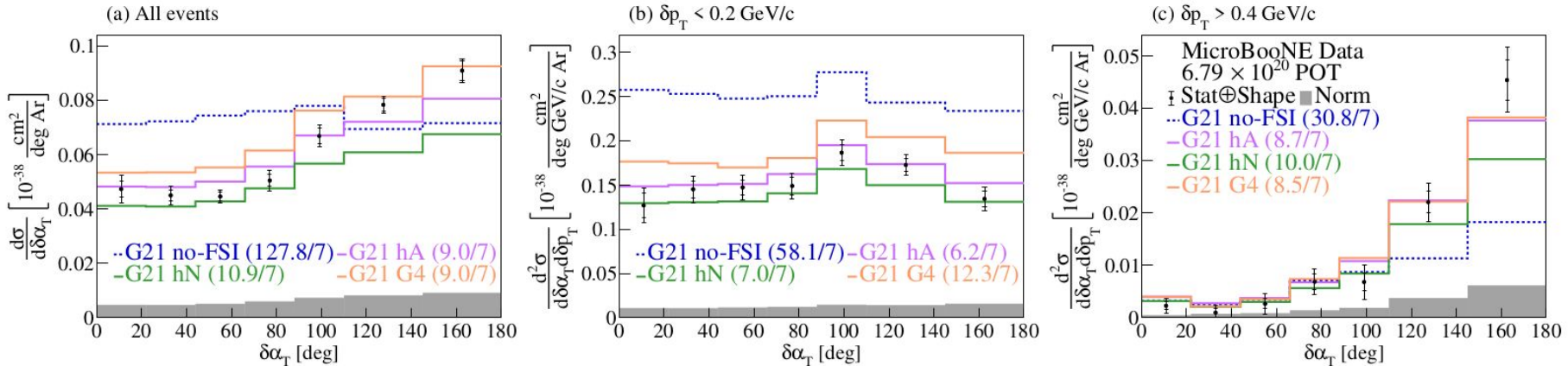


FIG. 2. The flux-integrated (a) single- and (b-c) double- (in δp_T bins) differential CC1p0 π cross sections as a function of the angle $\delta\alpha_T$. Inner and outer error bars show the statistical and total (statistical and shape systematic) uncertainty at the 1σ , or 68%, confidence level. The gray band shows the separate normalization systematic uncertainty. Colored lines show the results of theoretical cross section calculations with a number of FSI-modeling choices based on the GENIE event generator.

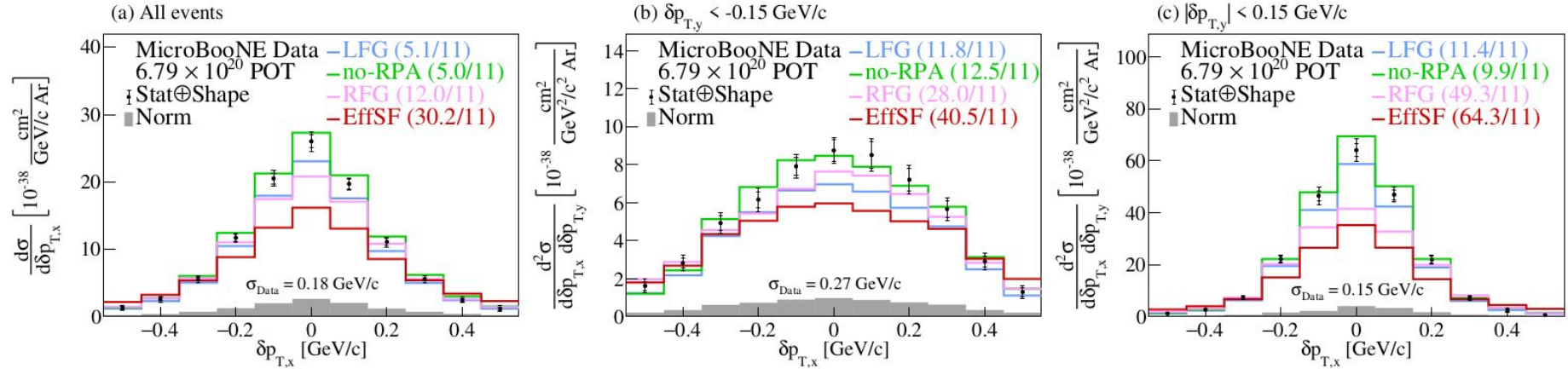


FIG. 3. The flux-integrated (a) single- and (b-c) double- (in $\delta p_{T,y}$ bins) differential CC1p0 π cross sections as a function of the transverse three-momentum transfer component, $\delta p_{T,x}$. Inner and outer error bars show the statistical and total (statistical and shape systematic) uncertainty at the 1σ , or 68%, confidence level. The gray band shows the separate normalization systematic uncertainty. Colored lines show the results of theoretical cross section calculations with a number of event generators. The standard deviation (σ_{Data}) of a Gaussian fit to the data is shown on each panel.

VI. MODELING CONFIGURATIONS

The nominal MC neutrino interaction prediction (**G18**) uses the local Fermi gas (LFG) model [50], the Nieves CCQE scattering prescription [51] which includes Coulomb corrections for the outgoing muon [52] and random phase approximation (RPA) corrections [53]. Additionally, it uses the Nieves MEC model [54], the KLN-BS RES [55–58] and Berger-Sehgal coherent (COH) [59] scattering models, the hA2018 FSI model [60], and MicroBooNE-specific tuning of model parameters [38].

Our results are also compared to a number of alternative event generators. **GiBUU** 2021 (**GiBUU**) uses similar models, but they are implemented in a coherent way by solving the Boltzmann-Uehling-Uhlenbeck transport equation [61]. The modeling includes the LFG model [50], a standard CCQE expression [62], an empirical MEC model and a dedicated spin dependent resonance amplitude calculation following the MAID analysis [61]. The DIS model is from PYTHIA [63]. **GiBUU**'s FSI treatment propagates the hadrons through the residual nucleus in a nuclear potential which is consistent with the initial state. **NuWro** v19.02.2 (**NuWro**) uses the LFG model [50], the Llewellyn Smith model for QE events [64], the Nieves model for MEC events [65], the Adler-Rarita-Schwinger formalism to calculate the Δ resonance explicitly [58], the BS COH [59] scattering model and an intranuclear cascade model for FSI [65]. **NEUT** v5.4.0 (**NEUT**) uses the LFG model [50], the Nieves CCQE scattering prescription [51], the Nieves MEC model [54], the BS RES [55–58] and BS COH [59] scattering models, and FSI with Oset medium corrections for pions [35, 36].

In addition to the alternative event generators, our results are compared to a number of different **GENIE** configurations. These include an older version, **GENIE** v2.12.10 (Gv2) [35, 36], which uses the Bodek-Ritchie Fermi Gas model, the Llewellyn Smith CCQE scattering prescription [64], the empirical MEC model [66], a Rein-Sehgal RES and COH scattering model [67], and a data driven FSI model denoted as “hA” [68]. Another model, “Untuned”, uses the **GENIE** v3.0.6 G18_10a_02_11a configuration without additional MicroBooNE-specific tuning. Finally, the newly added theory-driven **GENIE** v3.2.0 G21_11b_00_000 configuration (**G21**) is shown. This includes the SuSAv2 prediction for the QE and MEC scattering parts [69] and the hN2018 FSI model [70]. The modeling options for RES, DIS, and COH interactions are the same as for **G18**.

To quantify the data-simulation agreement, the χ^2/bins ratio data comparison for each generator is shown on all the figures and is calculated by taking into account the total covariance matrix. Ratios close to unity are indicative of a sufficiently accurate modeling performance. Theoretical uncertainties on the models themselves are not included.

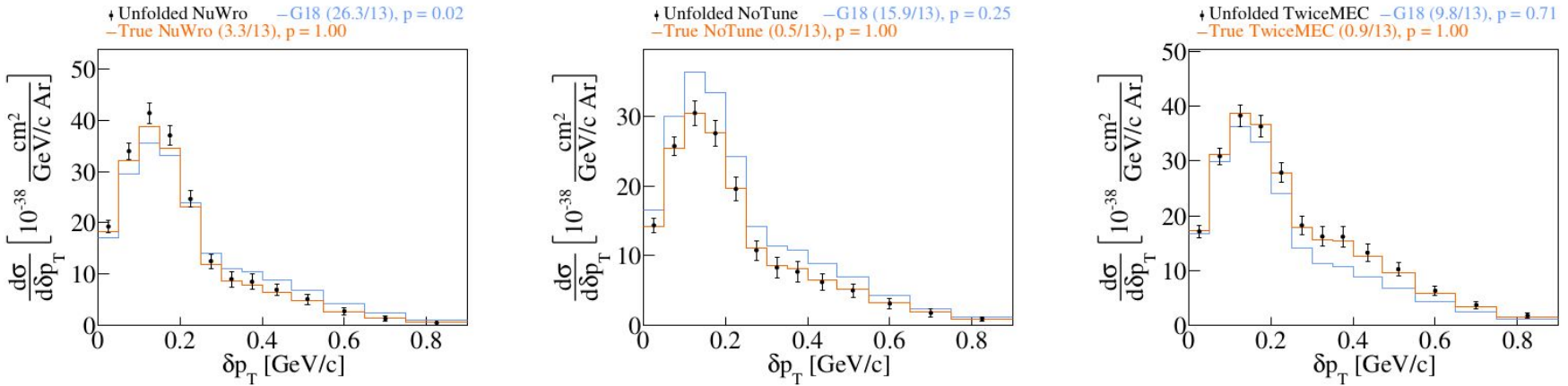


FIG. 1. Fake data studies for δp_T using (left) NuWro, (center) GENIE without the MicroBooNE tune (NoTune), and (right) twice the weights for MEC events (TwiceMEC) as fake data samples.

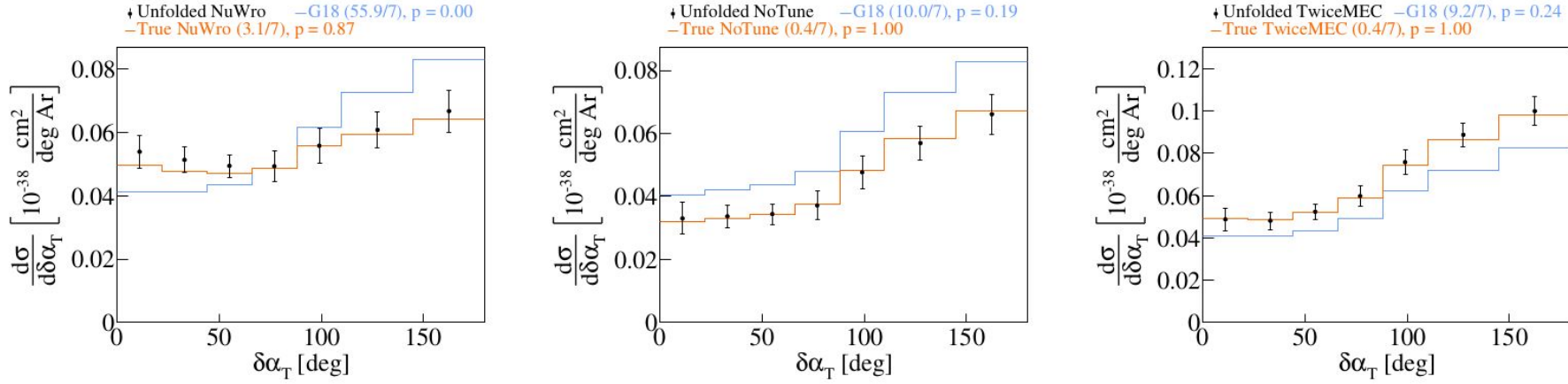


FIG. 2. Fake data studies for $\delta\alpha_T$ using (left) NuWro, (center) GENIE without the MicroBooNE tune (NoTune), and (right) twice the weights for MEC events (TwiceMEC) as fake data samples.

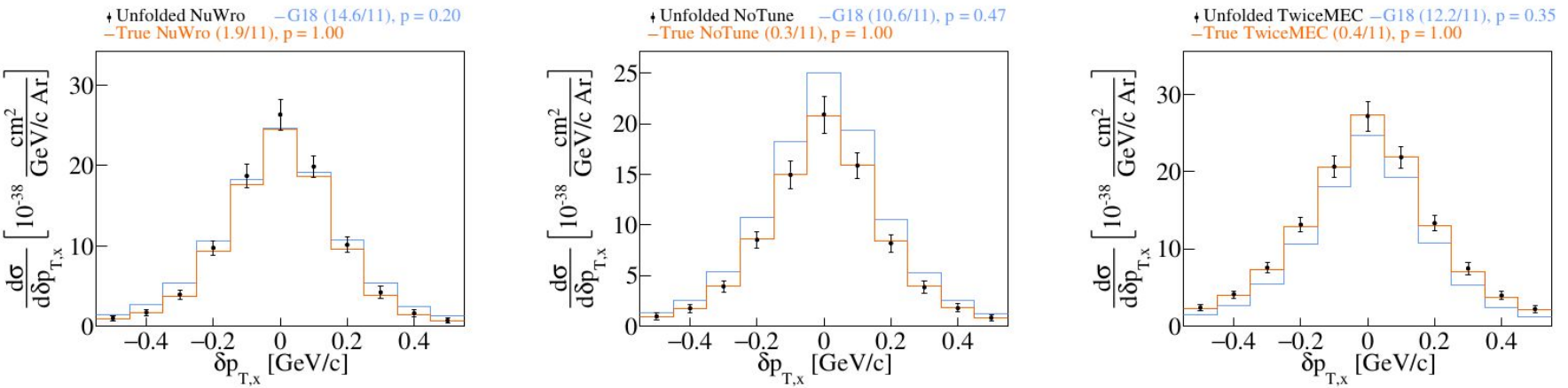


FIG. 3. Fake data studies for $\delta p_{T,x}$ using (left) NuWro, (center) GENIE without the MicroBooNE tune (NoTune), and (right) twice the weights for MEC events (TwiceMEC) as fake data samples.

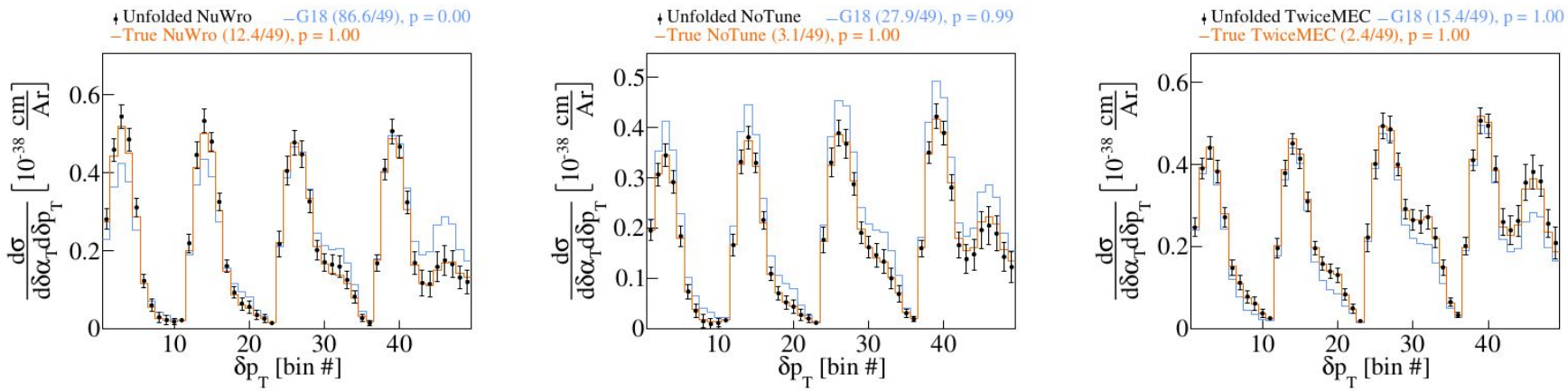


FIG. 4. Fake data studies for δp_T in $\delta\alpha_T$ bins using (left) NuWro, (center) GENIE without the MicroBooNE tune (NoTune), and (right) twice the weights for MEC events (TwiceMEC) as fake data samples.

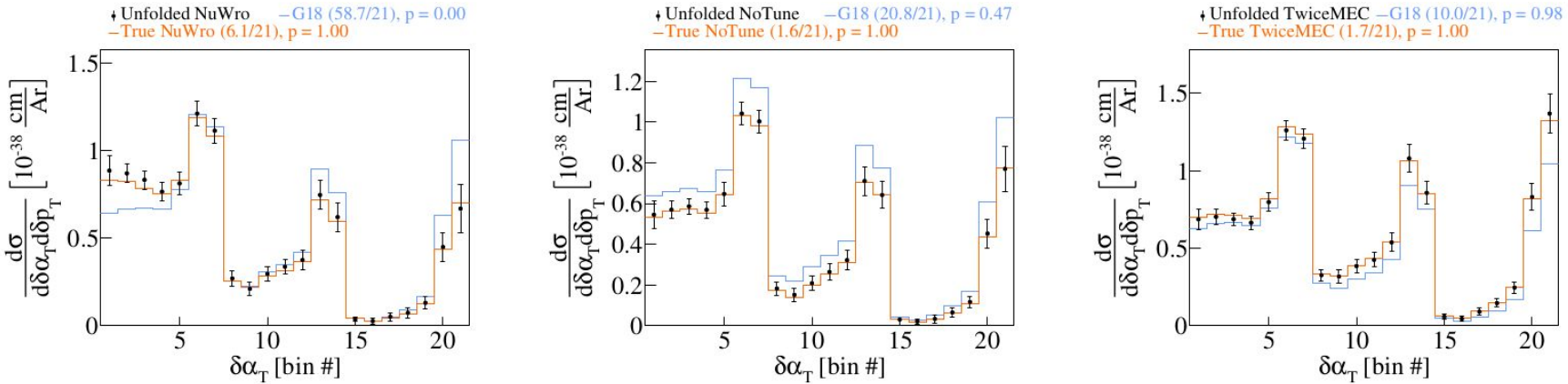


FIG. 5. Fake data studies for $\delta\alpha_T$ in δp_T bins using (left) NuWro, (center) GENIE without the MicroBooNE tune (NoTune), and (right) twice the weights for MEC events (TwiceMEC) as fake data samples.

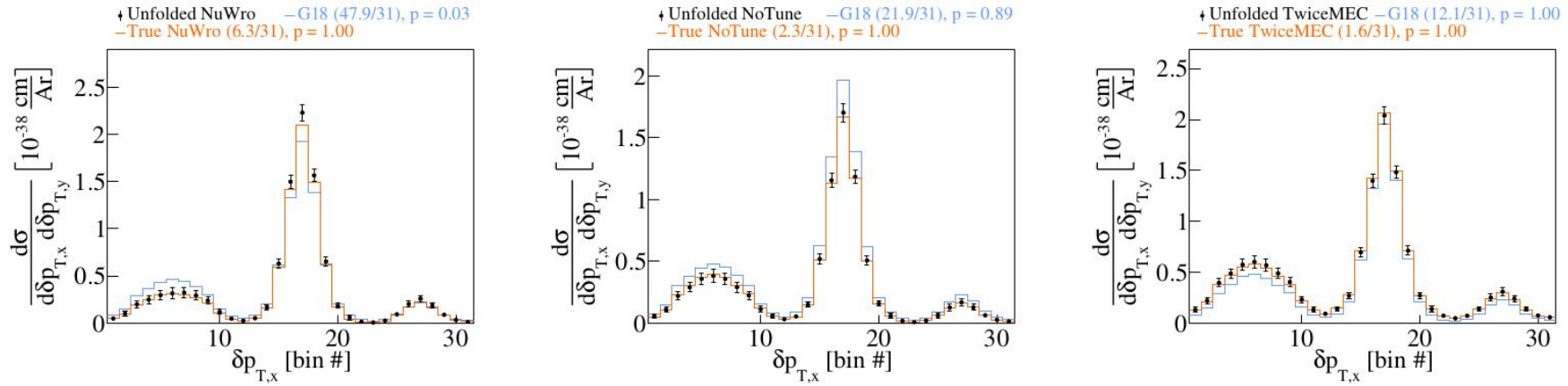


FIG. 6. Fake data studies for $\delta p_{T,x}$ in $\delta p_{T,y}$ bins using (left) NuWro, (center) GENIE without the MicroBooNE tune (NoTune), and (right) twice the weights for MEC events (TwiceMEC) as fake data samples.

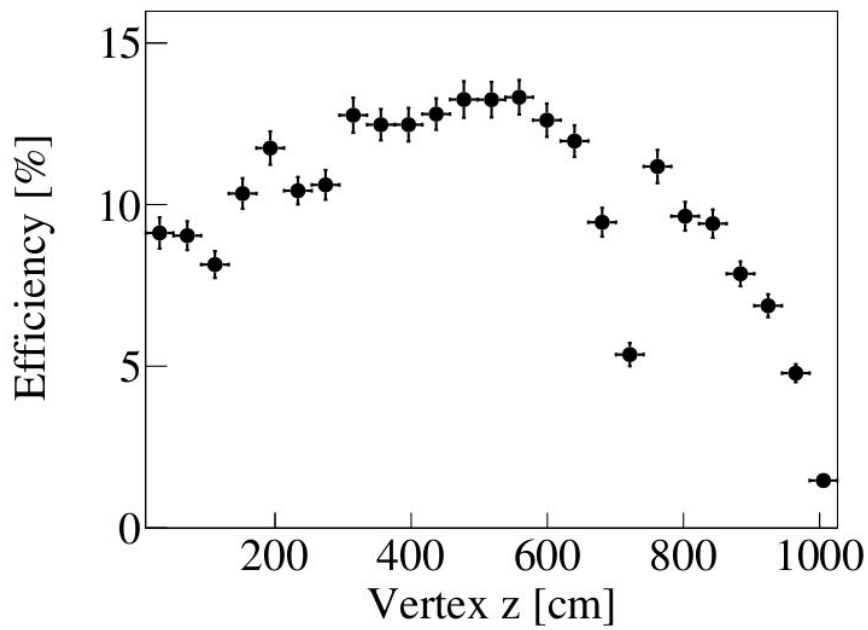
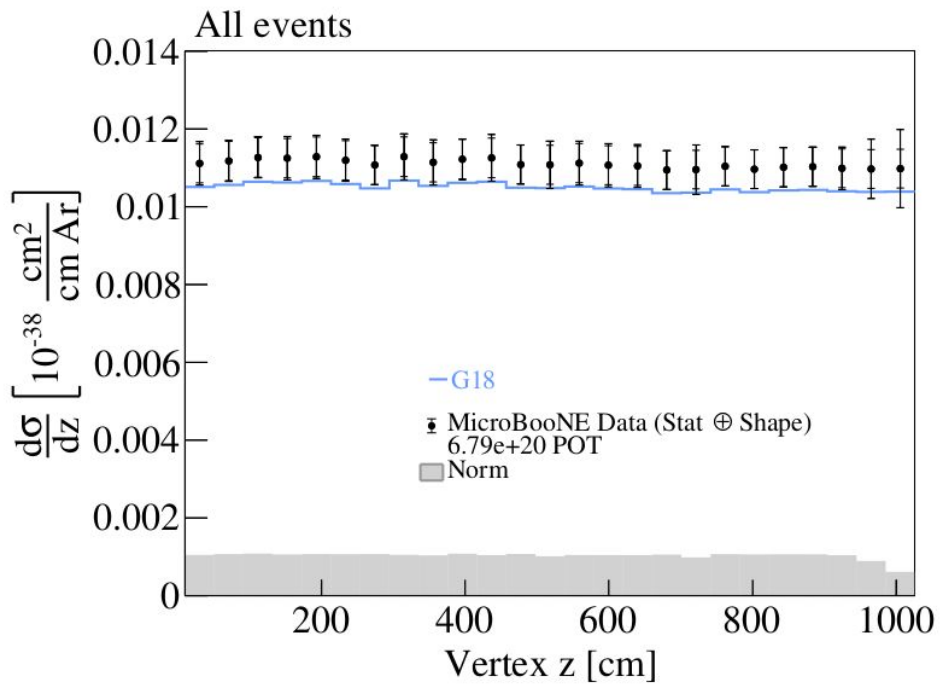


FIG. 7. (Left) extracted cross section as a function of the vertex z distribution. (Right) vertex z efficiency function.

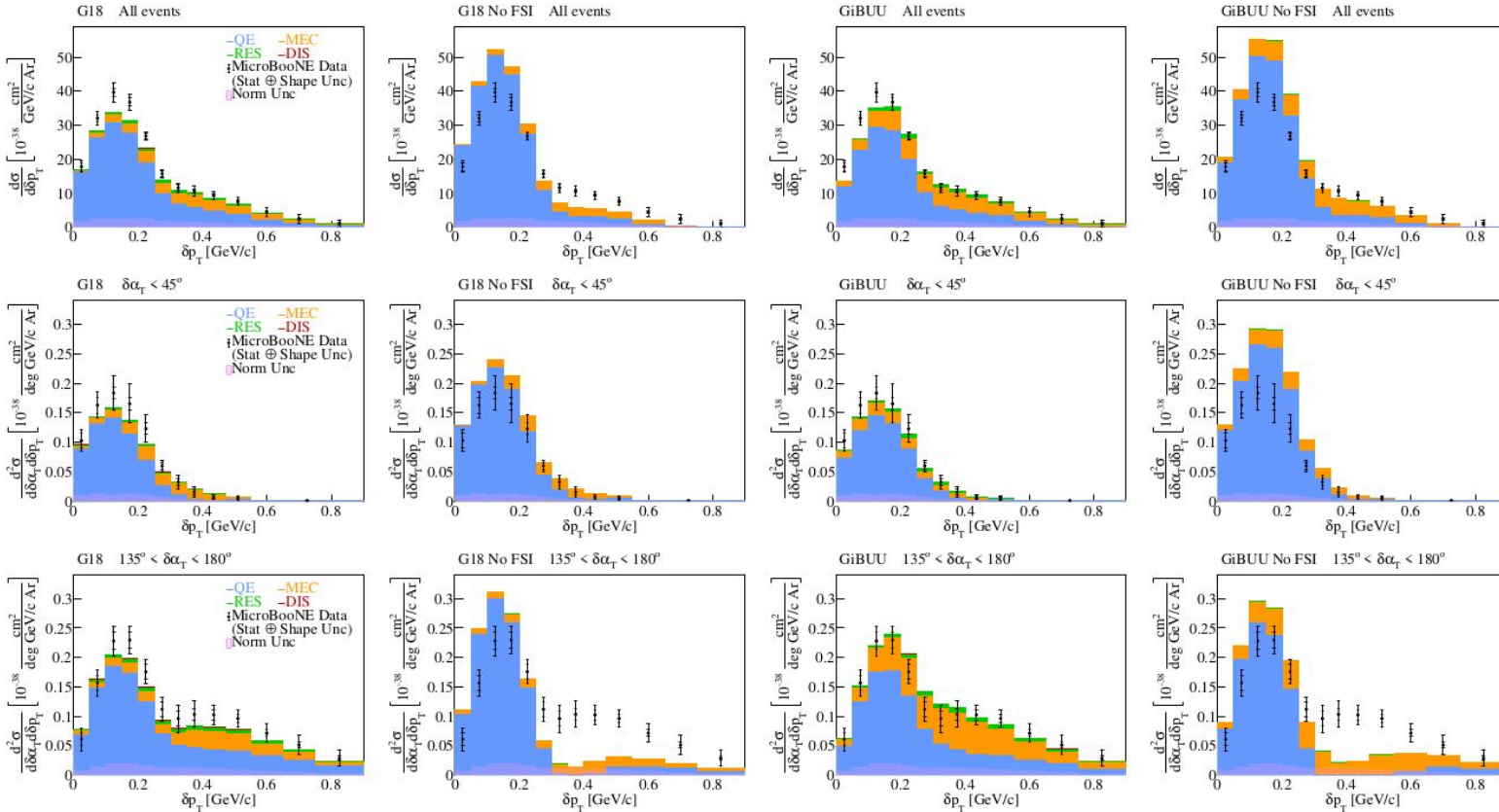


FIG. 8. Cross section interaction breakdown for (top) all the selected events, (middle) events with $\delta\alpha_T < 45^\circ$, and (bottom) events with $135^\circ < \delta\alpha_T < 180^\circ$. The breakdown is shown for (first column) the G18 configuration with FSI effects, (second column) the G18 configuration without FSI effects, (third column) GiB with FSI effects, and (forth column) GiB without FSI effects.

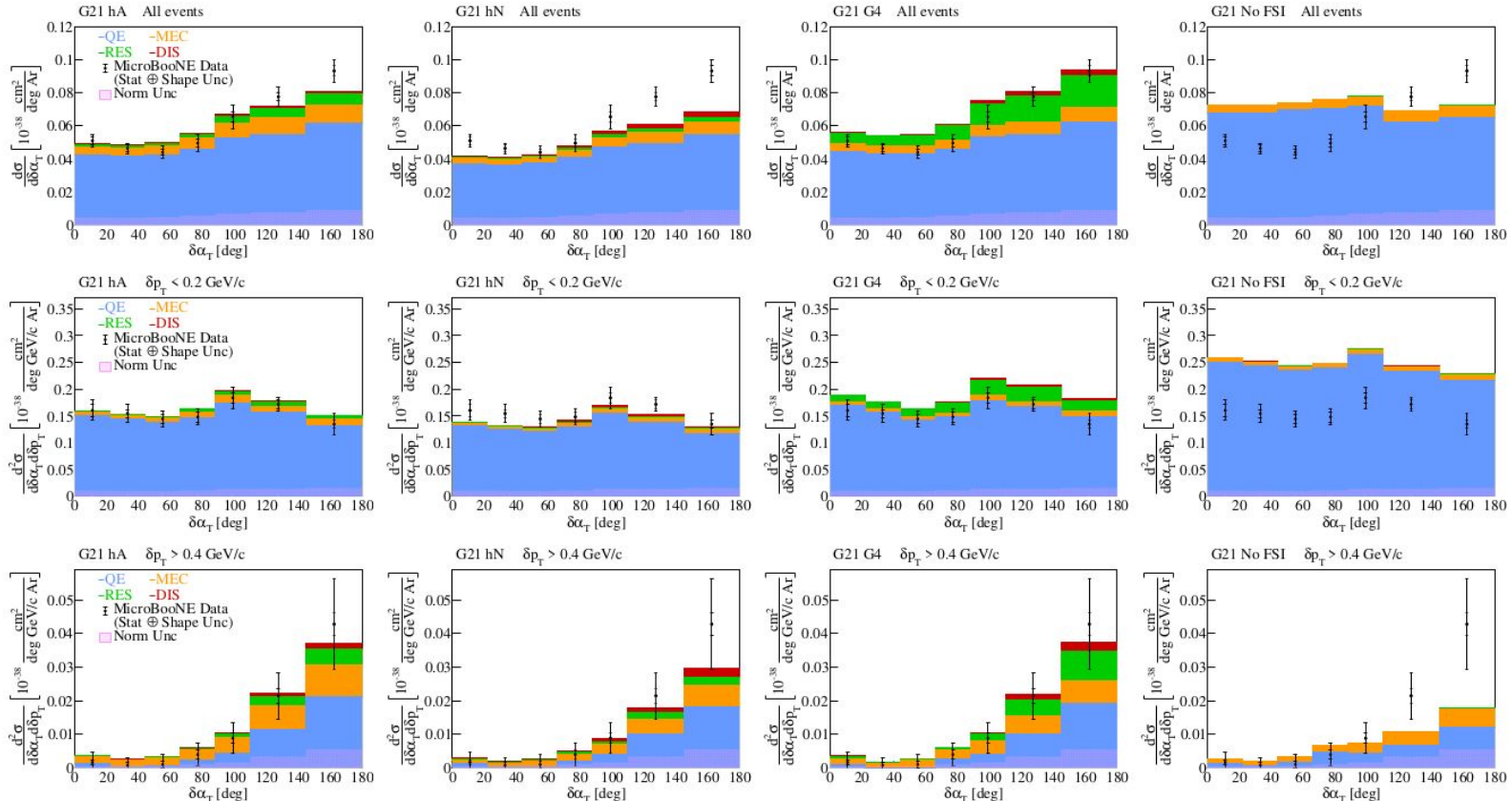


FIG. 9. Cross section interaction breakdown for (top) all the selected events, (middle) events with $\delta p_T < 0.2 \text{ GeV}/c$, and (bottom) events with $\delta p_T > 0.4 \text{ GeV}/c$. The breakdown is shown for (first column) the G21 hA configuration with the hA2018 FSI model, (second column) the G21 hN configuration with the hN FSI model, (third column) the G21 G4 configuration with the G4 FSI model, and (forth column) the G21 No FSI configuration without FSI effects.

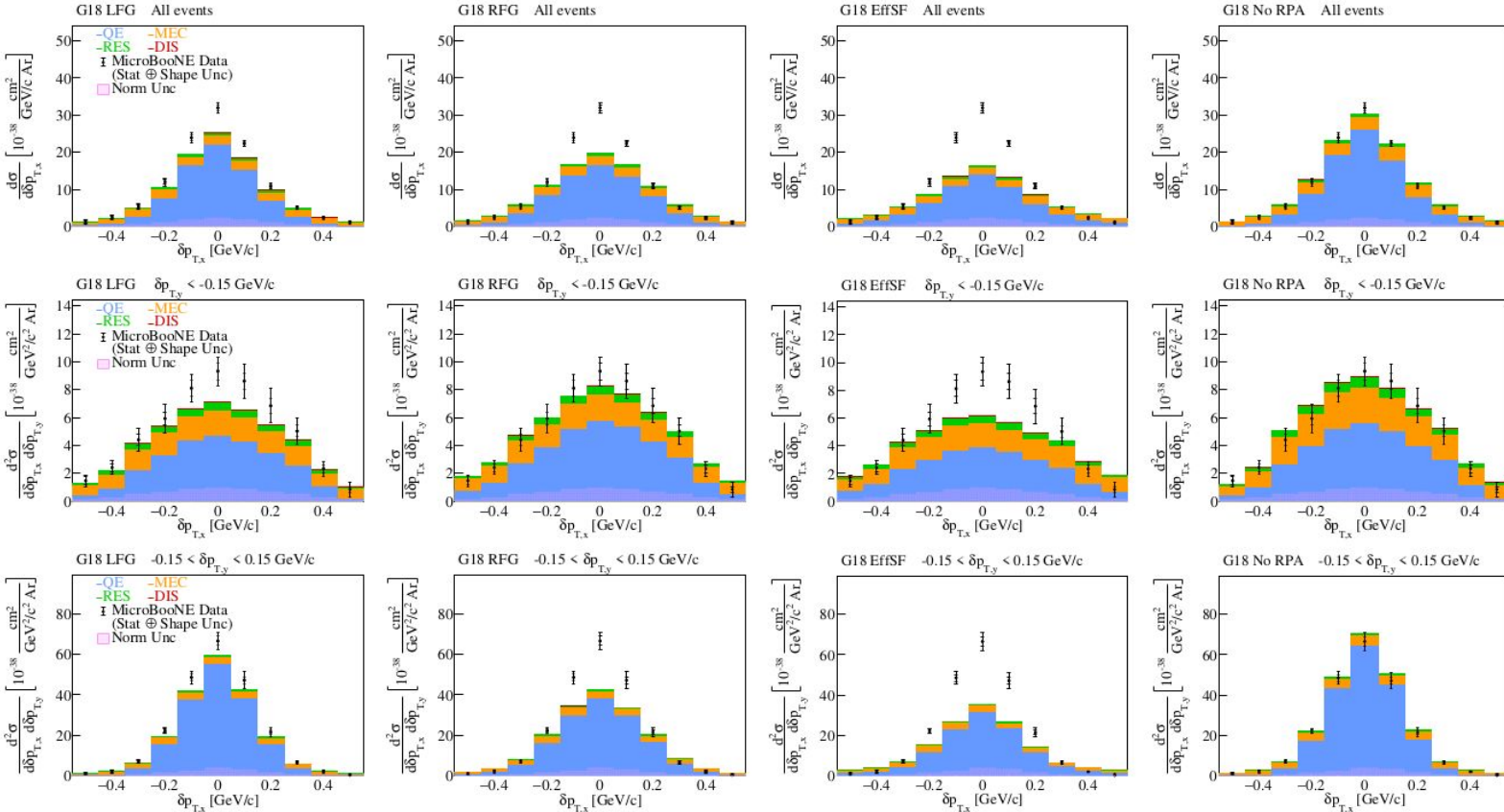


FIG. 10. Cross section interaction breakdown for (top) all the selected events, (middle) events with $\delta p_{T,y} < -0.15 \text{ GeV}/c$, and (bottom) events with $-0.15 < \delta p_{T,y} < 0.15 \text{ GeV}/c$. The breakdown is shown for (first column) the G18 LFG configuration, (second column) the G18 RFG configuration, (third column) the G18 EffSF configuration, and (forth column) the G18 No RPA configuration.

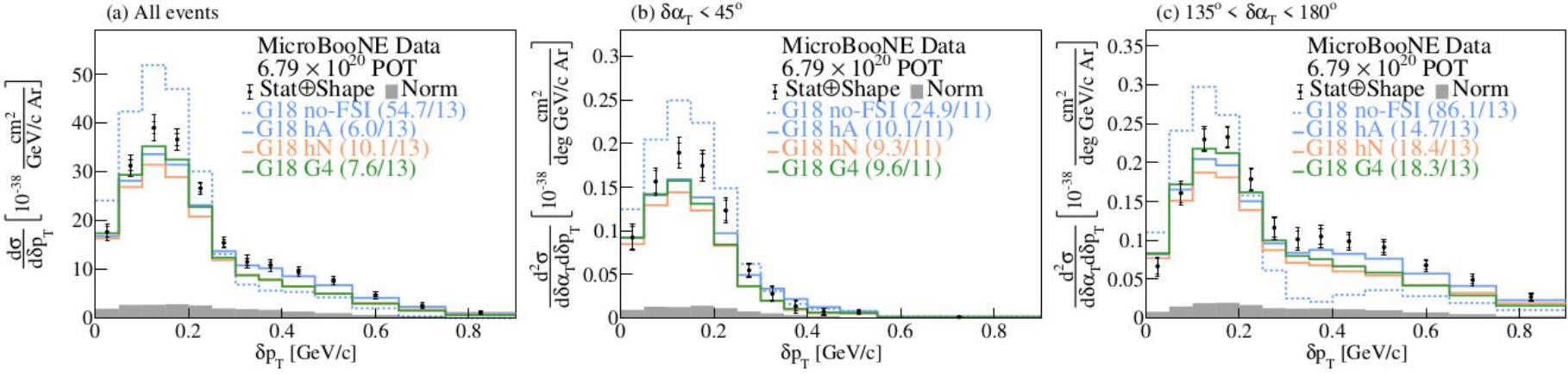


FIG. 11. The flux-integrated (a) single- and (b-c) double- (in $\delta\alpha_T$ bins) differential CC1p0 π cross sections as a function of the transverse missing momentum, δp_T . Inner and outer error bars show the statistical and total (statistical and shape systematic) uncertainty at the 1σ , or 68%, confidence level. The gray band shows the separate normalization systematic uncertainty. Colored lines show the results of theoretical cross section calculations with a number of G21 FSI modeling variations.

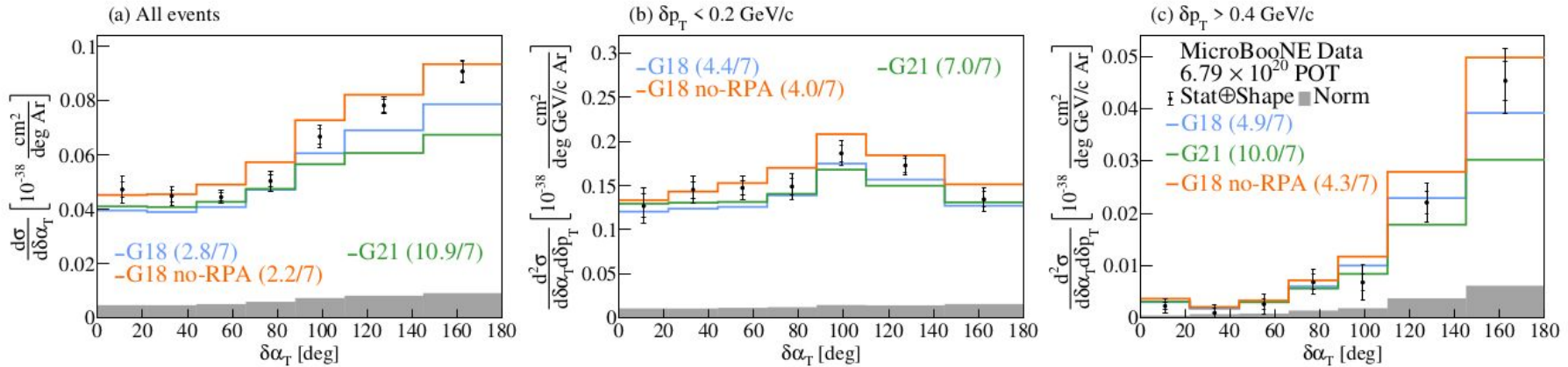


FIG. 12. The flux-integrated (a) single- and (b-c) double- (in δp_T bins) differential CC1p0 π cross sections as a function of the angle $\delta\alpha_T$. Inner and outer error bars show the statistical and total (statistical and shape systematic) uncertainty at the 1σ , or 68%, confidence level. The gray band shows the separate normalization systematic uncertainty. Colored lines show the results of theoretical cross section calculations with a number of QE-modeling choices based on the GENIE event generator.

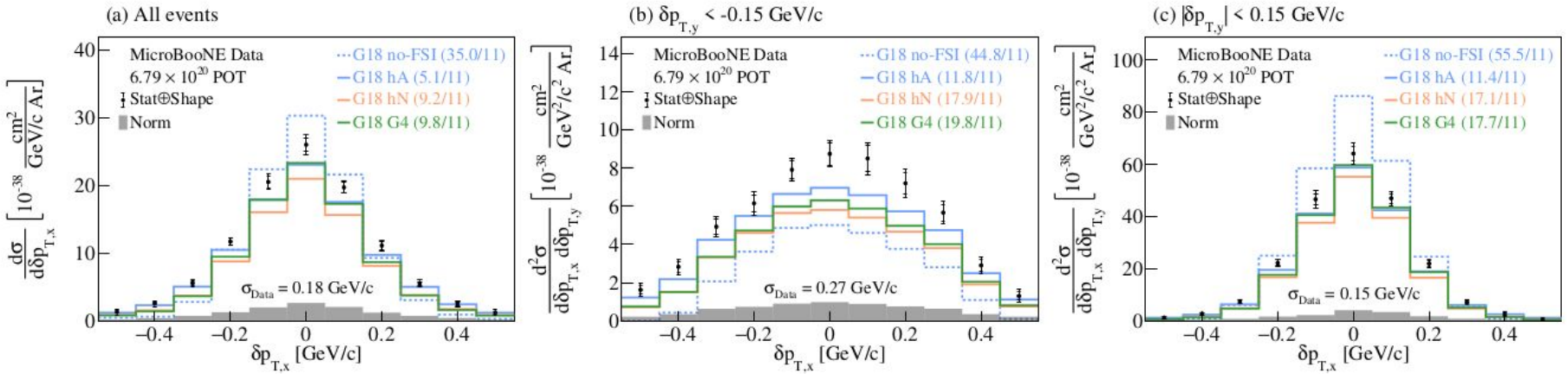
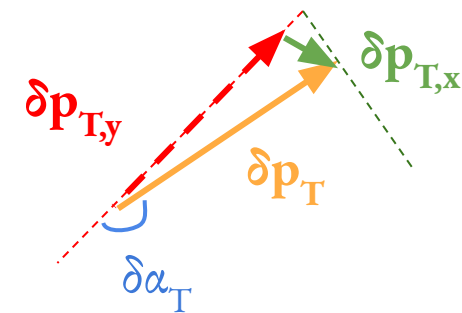
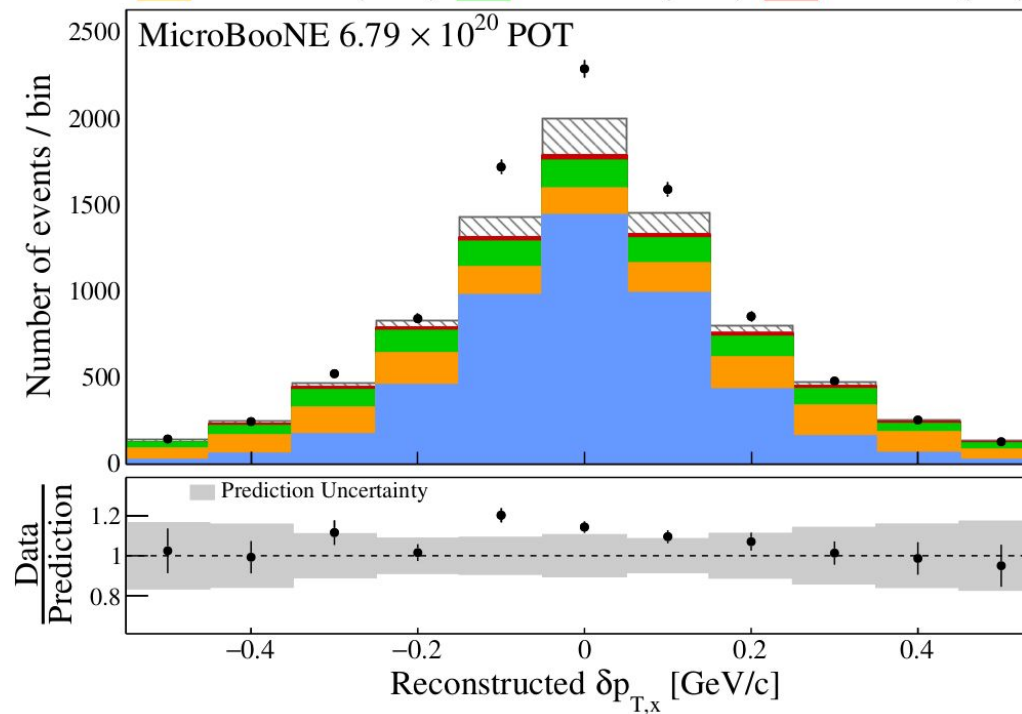


FIG. 13. The flux-integrated (a) single- and (b-c) double- (in $\delta p_{T,y}$ bins) differential CC1p0 π cross sections as a function of the transverse three-momentum transfer component, $\delta p_{T,x}$. Inner and outer error bars show the statistical and total (statistical and shape systematic) uncertainty at the 1σ , or 68%, confidence level. The gray band shows the separate normalization systematic uncertainty. Colored lines show the results of theoretical cross section calculations with a number of G18 FSI modeling variations. The standard deviation (σ_{Data}) of a Gaussian fit to the data is shown on each panel.

Transverse Component $\delta p_{T,x}$

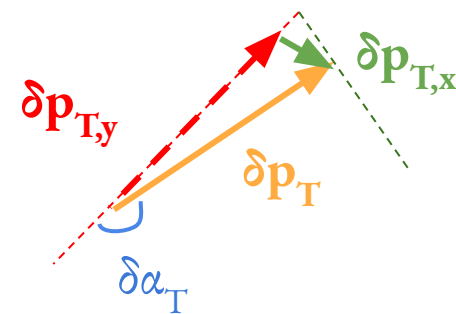
BNB Data
MC MEC (19%)
Cosmic (8%)
MC RES (13%)
MC QE (58%)
MC DIS (2%)



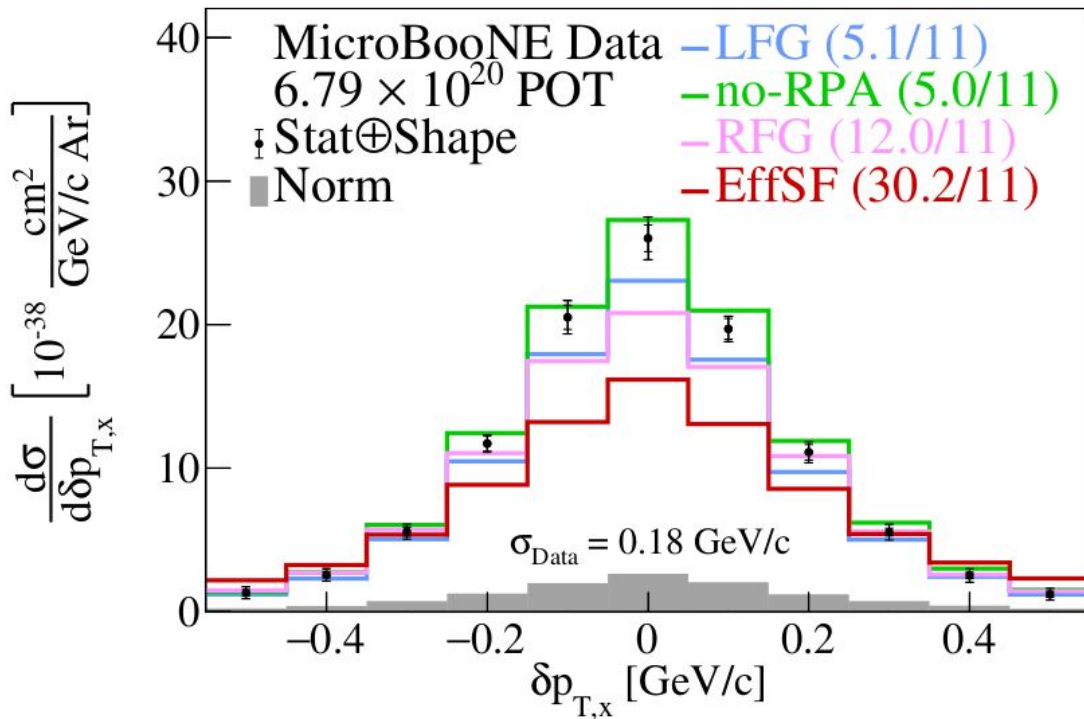
$$\delta p_{T,x} = \delta p_T \cdot \sin \delta \alpha_T$$

- Symmetric around 0 GeV/c
- QE dominance in central region
- MEC/RES events primarily in the tail

Transverse Component $\delta p_{T,x}$ Cross Section



All events

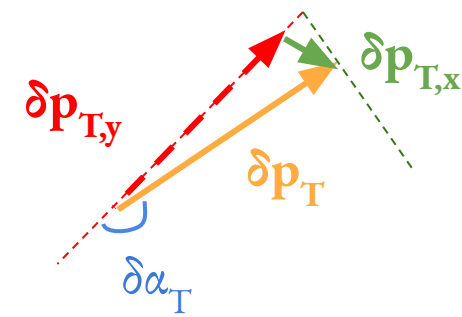
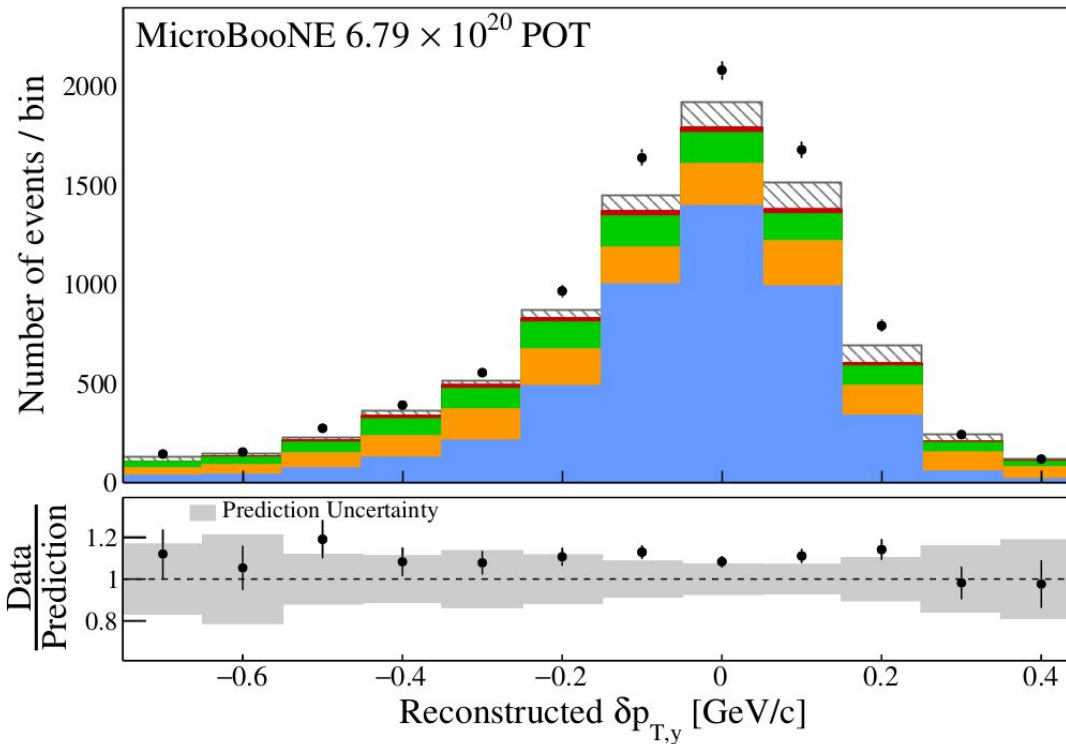


$$\delta p_{T,x} = \delta p_T \cdot \sin \delta \alpha_T$$

- G18 LFG = GENIE v3.0.6
G18_10a_02_11a (G18) + uB Tune
with local Fermi gas
- G18 no-RPA = G18 w/o RPA effects
- G18 RFG = G18 with relativistic
Fermi gas (RFG)
- G18 EffSF = G18 with spectral
function (EffSF)

Longitudinal Component $\delta p_{T,y}$

◆ BNB Data Cosmic (8%) MC QE (58%)
■ MC MEC (19%) MC RES (13%) MC DIS (2%)

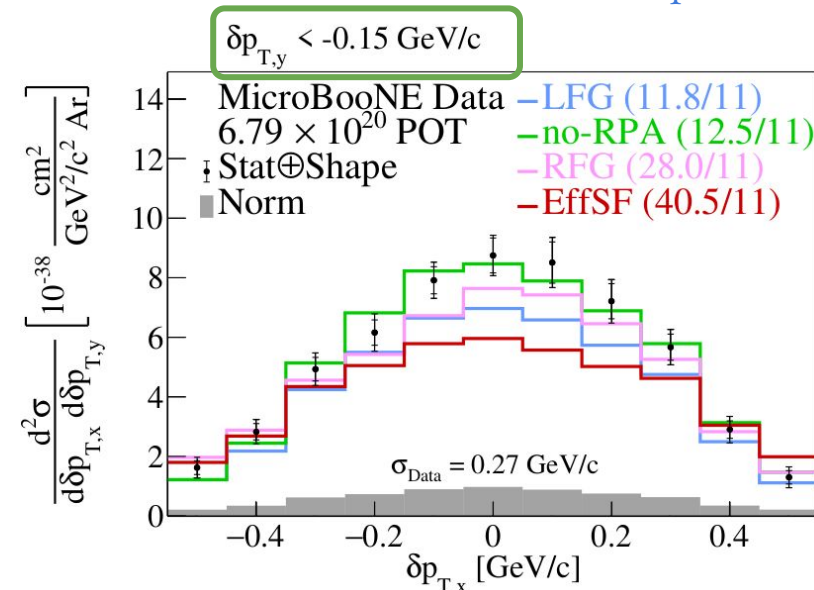
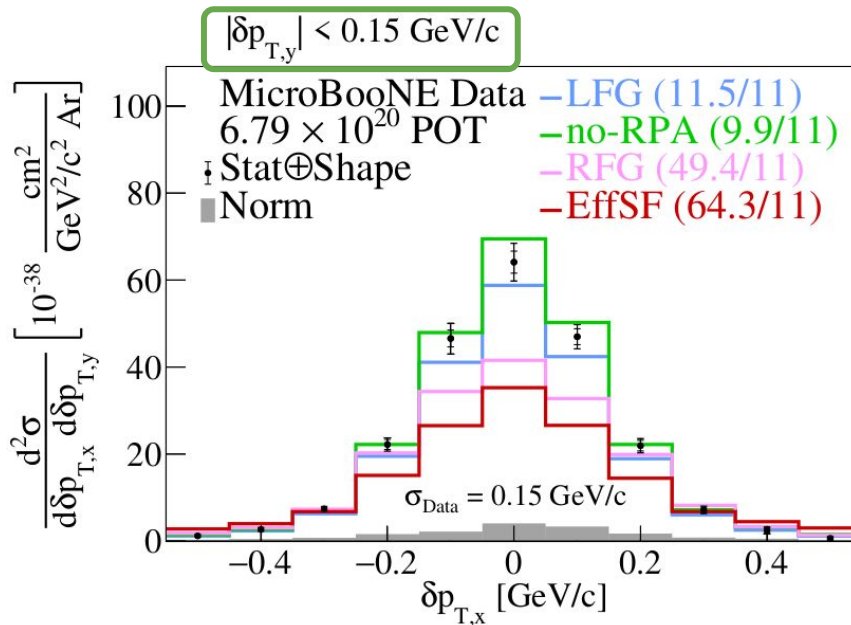
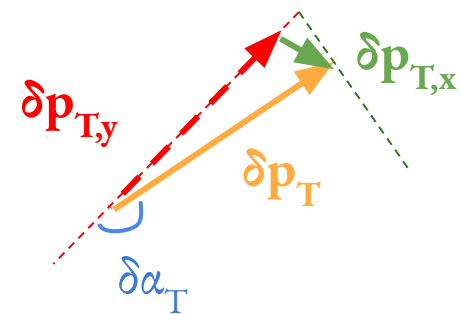


$$\delta p_{T,y} = \delta p_T \cdot \cos\delta\alpha_T$$

- Asymmetric due to $\delta\alpha_T$ enhancement at $\sim 180^\circ$
- **QE** dominance in central region
- Spread of tail sensitive to FSI strength & **MEC/RES**

High Statistics→Into the Multiverse!

- First neutrino-argon differential cross section in TKI variables
- Sensitive to initial nucleon motion & proton FSI modeling



CCQE-like vs TKI

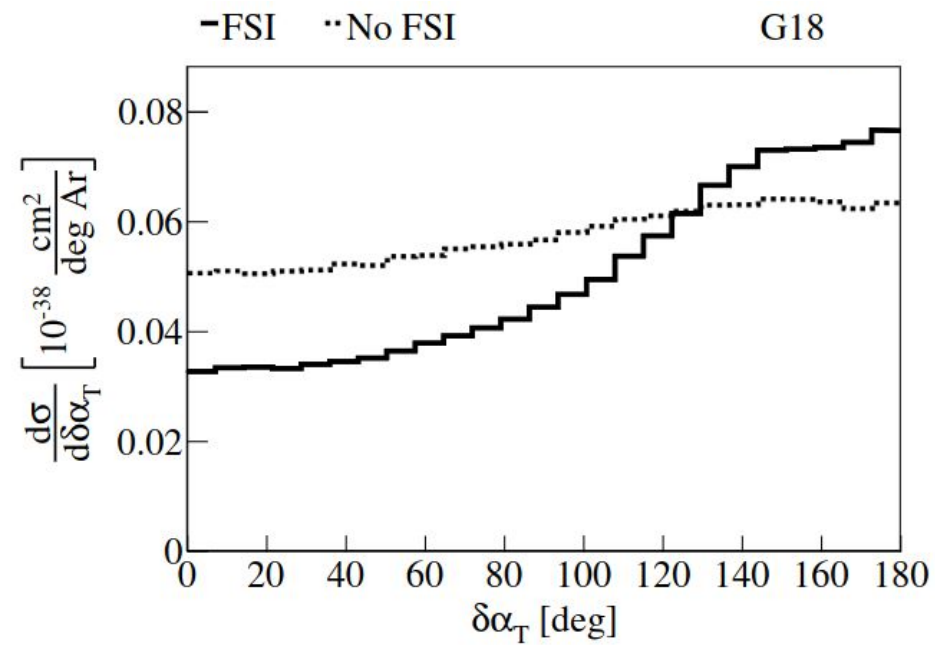
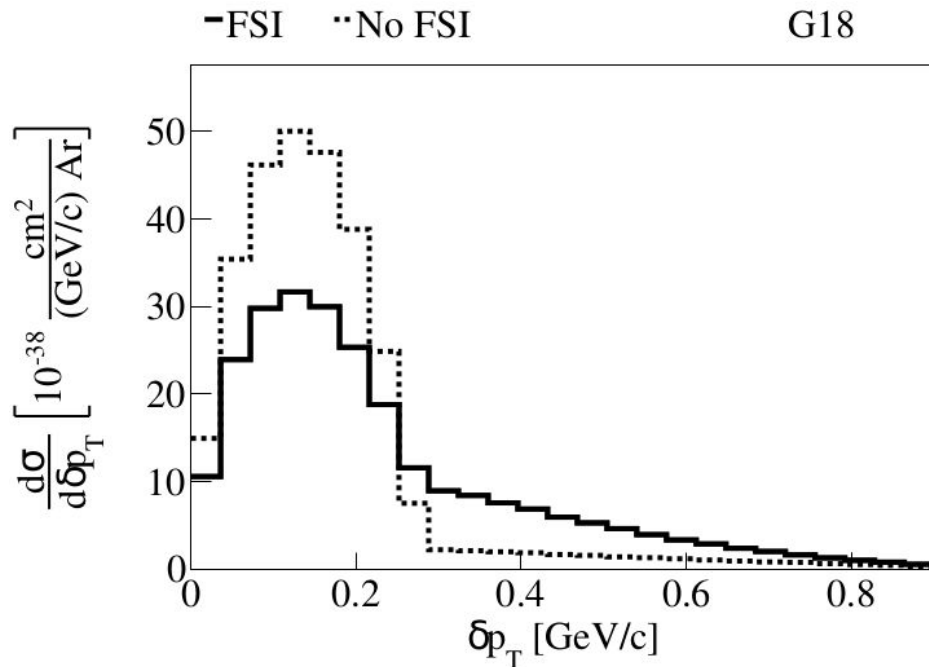
- 1 muon $100 < P_\mu < 1500$ MeV/c
- 1 proton $300 < P_p < 1000$ MeV/c
- No $\pi^\pm (> 70 \text{ MeV/c})$
- No π^0 of any momenta

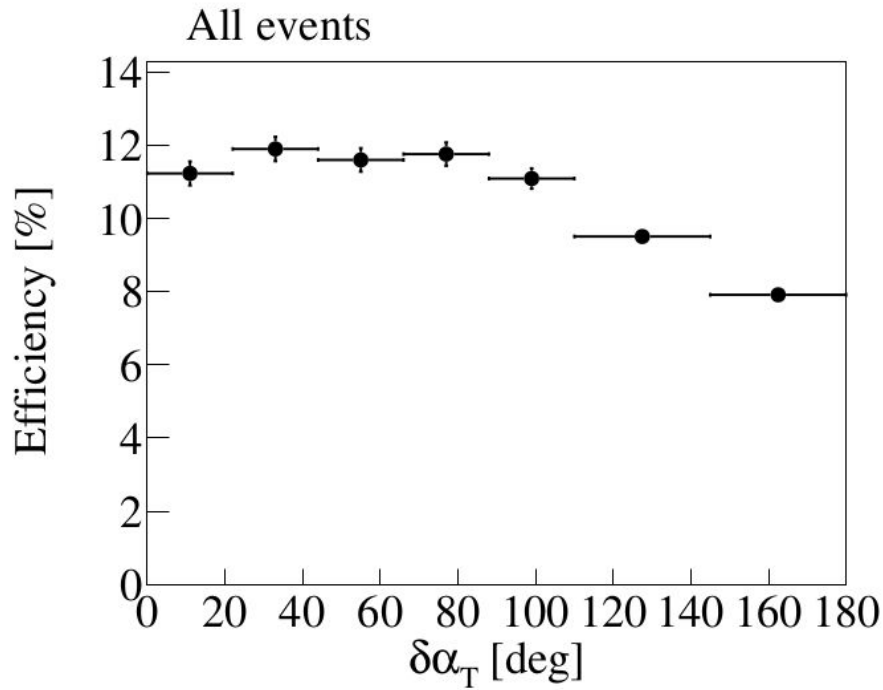
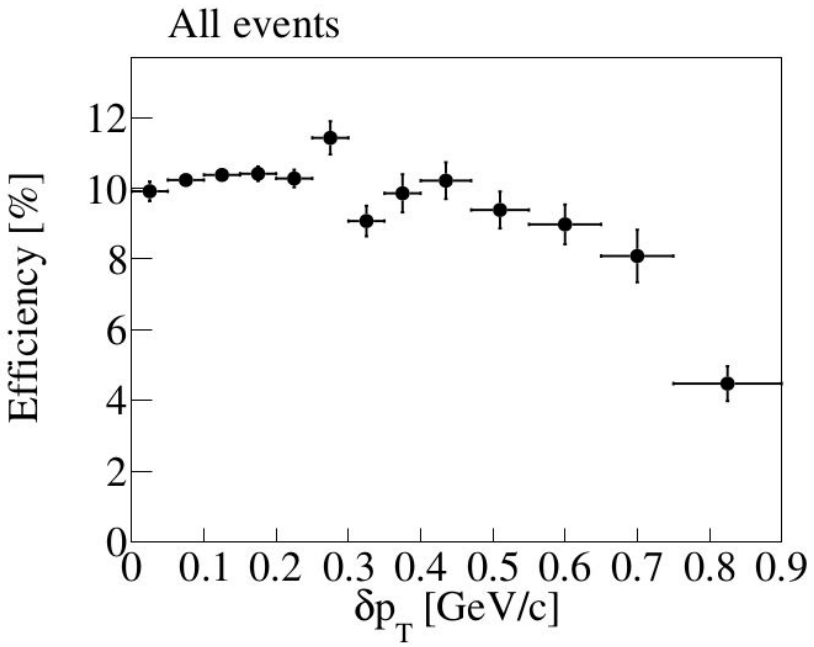
- $-0.65 < \cos \theta_\mu < 0.95$
- $\cos \theta_p > 0.15$

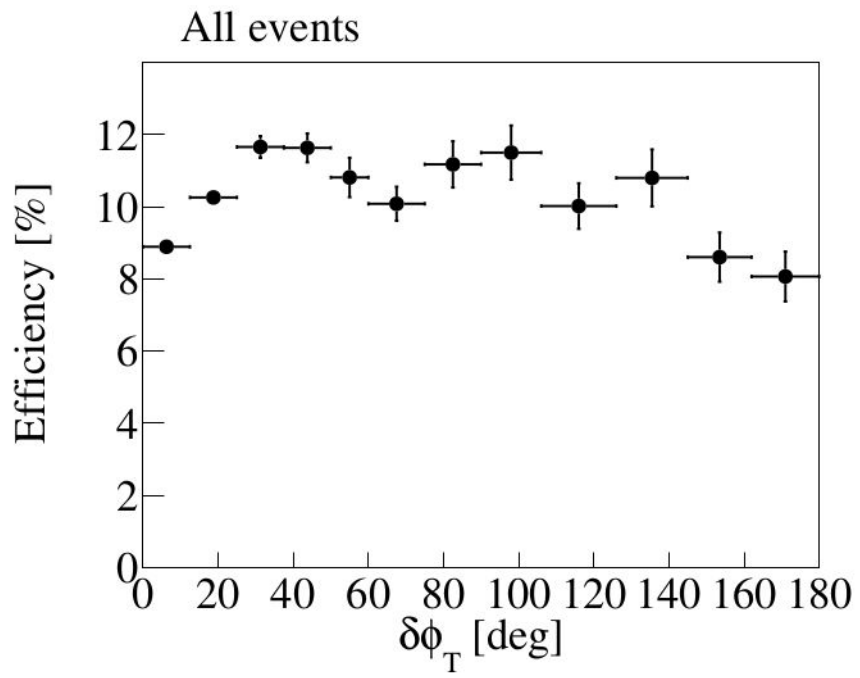
- $|\Delta\theta_{\mu,p} - 90^\circ| < 55^\circ$
- $|\Delta\phi_{\mu,p} - 180^\circ| < 35^\circ$
- $\mathbf{p}_T = |\mathbf{p}_T^\mu + \mathbf{p}_T^p| < 350 \text{ MeV/c}$

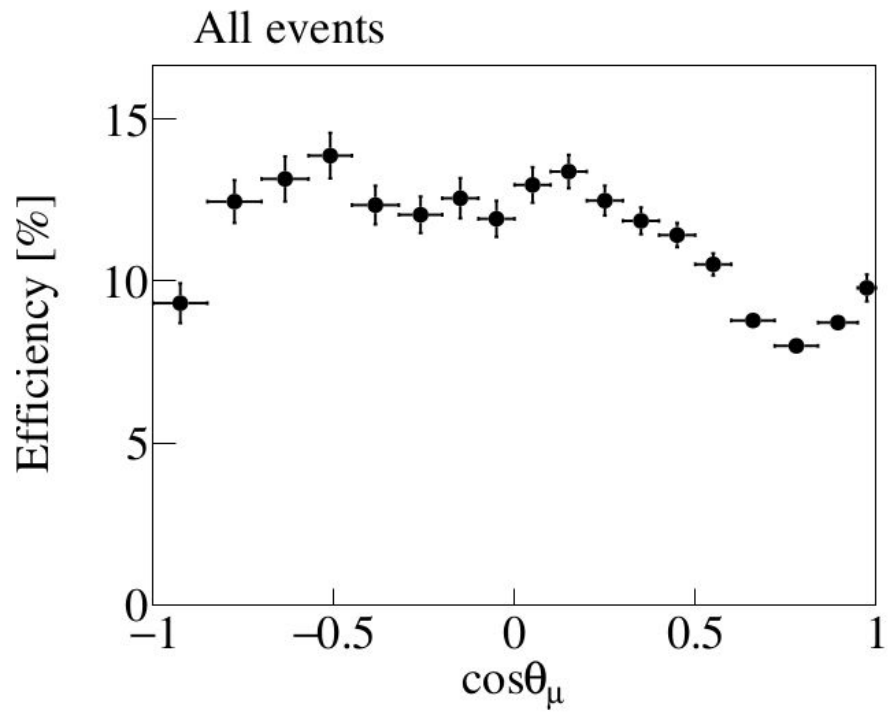
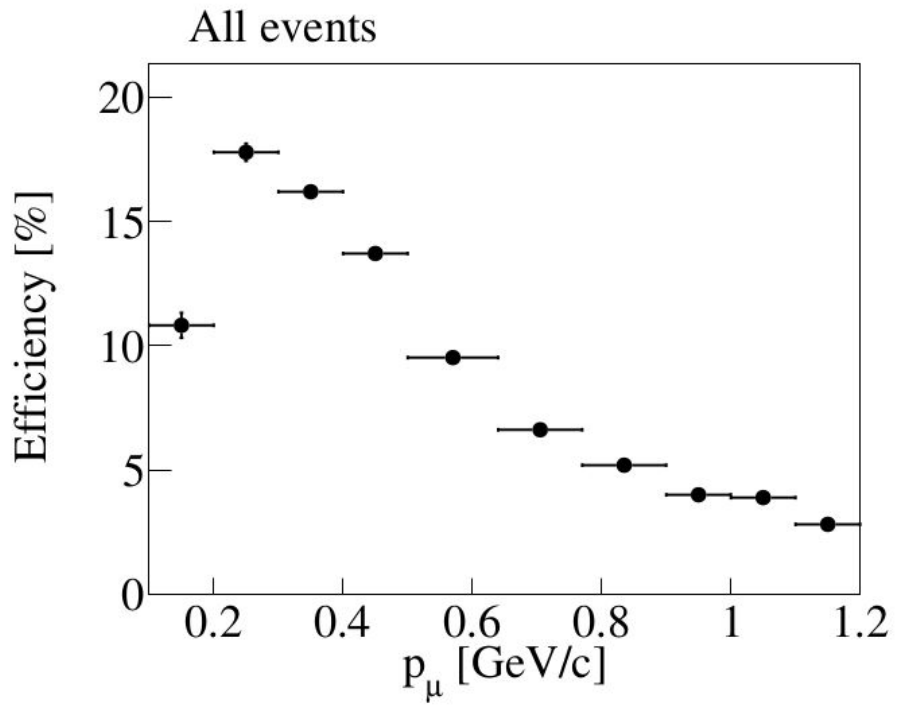
- 1 muon $100 < P_\mu < 1200$ MeV/c
- 1 proton $300 < P_p < 1000$ MeV/c
- No $\pi^\pm (> 70 \text{ MeV/c})$
- No π^0 of any momenta

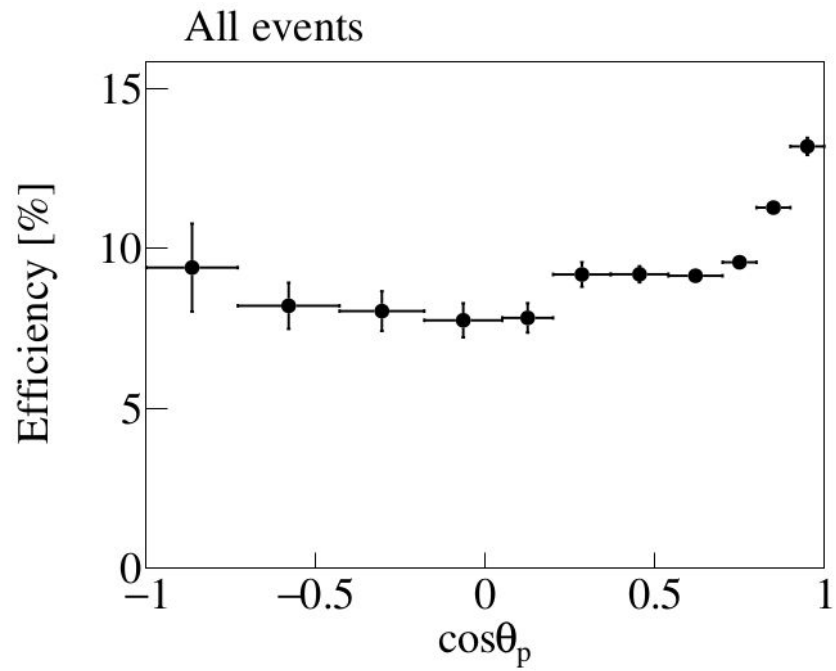
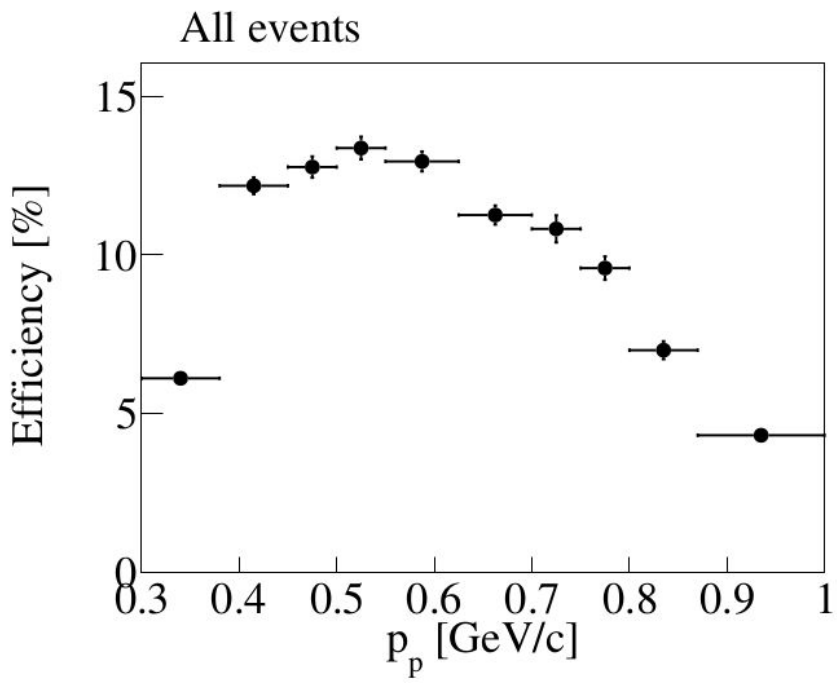
- $-1 < \cos \theta_\mu < 1$
- $-1 < \cos \theta_p < 1$

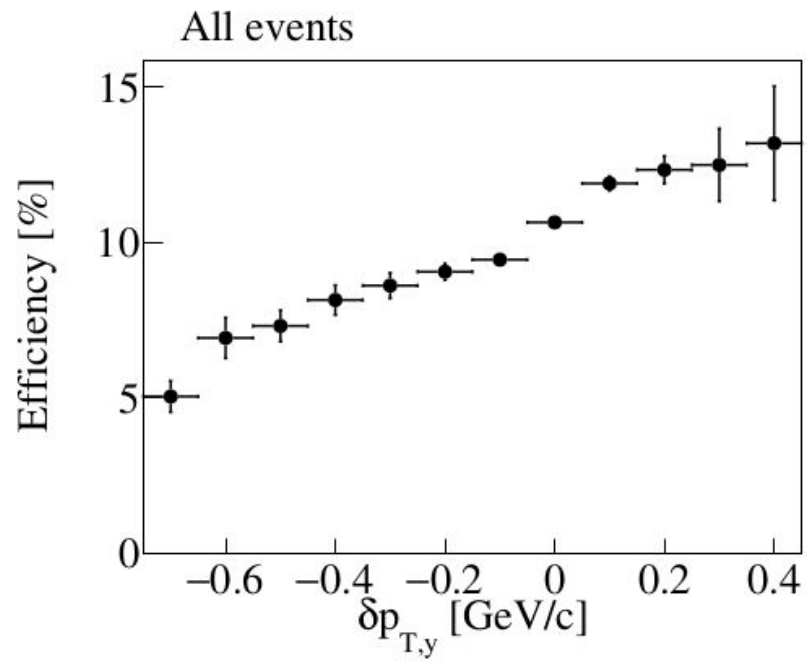
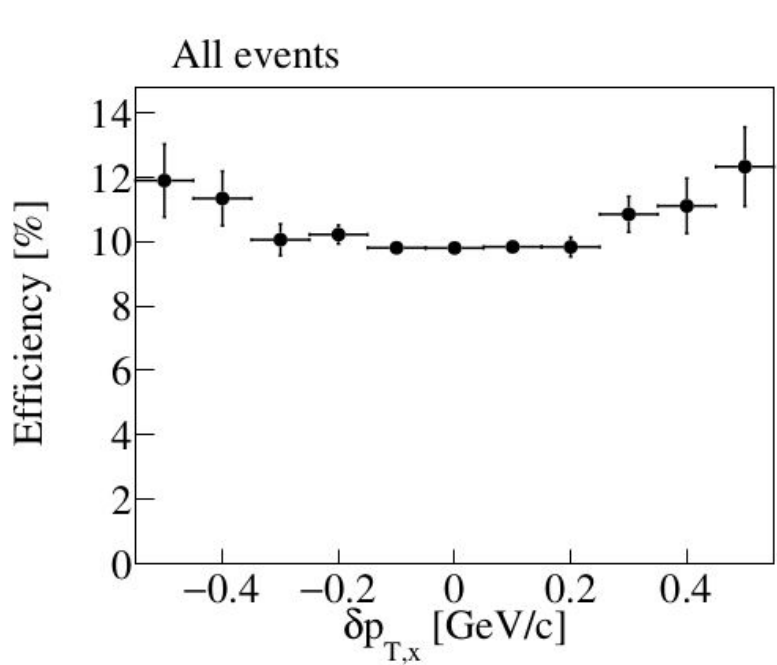












• MicroBooNE Data 6.79e+20 POT
— MC uB Tune

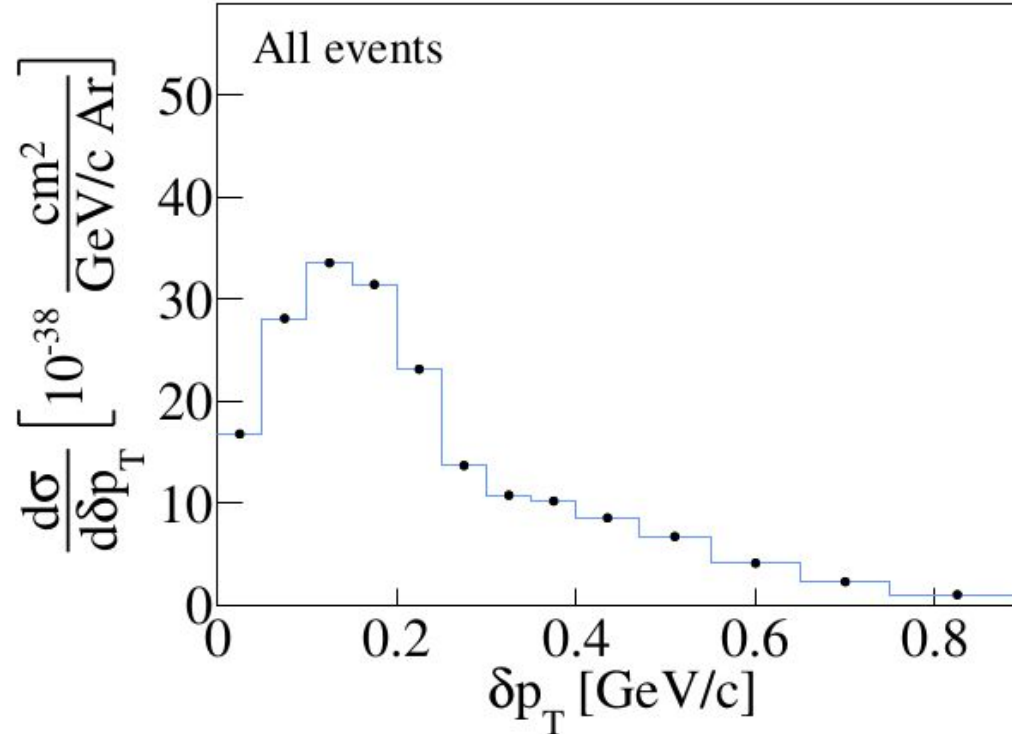


Figure 56: Closure test for δp_T .

